UNIVERSIDADE FEDERAL DO PARANÁ

THIAGO AUGUSTO FORMENTINI

MACROSCOPIC, MICROSCOPIC AND MOLECULAR SCALE INTERACTIONS AFFECTING COPPER AND ZINC TRANSFER WITHIN A CLAYEY HAPLUDOX SOIL SUBJECT TO LONG-TERM PIG SLURRY APPLICATION

CURITIBA

2016

THIAGO AUGUSTO FORMENTINI

MACROSCOPIC, MICROSCOPIC AND MOLECULAR SCALE INTERACTIONS AFFECTING COPPER AND ZINC TRANSFER WITHIN A CLAYEY HAPLUDOX SOIL SUBJECT TO LONG-TERM PIG SLURRY APPLICATION

A thesis submitted in partial fulfillment of the requirements for the degree of Doctor of Philosophy in Environmental Engineering, Graduate Program in Water Resources and Environmental Engineering, Federal University of Parana.

Supervisor: Cristovão V. S. Fernandes, Ph.D.
Co-Supervisor: Adilson Pinheiro, Ph.D.

CURITIBA
2016

Formentini, Thiago Augusto
Macroscopic, microscopic and molecular scale interactions affecting copper and zinc transfer within a clayey hapludox soil subject to long-term pig slurry application / Thiago Augusto Formentini. – Curitiba, 2016.
138 f. : il., tabs.

Thesis (doctor) – Universidade Federal do Paraná, Setor de Tecnologia, Programa de Pós-Graduação em Engenharia Ambiental.
Orientador: Cristovão V. S. Fernandes
Coorientador: Adilson Pinheiro
Bibliografia: p. 118-132

1. Metais pesados. 2. Adubação orgânica . 3. Extração (Química). I. Fernandes, Cristovão V. S. II. Pinheiro, Adilson. III. Título.

CDD 631.620

TERMO DE APROVAÇÃO

THIAGO AUGUSTO FORMENTINI

"Macroscopic, microscopic and molecular scale interactions affecting copper and zinc transfer within a clayey Hapludox soil subject to long-term pig slurry application"

Tese aprovada como requisito parcial à obtenção do grau de Doutor, pelo Programa de Pós-Graduação em Engenharia de Recursos Hídricos e Ambiental do Setor de Tecnologia da Universidade Federal do Paraná, pela comissão formada pelos professores:

PRESIDENTE:

Cristovão Vicente S. Fernandes
Universidade Federal do Paraná
Orientador

MEMBROS:

Adilson Pinheiro
Universidade Regional de Blumenau
Coorientador

Fabio Mallmann
Universidade Federal de Santa Maria

Emmanuel Doelsch
Cirad, UPR Recyclage et Risque, França

Julio Gomes
Universidade Federal do Paraná

Maria Cristina Borba Braga
Universidade Federal do Paraná

Curitiba, 21 de março de 2016

DEDICATION

This thesis is dedicated to Dr. Maria do Carmo Cauduro Gastaldini. When I started working at the Technology Center of the Federal University of Santa Maria, at the age of 19, I met someone to look after my career, rather than just a boss. She guided me for seven years, since I started as a second-year undergraduate student until I left holding my master's degree. Professor Maria do Carmo supported me to obtain my bachelor's degree, by allowing alternative work shifts in accordance with my classes schedules. Moreover, she supervised my coursework. During those seven years, she has made many efforts to integrate me in her research group, seeing me not only as a member of her staff, but also as a student and researcher. As a consequence, she was also my master's thesis supervisor. Finally, when an opportunity came to start this Ph.D. project in another university, she was the first person to give me full support, even if this would also mean my absence from the department.

Now, eleven years have passed by. I left and I am coming back. Everything that follows in this document was initiated in November 2004, at office 537, building 10, former Hydraulics and Sanitation Department, current Sanitary and Environmental Engineering Department, Federal University of Santa Maria.

It has been a long but exciting and learning journey.

Professora Maria do Carmo, meu muito obrigado!

ACKNOWLEDGMENTS

A Ph.D. is a life growing experience. By meeting great scientists, I hope I have become a better person. Supported by lifetime and temporary family and friends, I kept mentally healthy to go further in my research.

Mãe e pai. Vocês me ensinaram os valores mais importantes da vida. Vocês foram presentes no meu passado, importam-se com o meu presente, e torcem pelo meu futuro. Obrigado por me trazerem até aqui.

Mana, por ser minha melhor amiga, e por tudo o que isso significa.

To the five people without whom this thesis would have never been possible:

- Cris and Adilson: for all your efforts since the very beginning of this project. For teaching me about science, respect and teamwork. "*Você foi lá na rebimboca da parafuseta*". "*Toca pra frente*".
- Emmanuel: for receiving me in France and, thereby, pushing my life and research to another level. *"*This is science, not entertainment*"*.
- Fábio: for the partnership, both in and out of science. "*Se precisar, já sabe, prende o grito*".
- Milton: For conducting and making available a fantastic field experiment.

To all the lecturers, colleagues and staff from PPGERHA–UFPR. In special to Maria Cristina, Julio Gomes, Tobias Bleninger, Júlio Azevedo, Urivald Pawlowsky, Celmar, Marcelo, Patrícia and Marcus.

To all the lecturers, colleagues and staff from PPGEA–FURB. In special to Noemia, Thiago, Ruy, Rubia, Rafa and Jéssica.

To all the researchers and staff from CEREGE. In special to Samuel, Isabelle, Daniel, Bernard, Perrine, Clement, Jérôme L., Jerome R., Jean Paul, Lorette and Frauke.

To all my colleagues from DESA–UFSM. In special to Maria do Carmo, João Batista and Eloiza (*in memorian*). You supported me since the beginning of my career. Thank you for allowing my absence during these four years.

To other people who directly collaborated: Marcos Bender, Danilo Rheinheimer (PPGCS–UFSM), Olivier Grauby (CINaM–Luminy) and Isabelle Kieffer (ESRF).

À minha família em (ou de) Braga: Vô Nolly, Vó Helena, Vó Cleme, Tia Mada, Tia Noila, Tia Tere, Tio Carlos, João Antônio, Ana Rita, Rodrigo, Dudo, Fábio e Evandro.

To my second family in Santa Maria, Porto Alegre, Três Passos and throughout Rio Grande do Sul: Marina, Juli, Dessa, Má, Zé, Rafa, Alan, Frasson, Betânia, Marco, Diego, Lucas, Paulo, José, Josué, Pri, Zé Maedge, Cassio, Manu, Clá, Caio and Bauermann.

To my second family in Curitiba: Cesar, Maritza, Raissa, Fran, Bianca, Calicio, Adri, Gabi, Mizu, Jhonatas, Tábata, Steffany and João.

To my second family in Blumenau: Vitor, Vicente, Vinícius, Rodrigo, Batutinha, Helen, Ilya, Ariel and Neguinha. "*Casa Amarela é show!"*

To my second family in France: Danielle, Wuhib, William, Nathan, Pierre, Chloé, Nelly, Xavier, Cécile, P.A., Marrion, Alexia, Nicolas, Astrid, Maureen, Amalia, Gabe, Djordje, Juanito, Madjib, Gabriel, Antoine, Nadjib, Jojo, Julie, Sophie, Lucie, Camille, Louay and Jules.

My sincere and special thanks to other people that eventually were not named here. Every little smile, shared moment, word of comfort or motivation were very important during this long journey.

To UFSM: for the leave of absence.

To CAPES: for the scholarship (99999.000142/2014-00) during the sandwich period in France.

To FAPESC (17419/2011-0) and CNPq (403739/2013-6): for the financial support.

To EPAGRI: for providing the soil samples and the historical data.

To COOPERCAMPOS: for authorizing this study in its experimental area.

To my guitar: for being my most faithful companion during the last four years.

“It is paradoxical, yet true, to say, that the more we know, the more ignorant we become in the absolute sense, for it is only through enlightenment that we become conscious of our limitations. Precisely one of the most gratifying results of intellectual evolution is the continuous opening up of new and greater prospects.”

(Nikola Tesla)

ABSTRACT

Pig slurry (PS) recycling as fertilizer is commonly practiced as an option for minimizing livestock waste. The fate of trace metals from PS origin remains uncertain and only a few long-term field studies have been reported to date. This study was designed to assess the impact of 11-year continuous PS spreading on Cu and Zn behavior within a Brazilian clayey Hapludox soil. Three different PS application rates were monitored at six soil depths in comparison to a non-amended control soil. Experiments were carried out to investigate the accumulation and profile distribution, chemical fractionation, mineral and organic associations, and molecular-level incorporation of natural and exogenous heavy metal (HM) within the soil matrix. Firstly, the modified Geological Survey of Canada sequential extraction protocol was applied, resulting in six HM fractions with progressively weaker extractability. Significant increase in Cu and Zn total concentration (assessed by the sum of fractions) was noted only within the 0–5 cm soil layer for the 50 and 100 m^3 ha^{-1} $year^{-1}$ (PS50 and PS100) treatments, and up to 10–15 cm for the 200 m^3 ha^{-1} $year^{-1}$ (PS200) treatment. The mass balance, determined for the 22 PS amendments over the period, confirmed the overall exogenous Cu and Zn accumulation within the surface layers. More than 70% of the natural HM content was originally in the residual fraction. However, this was the only fraction not influenced by the PS amendments. Secondly, the HM phase associations with the soil matrix were assessed. Surface soil samples from the control and PS200 plots were fractionated according to density, resulting in five density fractions. Pedogenic HM were most likely associated to the phyllosilicates kaolinite and vermiculite and the Fe-oxide hematite. Exogenous Cu was mainly detected in the lightest density fraction, rich in organic matter (OM), whereas exogenous Zn distributed between the OM-rich and the phyllosilicate-rich fractions. Finally, synchrotron-based X-ray absorption spectroscopy was conducted on the same samples used for density fractionation. The soil Cu and Zn EXAFS data were analyzed by linear combination fitting, based on a library of EXAFS spectra of reference materials. Kaolinite and vermiculite accounted for the speciation of pedogenic Cu. The exogenous Cu was almost completely sorbed as inner-sphere into the kaolinite mineral structure. Kaolinite and hematite were the main minerals accounting for the Zn of natural occurrence. Exogenous Zn distributed about equally among Zn-kaolinite, Zn-hematite and Zn-OM. The speciation of Cu and Zn in the PS matrix was dominated by the sulfides Cu_2S and ZnS. However, these species were not detected at all within the soil after PS spreading. Scanning electron microscopy with X-ray microanalysis showed ZnS particles of about 1 µm diameter. Such small particles were reported for the first time in the PS matrix. It was hypothesized that the observed micro ZnS particles would rather consist of nano ZnS aggregates, more susceptible to solubilization. Results of this study reinforce the importance of long-term investigation under field conditions, and highlight the influence of the soil characteristics on the HM fate. The very high clay content of the soil was determinant for the strong attenuation of the PS-added HM mobility. Moreover, it opens a new line of investigation concerning the structure and stability of HM sulfides within the soil following organic amendments.

Keywords: Heavy metal. Organic amendment. Sequential extraction. Density fractionation. EXAFS.

RESUMO

A reciclagem de dejetos líquidos de suínos (DLS) como fertilizante é uma prática comum para diminuir os resíduos agropecuários. O destino de metais traço aplicados ao solo via DLS permanece incerto e poucos estudos de longa duração, em escala de campo, foram relatados até o momento. O presente trabalho visou avaliar o impacto de 11 anos de aplicação contínua de DLS em um solo argiloso no comportamento dos metais Cu e Zn. Três taxas de aplicação de DLS foram monitoradas em seis profundidades de solo, comparando-as com uma parcela de controle. Experimentos objetivaram avaliar a acumulação, distribuição no perfil, fracionamento químico, associações minerais e orgânicas e a incorporação ao nível molecular dos metais pesados (MP) de origem natural e exógena. Inicialmente, o protocolo de extração sequencial do *Geological Survey of Canada* foi aplicado às amostras de solo, resultando em seis frações de MP com extratabilidades progressivamente mais fracas. Observou-se um aumento significativo na concentração total de Cu e Zn apenas na camada de 0 a 5 cm, nos tratamentos de 50 e 100 m^3 ha^{-1} ano^{-1} de DLS. No tratamento de 200 m^3 ha^{-1} ano^{-1} (DLS200), o aumento foi até a camada de 10 a 15 cm. O balanço de massa, determinado para as 22 aplicações de DLS, confirmou a acumulação total do Cu e Zn exógenos nas camadas de solo superficiais. Mais de 70% do teor natural dos MP foi detectado na fração residual. Entretanto, esta foi a única fração não influenciada pelas adições de DLS. Em seguida, as associações entre os MP e as fases do solo foram investigadas. Amostras de superfície (0 a 5 cm) das parcelas de controle e DLS200 foram fracionadas de acordo com a densidade, resultando em cinco frações densimétricas. Os MP de origem pedogênica estavam possivelmente associados aos filossilicatos caulinita e vermiculita e ao óxido de Fe hematita. O Cu exógeno foi detectado sobretudo na fração densimétrica mais leve, rica em matéria orgânica (OM), enquanto o Zn exógeno distribuiu-se entre as frações rica em OM e rica em filossilicatos. Finalmente, aplicou-se a espectroscopia de absorção de raios-X baseada em luz síncrotron às mesmas amostras utilizadas no fracionamento densimétrico. Os dados de EXAFS foram submetidos ao ajuste por combinações lineares, considerando uma base de dados de materiais de referência. A especiação do Cu pedogênico foi dominada pelos minerais caulinita e vermiculita, enquanto o Cu exógeno foi detectado quase totalmente sorvido em *inner-sphere* na estrutura mineral da caulinita. A ocorrência natural do Zn deu-se associada aos minerais caulinita e hematita, enquanto sua distribuição exógena foi verificada entre Zn-caulinita, Zn-hematita e Zn-MO. A especiação dos MP no DLS foi dominada pelos sulfetos Cu_2S e ZnS. Entretanto, estas espécies não foram detectadas no solo após as aplicações de DLS. Análise do DLS via microscopia eletrônica de varredura revelou partículas de ZnS de aproximadamente 1 μm de diâmetro, inéditas na literatura científica. Postulou-se que tais micropartículas poderiam consistir de nano-agregados de ZnS, mais suscetíveis a solubilização. Os resultados do presente estudo reforçam a importância da investigação de longa duração, em condições de campo, e destacam a influência das características do solo no destino dos MP. O alto teor de argila do solo foi determinante para a forte atenuação da mobilidade dos MP adicionados via DLS. Ademais, abre-se caminho à uma nova linha de investigação relacionada à estrutura e estabilidade de sulfetos metálicos no solo após aplicação via rejeitos orgânicos.

Palavras-chave: Metal pesado. Adubação orgânica. Extração sequencial. Fracionamento densimétrico. EXAFS.

LIST OF FIGURES

FIGURE 2.1 – Soil textural triangle 27

FIGURE 2.2 – Biogeochemical cycling of soil contaminants, as controlled by the soil solution 33

FIGURE 2.3 – Time ranges required to attain equilibrium by different types of reaction in soil environments..... 36

FIGURE 3.1 – Materials and methods diagram..... 48

FIGURE 3.2 – Experiment location and design 50

FIGURE 4.1 – Cu and Zn fractionation among the six fractions within the CT, PS50, PS100 and PS200 deepest (25–30 cm) and topmost (0–5 cm) soil layers 70

FIGURE 4.2 – Soil profile distribution of Cu and Zn concentrations associated with the first five fractions and the deepest soil layer significantly affected ($p < 0.05$) by the PS application rate, comparing PS50, PS100 and PS200 with the CT plot 73

FIGURE 4.3 – Cu fractions, SUMF and soil organic C profile within CT, PS50, PS100 and PS200 plots 74

FIGURE 4.4 – Zn fractions, SUMF and soil organic C profile within CT, PS50, PS100 and PS200 plots 77

FIGURE 4.5 – Soil mass distribution (in percentage) among density fractions and XRD characterization 81

FIGURE 4.6 – Organic C and N concentrations and mass distribution among density fractions 83

FIGURE 4.7 – (a) Cu concentration within soil density fractions in the CT and PS200 samples and Cu concentration increase within each fraction. (b) Resulting exogenous Cu distribution..... 86

FIGURE 4.8 – (a) Zn concentration within soil density fractions in the CT and PS200 samples and Zn concentration increase within each fraction. (b) Resulting exogenous Zn distribution 87

FIGURE 4.9 – k^2-Weighted Cu K-edge EXAFS and FT spectra of CT, PS200 and pig slurry samples as compared to Cu-containing or Cu sorbed on selected mineral and organic references 92
FIGURE 4.10 – k^2-Weighted Zn K-edge EXAFS and FT spectra of CT, PS200 and pig slurry samples as compared to Zn-containing or Zn sorbed on selected mineral and organic references 94
FIGURE 4.11 – k^2-Weighted Cu K-edge EXAFS and FT spectra of CT, PS200 and pig slurry samples, superposed by the best LCF fits for each sample 97
FIGURE 4.12 – (a) Absolute and percentage distribution of Cu species within CT, PS200 and pig slurry samples. (b) Absolute and percentage distribution of exogenous Cu 98
FIGURE 4.13 – k^2-Weighted Zn K-edge EXAFS and FT spectra of CT, PS200 and pig slurry samples, superposed by the best LCF fits for each sample 99
FIGURE 4.14 – (a) Absolute and percentage distribution of Zn species within CT, PS200 and pig slurry samples. (b) Absolute and percentage distribution of exogenous Zn..... 101
FIGURE 4.15 – (a, b) Scanning electron microscopy micrograph of the pig slurry 20 µm > PS > 0.2 µm particle size fraction; arrows indicate regions selected for energy dispersive spectrometer spectrum (c) 102
FIGURE 4.16 – (a) Scenario comparing hypothetical EXAFS and FT spectra of the amended plot if the ZnS detected within PS was preserved in the soil (CT + PS) with the spectra of the CT plot. (b) EXAFS and FT spectra actually recorded for the PS200 plot as compared to the spectra of the CT plot 108

LIST OF TABLES

TABLE 2.1 – Cu and Zn concentrations worldwide and in Brazilian and Santa Catarina State soils 28
TABLE 2.2 – Average nutrient composition of swine manure..... 29
TABLE 2.3 – Cu and Zn limits for agricultural use of biosolids 32
TABLE 3.1 – Total Cu, Zn and organic C concentrations within the soil 0–5, 5–10, 10–15, 15–20, 20–25 and 25–30 cm layers of the CT, PS50, PS100 and PS200 plots, after 22 PS amendments..... 51
TABLE 3.2 – Operating conditions for the *m*GSC sequential extraction procedure for 1 g of air-dried soil 53
TABLE 4.1 – SUMF-Cu and SUMF-Zn concentrations (mean ± SD) within the soil layers of the CT, PS50, PS100 and PS200 plots 67
TABLE 4.2 – Cu and Zn quantities (mean ± SD) applied via 22 PS amendments and accumulated within the 0–30 cm profile of PS50, PS100 and PS200 plots after 11 years 68

LIST OF ABBREVIATIONS AND ACRONYMS

ANOVA	Analysis of variance
ATSDR	Agency for Toxic Substances and Disease Registry
BCR	Community Bureau of Reference
CEC	Council of the European Communities
CEC	Cation exchange capacity
CETESB	*Companhia Ambiental do Estado de São Paulo* (Sao Paulo Environmental Company)
CONAMA	*Conselho Nacional do Meio Ambiente* (Brazilian National Environmental Council)
CT	Control plot
e.g.	*Exemplī grātiā* (for example)
EC	European Commission
EMBRAPA	*Empresa Brasileira de Pesquisa Agropecuária* (Brazilian Agricultural Research Company)
EPR	Electron paramagnetic resonance
EXAFS	Extended X-ray absorption fine structure
F1	Fraction 1 – exchangeable
F2	Fraction 2 – adsorbed
F3	Fraction 3 – organic matter
F4	Fraction 4 – amorphous oxyhydroxides
F5	Fraction 5 – crystalline oxides
F6	Fraction 6 – residual
FAO	Food and Agriculture Organization of the United Nations
FT	Fourier transform
HDL	High-density lipoprotein
HIM	Hydroxy-interlayered minerals
HM	Heavy metal
HSD	Honest significant difference
i.e.	*id est* (that is)
IAP	*Instituto Ambiental do Paraná* (Parana Environmental Institute)
ICP–OES	Inductively coupled plasma–optical emission spectrometer

IRIS	Integrated Risk Information System
LCF	Linear combination fitting
LDH	Layered double hydroxides
LoQ	Limit of quantification
*m*GSC	Modified Geological Survey of Canada protocol
NC	North Carolina State
OM	Organic matter
PCA	Principal component analysis
pH	Potential of hydrogen
PS	Pig slurry
PS50	50 m^3 ha^{-1} $year^{-1}$ of pig slurry plot
PS100	100 m^3 ha^{-1} $year^{-1}$ of pig slurry plot
PS200	200 m^3 ha^{-1} $year^{-1}$ of pig slurry plot
Res	Residual parameter
RS	Rio Grande do Sul State
RSF	Radial structure function
SC	Santa Catarina State
SD	Standard deviation
SEMA	*Secretaria do Meio Ambiente e Recursos Hídricos* (Parana Environmental and Water Resources Secretariat)
SI	Supporting information
SUMF	Sum of fractions
USDA	United States Department of Agriculture
USEPA	United States Environmental Protection Agency
XANES	X-ray absorption near edge structure
XAS	X-ray absorption spectroscopy

LIST OF SYMBOLS

B	Boron
C	Carbon
Ca	Calcium
Cd	Cadmium
Cr	Chromium
Cu	Copper
Cu^{2+}	Copper ion
CH_3COOH	Acetic acid
CH_3COONa	Sodium acetate
Cl	Chlorine
E	Energy
E_0	Absorption edge energy
Fe	Iron
Ge	Germanium
HCl	Hydrochloric acid
He	Helium
HNO_3	Nitric acid
K	Potassium
k	Wave number of the photo-electron
K_2O	Potassium oxide
Mg	Magnesium
Mn	Manganese
Mo	Molybdenum
N	Nitrogen
Na	Sodium
$Na_4P_2O_7$	Sodium pyrophosphate tetrabasic
$NaNO_3$	Sodium nitrate
$NH_2OH{\cdot}HCl$	Hydroxylamine hydrochloride
Ni	Nickel
P	Phosphorus
p	p-value; significance level

P_2O_5	Phosphorus pentoxide
Pb	Lead
S	Sulfur
Zn	Zinc
$\chi(E)$	EXAFS function
$\chi(k)$	EXAFS oscillations as a function of k
$\mu(E)$	Measured absorption coefficient
$\mu_0(E)$	Background function (absorption of an isolated atom)

LIST OF UNITS

Å	Angstron
cm	Centimeter
$cmol_c\ dm^{-3}$	Centimole of charge per cubic decimeter
eV	Electronvolt
$g\ cm^{-3}$	Gram per cubic centimeter
$g\ kg^{-1}$	Gram per kilogram
$g\ l^{-1}$	Gram per liter
$g\ m^{-3}$	Gram per cubic meter
h	hour
kD	Kilodalton
$kg\ ha^{-1}$	Kilogram per hectare
$kg\ ha^{-1}\ year^{-1}$	Kilogram per hectare per year
l	Liter
$m^3\ ha^{-1}\ year^{-1}$	Cubic meter per hectare per year
$mg\ kg^{-1}$	Milligram per kilogram
$mg\ l^{-1}$	Milligram per liter
min	Minute
ml	Milliliter
mm	Millimeter
$mol\ l^{-1}$	Mole per liter
rpm	Revolutions per minute
v/v	Volume/volume percent
µm	Micrometer
µM	Micromolar
$\mu mol\ g^{-1}$	Micromole per gram
ºC	Degree Celsius

SUMMARY

1 INTRODUCTION 20

1.1 RESEARCH PROBLEMS AND QUESTIONS 22

1.1.1 Problem and question #1 22

1.1.2 Problem and question #2 23

1.2 HYPOTHESIS 23

1.3 AIM AND OBJECTIVES 23

1.4 EXPECTED CONTRIBUTION 24

1.5 THESIS ORGANIZATION 25

2 THEORETICAL FRAMEWORK 26

2.1 THE SOIL 26

2.2 HEAVY METALS IN SOILS 28

2.3 PIG SLURRY 29

2.4 HEALTH ASPECTS 30

2.5 LEGISLATION 31

2.6 HEAVY METAL FATE IN SOILS 33

2.7 STATE OF THE ART 36

2.7.1 Chemical sequential extractions 38

2.7.2 Density fractionation 42

2.7.3 X-ray absorption spectroscopy 43

2.7.4 Remarks 47

3 MATERIALS AND METHODS 48

3.1 OBJECTS OF STUDY 49

3.1.1 Experiment location and design 49

3.1.2 Soil and PS characteristics 51

3.2 ACCUMULATION AND FRACTIONATION METHODS 52

3.2.1 Sequential extraction procedure 52

3.2.2 Statistical analysis and calculations 54

3.3 PHASE ASSOCIATION METHODS 55
3.3.1 Density fractionation procedure 55
3.3.2 Characterization and chemical analysis of soil density fractions ..57
3.3.3 Calculations 58
3.4 MOLECULAR ENVIRONMENT METHODS 59
3.4.1 X-ray absorption spectroscopy 59
3.4.2 Cu sorption experiments 61
3.5 COMPLEMENTARY PIG SLURRY ANALYSIS 64
3.5.1 Particle size fractionation of pig slurry 64
3.5.2 Scanning electron microscopy with X-ray microanalysis 65

4 RESULTS AND DISCUSSION 66
4.1 ACCUMULATION AND FRACTIONATION 66
4.1.1 Sequential extraction recoveries and Cu and Zn natural contents 66
4.1.2 Cu and Zn accumulation 67
4.1.3 Cu and Zn fractionation 69
4.1.3.1 Residual fraction 71
4.1.3.2 Fractions influenced by PS amendments and the exogenous Cu and Zn distribution 72
4.1.4 Remarks 78
4.2 PHASE ASSOCIATION 80
4.2.1 Mass distribution and mineral characterization of soil density fractions 80
4.2.2 Organic C and N 82
4.2.3 Cu and Zn 84
4.2.4 Discussion 87
4.2.4.1 Cu and Zn natural occurrence 87
4.2.4.2 Cu and Zn exogenous distribution 89
4.2.5 Remarks 90
4.3 MOLECULAR ENVIRONMENT 91
4.3.1 Linear combination fitting 96
4.3.2 Pig slurry SEM–EDS analysis 101
4.3.3 Discussion 102
4.3.3.1 Cu and Zn natural occurrence 102

4.3.3.2 Cu and Zn exogenous distribution 104
4.3.3.3 Cu and Zn in the pig slurry..... 106

5 CONCLUDING REMARKS 109
5.1 THE HM ACCUMULATION WITHIN THE SOIL SURFACE AND THE ENVIRONMENTAL ISSUE 109
5.2 TOWARDS A MICROSCOPIC AND MOLECULAR LEVEL EXPLANATION FOR THE MACROSCOPIC OBSERVATION 110
5.2.1 A novel application for soil density fractionation: assessing the HM fate within organically amended soils 111
5.2.2 The Cu and Zn molecular environment: confirming the leading role of clay minerals for HM retention and observing a novel Zn speciation in PS followed by a unique behavior after spreading on the soil 112
5.3 FUTURE RESEARCH 114
5.3.1 Type of soil 114
5.3.2 Scenarios of PS application 115
5.3.3 Modeling 115
5.3.4 Analytical approach..... 116
5.3.5 The big picture 116

REFERENCES 118

APPENDICES 133

1 INTRODUCTION

The recycling of organic waste such as pig slurry (PS) in agriculture, as commonly practiced throughout much of the world, is one of the most cost-effective ways of managing these wastes (ASADA et al., 2012; L'HERROUX et al., 1997). This practice lowers treatment, transportation and disposal costs, while it improves soil physicochemical attributes for crops (GIROTTO et al., 2010). In this context, it might be regarded as an environment-friendly strategy and a relevant part for water resources planning and management towards a more sustainable waste residue control.

However, it may cause adverse environmental impacts, such as nitrate (PEU et al., 2007) or phosphate (SMITH et al., 2004) contamination of groundwater. Furthermore, problems related to runoff may arise in regions where rainfall is frequent and intense, causing the transfer of these contaminants to superficial waters (XUE et al., 2003).

One additional concern is related to the heavy metal (HM) concentration in PS, particularly copper (Cu) and zinc (Zn). They are abundantly added as supplements in pig feed, owing to their growth factor (Cu) and antibiotic (Zn) attributes (JONDREVILLE et al., 2003). Nevertheless, the animals retain only a small portion of these metals, thus a substantial amount of HM is excreted in the manure and subsequently spread on the soil during PS recycling (ORIHARA et al., 2002; POULSEN, 1998). As a result, pig manure is the most significant anthropogenic source of Cu and Zn in agricultural soils (BACH et al., 2002).

Most crops use only a small amount of Cu and Zn to complete their life cycles (NOVAK et al., 2004). Therefore, phytotoxicity or HM accumulation in plant tissues and grains may occur, ultimately including them into the food chain. Moreover, HM leaching through the soil profile is of major concern regarding groundwater quality (LIPOTH & SCHOENAU, 2007; HAO et al., 2008). Unlike macronutrients, whose mobility and transfer mechanisms are to date fairly well studied and understood, HM fate in soils is still under evolving investigation.

The total soil HM content may represent the level of accumulation. However, it is acknowledged that the environmental risk is dependent on mechanisms acting in the retention and migration of (potentially) mobile and bioavailable fractions.

Interactions between HM and soils mainly include complexation, ion exchange, adsorption and precipitation. Due to the highly variable characteristics of soils, diverse nature and strength of the bond between HM and the soil matrix, multiple properties of the solution in contact with the solid phase, and the typically trace level concentration of HM in soils, investigation within this environment is not straightforward (ASADA et al., 2012; FILGUEIRAS et al., 2002; KABALA & SINGH, 2001).

Moreover, transformations governing HM retention and migration, especially those occurring in the soil solid phase, may take years or even centuries to be completed. They may also change over time due to saturation of sorbing sites or changes in the contaminant speciation, which are dependent, among other factors, on the HM amounts applied to the soil (HESTERBERG, 1998; SELIM & AMACHER, 1996; ZHENG & BENNETT, 2002).

In a previous modelling study, Mallmann (2013) reported the high potential of accumulation of Cu and Zn in a Brazilian clayey Hapludox soil that had received 22 PS applications over 11 years. This provided an opportunity for further investigation in the same field experiment, this time focusing on the interactions between HM and the soil environment. A complementary experimental study was thus envisioned as an attempt to explain the previously observed modelling behavior and thereby enhancing the comprehension of phenomena governing HM mobility within soils.

In the present research, a multi-scale investigation was proposed using chemical (contaminant) and physical (soil) fractionation protocols, followed by state-of-the-art analytical tools such as inductively coupled plasma optical emission and mass spectrometry, scanning electron microscopy and synchrotron-based X-ray absorption spectroscopy. Furthermore, the field trial used in this study presented unique characteristics making it relevant for the proposed investigation and building knowledge, such as: (i) long-term PS application at different rates; (ii) field scale design; and (iii) narrow soil layer partitioning. Such complete design is rare throughout the world and, in combination with the multi-scale investigation approach, should provide a concrete contribution for the understanding of HM fate in soils following long-term organic amendments, still scarce in the literature.

1.1 RESEARCH PROBLEMS AND QUESTIONS

Based on the foregoing discussion, two aspects were identified as critical for a comprehensive description of HM fate within organically amended soils. The first is related to the HM spatial distribution within the soil profile following long-term PS spreading. The second is related to their transfer mechanisms, *i.e.* the understanding of the observed spatial distribution, which involves different types of interactions between HM and soil. Both points are detailed below, followed by key questions seeking to guide the conduction of the present study.

1.1.1 Problem and question #1

The fate and behavior of Cu and Zn within organically amended soils are incompletely described and understood. Nevertheless, their migration through the soil profile has been reported as slow, due to the usually HM strong affinity for the soil matrix. Moreover, local conditions such as climate, soil mineralogy and organic content, and contaminant characteristics may drastically change the expected or most likely behavior. In order to assess thoroughly the HM fate following PS spreading on the soil under field natural conditions, continued long-term PS amendments are necessary. Investigation should take into account the HM sources and the profile distribution within the soil after application.

- How are Cu and Zn spatially distributed within the studied soil profile after 11 years of PS application? Which information can be drawn on their accumulation and mobility?

1.1.2 Problem and question #2

Total HM content in soils may not reflect the degree of contamination. Heavy metal retention and transfer within the soil, and therefore its potential mobility and availability, are dependent on the contaminant speciation and matrix characteristics. Therefore, the explanation and better understanding of the macroscopic behavior requires investigation on the HM local environment.

- Should a combination of chemical and physical HM-soil fractionation, followed by analysis at different scales of observation, be explored in association, and therefore improve the understanding on the Cu and Zn macroscopic behavior within a PS-amended soil?

1.2 HYPOTHESIS

The long-term fate of Cu and Zn in a soil following continued PS applications may be assessed by matching the HM inputs over time with the exogenous HM detected within the soil and comparing the HM concentration at different soil depths in PS-amended plots to their natural concentration in a control plot. Once this step is achieved, additional understanding on the observed HM macroscopic behavior may be attained by analyzing the HM speciation, determining the soil constituents, and thereby the interactions among them, by combining macroscopic, microscopic and molecular scale approaches.

1.3 AIM AND OBJECTIVES

The aim of the present study was to evaluate the effects of long-term PS applications on the Cu and Zn behavior within a clayey Hapludox soil. For this purpose, an 11-year term field trial involving 22 PS applications was studied. Soil samples were collected in the 0–30 cm horizon, divided into 6 layers of 5-cm depth each, in field plots

that had received three different PS application rates, plus a non-amended control plot. Experiments were carried out to investigate the accumulation and profile distribution, chemical fractionation, mineral and organic associations, and molecular-level incorporation of natural and exogenous Cu and Zn within the soil matrix. The following objectives were pursued:

- to assess the Cu and Zn accumulation and profile distribution within PS-amended plots, by comparing the amounts of HM added into and detected within the soil;
- to investigate the Cu and Zn chemical fractionation within amended and non-amended plots and, thereby, to explore the HM mobility through the soil profile;
- to recognize the nature of the soil solid phases and thus to identify potential HM-bearing minerals and organics;
- to analyze the Cu and Zn local environment, *i.e.* the incorporation of natural and exogenous HM into soil constituents at the molecular level.

1.4 EXPECTED CONTRIBUTION

Conditioned to the attainment of the proposed aim and objectives, the present study is expected to pose a contribution on the following domains:

- expansion of the scientific basis for maintaining quality of soils and adjacent systems;
- prediction of the evolution of HM behavior in organically amended soils;
- formulation of appropriate strategies to stabilize or remediate contaminated areas.

1.5 THESIS ORGANIZATION

The structure of this manuscript consists of five chapters, arranged in order to cover the aspects needed for (i) contextualizing the studied subject; (ii) describing the methodological approach, and (iii) presenting and discussing the results.

Chapter 1 aims to introduce the overall research problem and therefore justify this research. It establishes fundamental questions that guide the proposition of research hypothesis, objectives and contribution.

Chapter 2 presents consolidated background information on the studied topic. A brief description on soils, HM and PS is introduced. Moreover, basic transfer mechanisms affecting HM fate within soils, as well as health and legislation aspects are addressed. Lastly, the state of the art subsection presents the latest published efforts for understanding the previously discussed outline, reflecting thus the edge of knowledge to date. It also intends to highlight the literature gaps and therefore justifying the original methodological approach herein proposed.

Chapter 3 is the materials and methods section. Firstly, the experiment location and design, as well as the soil and PS basic characteristics are presented. Then, three well defined lines of investigation – complementary among each other – on the Cu and Zn interactions with the soil matrix are described.

Chapter 4 presents the core results of this research. It is roughly divided according to the three-line arrangement defined in the materials and methods section. A particular discussion on the results obtained in each of the three main investigation approaches is also pursued. For convenience, the discussion may be presented either along with the results or in a separate subsection, in order to properly make the link among the results from each approach.

Chapter 5 consists of a broader discussion on the results. Eventually, it may take into account aspects not directly addressed in the methodological approach, but that might be relevant for instigating upcoming studies. Finally, it presents the conclusions based on proposed questions, hypothesis and objectives.

2 THEORETICAL FRAMEWORK

“Science is organized knowledge.”

(Herbert Spencer)

2.1 THE SOIL

The soil is a heterogeneous, polyphasic, particulate, disperse, and porous system. It exhibits a large specific surface area. Phenomena such as adsorption of water and chemicals, capillarity, ion exchange, swelling and shrinking, dispersion and flocculation take place due to its disperse nature and resulting interfacial activity (HILLEL, 2003).

Mineral soils are formed by a mixture of solid particles of mineral and organic nature, water and air. They constitute thus a three-phase system, solid, liquid and gaseous. The solid phase forms the soil matrix, the liquid phase, along with dissolved substances, forms the soil solution, and the gaseous phase is the soil atmosphere (HILLEL, 2003; REINERT & REICHERT, 2006; LIBARDI, 2005).

A rough proportion of soil components in a medium-textured soil at an optimal condition for plant growth is: 45% minerals, 5% organic matter, 25% air, and 25% water. Depending on how individual soil granules clump or bind together and aggregate, the arrangement of the solid parts and of the pore space located between them, *i.e.* the soil structure, is formed. Roughly half of the space is occupied by solid particles, while the other half is formed by pores. The proportion of air and water filling the pores are subject to great variations under natural conditions, especially due to meteorological factors (BRADY, 1989).

Particles forming the soil matrix may vary largely in size, shape, chemical and mineralogical composition. The differences among soils are due to the differences in the type and relative abundance of such particles. The soil texture derives from the particle-size distribution, and it is considered the soil’s most stable physical characteristic (SANCHEZ, 2012). It is classified in several categories, according to the

proportion of each soil separate: clay (particles smaller than 0.002 mm diameter), silt (particles in the 0.002–0.05 mm range) and sand (particles in the 0.05–2.00 mm range). Figure 2.1 presents the United States Department of Agriculture (USDA) triangle used for the textural classification of soils (USDA, 2013).

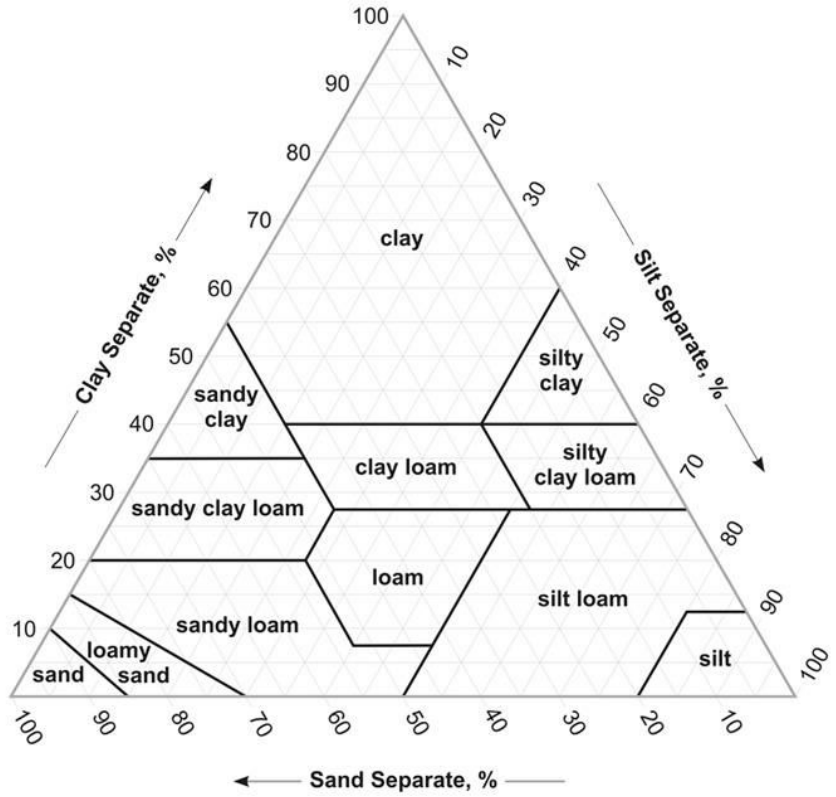

Figure 2.1 – Soil textural triangle (USDA, 2013).

The clay fraction is the most active part of the soil. Because of its high surface area, this fraction controls many of the chemical and physical properties of the soil. It is mainly composed of secondary silicate minerals such as kaolinite, illite and montmorillonite, also known as clay minerals. The sand and silt fractions influence essentially the physical properties of the soil. They consist mainly of quartz and other primary minerals (feldspars, micas, pyroxene, olivine), along with small amounts of secondary minerals such as aluminium (gibbsite) and iron (hematite) oxides (FAO, 1987).

2.2 HEAVY METALS IN SOILS

Heavy metals are defined as metallic elements with high atomic weights that can damage living things at low concentrations and tend to accumulate in the food chain (USEPA, 2016). They occur naturally in soils, usually at relatively low concentrations. They arise from pedogenic processes such as weathering of rocky fragments from which soils develop. The elemental and mineralogical composition of rocks widely vary, resulting in marked differences in HM concentration among different types of soils (ALLOWAY, 1995). Heavy metal concentration in soils may also be altered by evolving pedogenic processes, or influenced by either atmospheric deposition (*e.g.* dust particles derived from soil, rocks and volcanic ash) or anthropogenic inputs (*e.g.* fertilizers, pesticides, wastewater, sewage sludge and biosolids) (ALLOWAY, 1995; ADRIANO, 2001).

In the context of this research, Table 2.1 presents the Cu and Zn concentration in soils, according to worldwide (ALLOWAY, 1990; USEPA, 1983), Brazilian (FADIGAS et al., 2006) and regional (Santa Catarina State; PELOZATO, 2008; HUGEN et al., 2013) surveys. Of note, the regional concentration ranges in Table 2.1 refer to soils from throughout the State of Santa Catarina, whereas the regional average concentrations were actually selected from samples representing the soil studied in this work, *i.e.* a Hapludox soil from basaltic origin. Copper and Zn concentrations in the latter are markedly higher than Brazilian average contents, due to its development on basalt parent material (HUGEN et al., 2013).

Table 2.1 – Cu and Zn concentrations worldwide and in Brazilian and Santa Catarina State soils

	Cu (mg kg^{-1})		Zn (mg kg^{-1})	
Source	Range	Average	Range	Average
	Worldwide			
Alloway (1990)	20–30	25	10–300	50
USEPA (1983)	2–100	30	10–300	50
	Brazil			
Fadigas et al. (2006)	–	16	–	24
	Santa Catarina State			
Pelozato (2008)	7–250	165	40–250	147
Hugen et al. (2013)	2–200	149	10–80	72

2.3 PIG SLURRY

Pork has been globally established as the most important source of animal protein since 1978 (EMBRAPA, 2010). In 2008, it represented some 40% of the worldwide meat consumption (USPCE, 2009). The world pig stock in 2013 was of nearly 1 billion pigs. In the same year, Brazil was the third larger producer, with a pig stock of 36.7 million, being surpassed only by the United States (64.8 million) and China (475.9 million) (FAO, 2013). As a result, pig manure is produced in massive quantities. In 2008, swine activity generated more than 930 million cubic metres of PS in the European Union alone. Spreading manure on agricultural lands as fertilizer is its most common destination (EC, 2014).

Pig manure contains all the 13 nutrients and micronutrients essential to plant development: N, P, K, Ca, Mg, S, Mn, Cl, B, Fe, Mo, Cu and Zn (CHASTAIN et al., 2003). Manure nutrient and solid content may widely vary depending on feed digestibility, animal age and the amounts of water used for removing and eventually treating the waste. Manures with humidity greater than 90% are considered liquid, and usually referred to as slurry. Most swine manure is handled as a liquid. They have the advantage of being easily pumped (SASKATCHEWAN, 2013).

Table 2.2 – Average nutrient composition of swine manure

Manure Type	Total N	Ammonium NH_4–N	Phosphorus P_2O_5	Potassium K_2O	Copper	Zinc
	g kg^{-1}					
Fresh	6	3.5	4.5	4.5	0.015	0.060
Scraped[1]	6.5	3.5	6	4.5	0.075	0.175
	g L^{-1}					
Liquid slurry (NC, USA)[2]	3.7	2.3	2.6	2.0	0.013	0.047
Liquid slurry (RS, SC, Brazil)	2.8	1.4	2.4	1.5	0.016	0.043
Anaerobic lagoon sludge	2.6	0.7	5.9	0.8	0.028	0.080
Anaerobic lagoon liquid	0.6	0.5	0.2	0.6	0.001	0.007

[1] Collected within 1 week.
[2] Six to 12 months accumulation of manure, urine, and excess water usage; does not include fresh water for flushing or lot runoff.
Source: Zublena et al. (2004), SBCS (2004).

Average nutrient values for different swine manure types (fresh, scraped, liquid slurry and anaerobic lagoon sludge and liquid) for the State of North Carolina, USA and for the States of Rio Grande do Sul and Santa Catarina, Brazil (liquid slurry only) are presented in Table 2.2. Ideally, manure application rates into soils might take into account the nutritional value of the manure, the nutrients available in the soil, and the nutritional assimilation expected by cultivars (CHASTAIN et al. 2003; SASKATCHEWAN, 2013).

2.4 HEALTH ASPECTS

Metals such as Na, K, Mg, Ca (macronutrients), Mn, Fe, Cu and Zn (micronutrients) are considered essential from the biological point of view. Others such as Ag, As, Cd and Pb are considered non-essential. However, even essential elements may, under specific conditions, cause negative impacts to terrestrial and aquatic ecosystems, when present in concentrations not consistent with natural levels (VAZ & LIMA, 2003).

The tendency of some HM to accumulate in the soil is one of the factors enhancing their potential toxicity. High HM levels may induce incorporation by cultivars, lowering yields and ultimately reaching animals and humans through the food chain. Moreover, HM leaching is of major concern regarding groundwater contamination (MORTVEDT, 1996).

Among the harmful human health effects arising from exposure to excessive levels of Cu are liver and kidneys damages, anemia, immunotoxicity, and congenital anomalies such as Wilson’s disease, Indian childhood cirrhosis, or idiopathic Cu toxicosis. The most common symptoms associated with Cu exposure are gastrointestinal discomfort, such as nausea, vomiting, diarrhea or abdominal pain, and green color of hair and teeth (ATSDR, 2004).

Exposure to high doses of Zn may cause anemia, pancreas damages, and lower the high-density lipoprotein (HDL, the so-called "good cholesterol”) levels in the body. The most common symptoms associated with Zn exposure are nausea, headaches, vomiting and abdominal pain (ATSDR, 2005; AZEVEDO & CHASIN, 2003).

Nevertheless, the elements Cu and Zn receive the “weight-of-evidence characterization D” in the carcinogenicity assessment for lifetime exposure of the Integrated Risk Information System (IRIS), by the United States Environment Protection Agency (USEPA, 2015). It means that they are not classifiable as to human carcinogenicity, although the report narrative express that data on the assessment of carcinogenic potential of Cu and Zn are to date either equivocal, inadequate or inconclusive.

2.5 LEGISLATION

Governments have been concerned in regulating HM concentration and biosolid application in soils. Limits of application usually refer to sewage sludge. Nevertheless, it may be extended to PS, due to analogous characteristics among them, *e.g.* the organic nature, fermentation and storage processes (GIROTTO, 2007). Two different approaches for limiting HM application in soils via biosolids have been traditionally used: the European (Directive 86/278/EEC) (CEC, 1986) and the North American, referred to as EPA 503 (USEPA Clean Water Act 503 Regulations) (USEPA, 1993).

The European directive is known for its "zero-impact" or "metal balance" approach. It is based on the concept that HM amounts added to the soil must not exceed the amounts removed by natural processes such as assimilation by cultivars, leaching and soil erosion (SAMPAIO, 2013).

The North American directive is based on risk assessment. Pre-established routes of exposure to HM after their application on agricultural soils are taken into account. It assumes that the toxicity of each element to cultivars is independent, *i.e.* there is no associated effect arising from a combination of contaminants. Moreover, phytotoxic response in plants is not regarded as linearly dependent on the element concentration within the soil or the plant tissue. It thus presumes that phytotoxicity arises fairly abruptly, at a certain plateau concentration, allowing for a HM storage limit within the soil (MCBRIDE, 2003).

In Brazil, the first nationwide regulation on the subject was issued in 2006. The CONAMA Resolution No. 375/2006 defines criteria and procedures for the agricultural

use of sewage sludge generated by sewage treatment and its derived products (CONAMA, 2006). The existing regulations by then were limited to technical rules from the Sao Paulo Environmental Sanitation Company – CETESB (P4.230 Aug/99) (CETESB, 1999) and the Parana Environmental Institute – IAP (CEP/DTA No. 001/2002) (SEMA/IAP, 2002). More recently, guiding values for soil quality and preservation regarding HM concentrations were issued for the state of Sao Paulo (DD No. 045/2014/E/C/I) (CETESB, 2014) and at the national level by the CONAMA Resolution No. 420/2009 (CONAMA, 2009).

Table 2.3 presents a summary of legislation focused on Cu and Zn concentration within soils and biosolids, as well as application rates and loads. Clearly, parameters adopted by Sao Paulo's CETESB concerning the maximum annual application rate and accumulated load of HM in the same area are based on the North American approach. Conversely, the national CONAMA resolution is inspired by the European approach. It places the Brazilian legislation on the subject among the strictest in the world.

Table 2.3 – Cu and Zn limits for agricultural use of biosolids.

Criteria	Max concentration within soil (mg kg^{-1})		Max concentration within biosolid (mg kg^{-1})		Max annual application rate (kg ha^{-1} $year^{-1}$)		Max accumulated load in the same area (kg ha^{-1})	
Agency	Cu	Zn	Cu	Zn	Cu	Zn	Cu	Zn
USEPA[1]	-	-	1500	2800	75	140	1500	2800
CETESB[2,3]	60	86	4300	7500	75	140	1500	2800
CEC[4]	50–140	150–300	1000–1750	2500–4000	12	30	120	300
CONAMA[5,6]	60	300	1500	2800	N/pH	N/pH	137	445
IAP[7]	-	-	1000	2500	5	12.5	50	125

[1] Clean Water Act 503 Regulations (USEPA, 1993);
[2] P4.230 (CETESB, 1999); [3] DD No. 045/2014/E/C/I (CETESB, 2014);
[4] Directive 86/278/EEC (CEC, 1986);
[5] Resolution No. 375/2006 (CONAMA, 2006); [6] Resolution No. 420/2009 (CONAMA, 2009);
[7] CEP/DTA No. 001/2002 (SEMA/IAP, 2002).

Regardless the approach, adopting a regulation at the national level is a remarkable advance, as establishing concrete basis for discussion and further improvements on the subject. It is also worth noting that legislation only refer to total

HM contents, although the nature of soils and potential contaminants – and therefore the interaction between them – largely influence HM mobility through the soil profile and availability to crops.

2.6 HEAVY METAL FATE IN SOILS

The complexity of soils and HM characteristics results in a broad variety of interactions between them. Understanding such interactions is thus essential to describe and predict how they interfere in the natural and exogenous HM fate (DUBE et al., 2001; RIEUWERTS et al., 2006). The biogeochemical cycle of contaminants in soils, as controlled by the soil solution, may occur by the different processes illustrated in Figure 2.2.

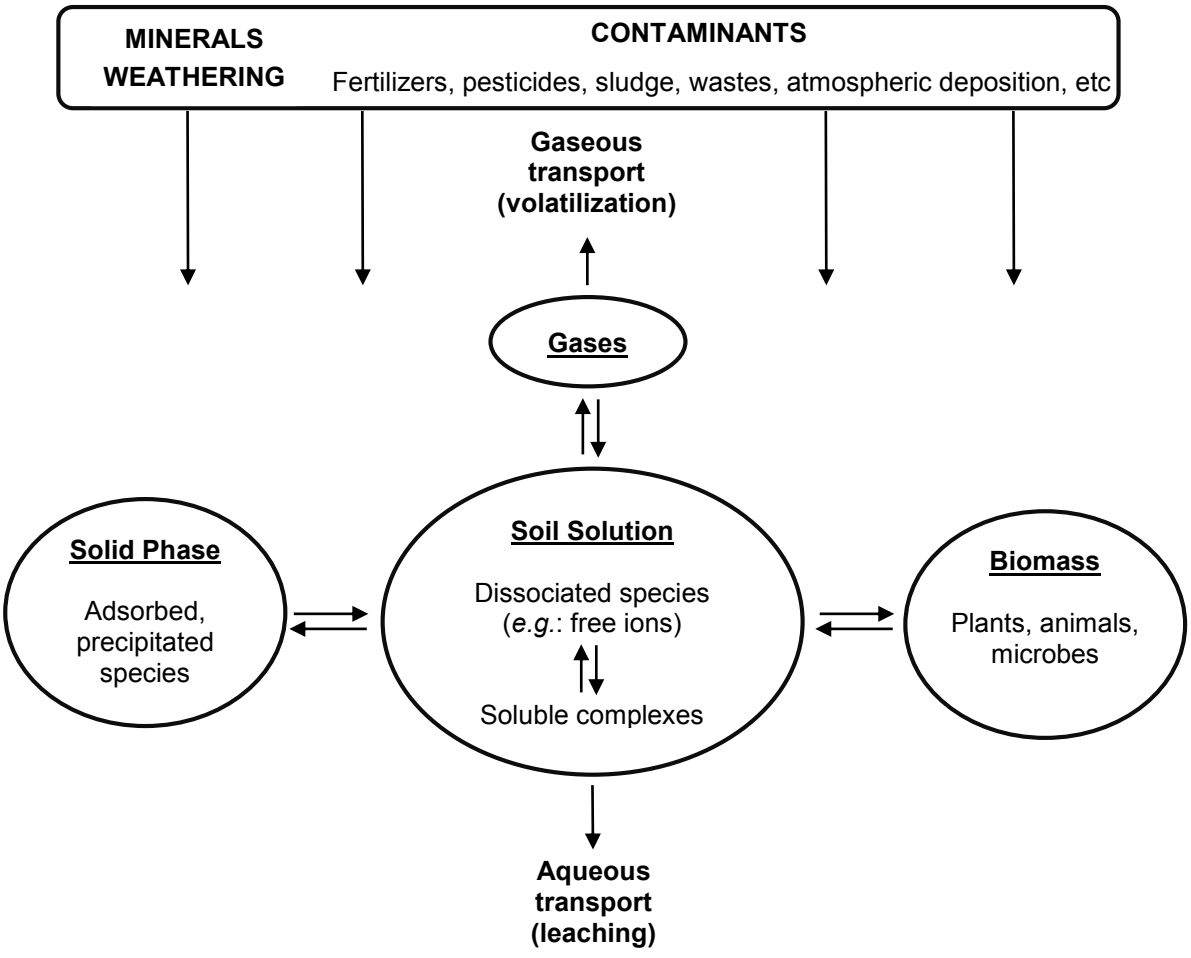

Figure 2.2 – Biogeochemical cycling of soil contaminants, as controlled by the soil solution (adapted from HESTERBERG, 1998 and ALLOWAY, 1995).

The main physical mechanisms involved in the contaminant transport are advection and dispersion. The former is controlled by the percolation of the soil solution. The latter arises from the contribution of mechanical dispersion – *i.e.* local variations in velocity around the mean velocity of flow – and diffusion – *i.e.* the movement of a substance due to a concentration gradient (DEMUELENAERE, 2004). Physical transport mechanisms acts only in the contaminant dissolved or dispersed fraction, which is usually low in the case of HM within soils.

Biological mechanisms comprises plant uptake and microbial degradation. Plant uptake has been demonstrated to be virtually negligible in the overall HM balance within soils (DEL CASTILHO et al., 1993; LEGROS et al., 2013), although small concentrations may affect crops development. Microbial degradation may be important for persistent organic pollutants, such as pesticides, but not for HM.

Chemical mechanisms, on the other hand, play a major role on the HM behavior within soils. Reactions such as acid/base, redox and complexation take place in the soil solution. They are highly dependent on the pH and redox potential. Moreover, the soil solution close linkage with the soil matrix gives rise to interactions such as ionic exchange, adsorption/desorption and precipitation/dissolution (HESTERBERG, 1998; ESSINGTON, 2004). Phenomena occurring in the solid–liquid interface are the most important chemical phenomena regulating HM behavior and availability in soils (ALLOWAY, 1990).

The likely best available summary of chemical processes affecting contaminant mobility in soils is given by the US Environmental Protection Agency (USEPA, 1999). Details related to HM were compiled and transcribed below. Of note, colloid-mediated transport is usually not addressed in classical description, due to its difficult delineation. Moreover, HM occluded in Fe and Al oxides, or incorporated into the crystal structure of silicate minerals – generally related to the parent material – may constitute a highly stable HM pool, not subject to mobilization.

> Aqueous Complexation
> Reaction where an aqueous molecular unit (ion) acts as a central group to attract and form a close association with other atoms or molecules. May enhance attenuation or mobility, depending on contaminant and geochemical conditions.
> (a) Function of pH and redox; (b) may lower the potential for adsorption and/or increase solubility, both of which can enhance potential for mobility; (c) complexes may more readily bond to soils and thus retard migration; (d) organic ligands from humic materials can be present in significant concentrations and dominate contaminant complexation in some systems.

> Adsorption and Ion Exchange
> Special case of a complexation reaction where there is a net accumulation of a contaminant at the interface between a solid phase and an aqueous-solution phase. Does not include the development of a 3-dimensional molecular structure. Enhances attenuation.
> (a) Occurs primarily in response to electrostatic attraction; (b) very dependent on pH and mineralogy; (c) cation adsorption is greatest at high pH and decreases with deceasing pH; (d) Totally-to-partially reversible; (e) Likely key process controlling contaminant mobility in areas where chemical equilibrium exists.
>
> Precipitation
> Special case of a complexation reaction in which the complex formed by 2 or more aqueous species is a solid with 3-dimensional molecular structure. Enhances attenuation.
> (a) Dependent on pH and redox; (b) totally-to-partially reversible; (c) likely key process where chemical nonequilibium exists, areas where high contaminant concentrations exist, or where steep pH and/or redox gradients exist.
>
> Subsurface Colloids
> Contaminants associated with suspended fine-grained material (smaller than clay size) that may be transported with flowing groundwater. Enhances mobility.
> (a) Little information on occurrence, mineralogical and physicochemical properties, or conditions conducive to the generation of mobile colloids; (b) may originate from the dispersion of soils, decementation of secondary mineral phases, and/or precipitation of groundwater constituents; (c) difficult to collect colloids from subsurface in a manner that minimizes or eliminates sampling artifacts; (d) difficult to unambiguously delineate between the contaminants in the mobile aqueous and mobile-solid phases. (USEPA, 1999).

However, distinguishing specific mechanisms acting in the HM mobility in real soil systems – and therefore their contribution to the overall process – is not straightforward. A classical simplified approach is to describe the interactions by means of the proportion between the amounts of HM bound at the surface as a function of the same HM in the equilibrium solution. This proportion is known as the distribution coefficient K_d (ZHENG & BENNETT, 2002; USEPA, 1999). However, isotherms fail to reflect dynamic process, as they are obtained under controlled conditions. Moreover, their timescale coverage is usually from minutes to days; small when compared to field situations, where changes in contaminant speciation may take longer to be completely processed, as indicated in Figure 2.3 (MCBRIDE, 1994).

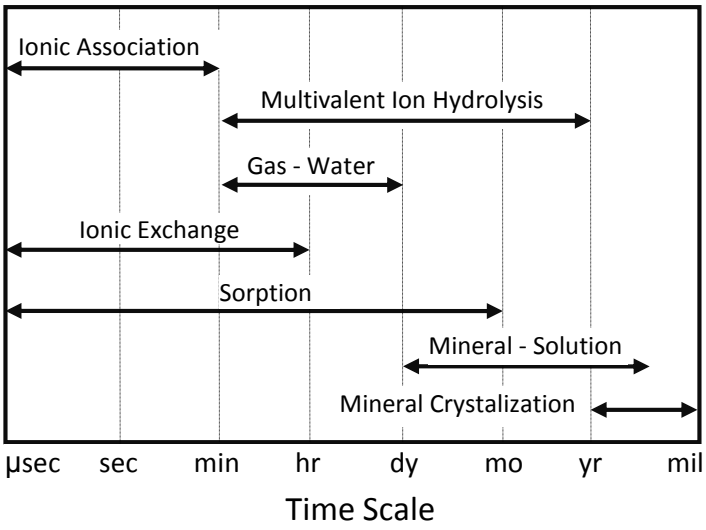

Figure 2.3 – Time ranges required to attain equilibrium by different types of reaction in soil environments (SELIM & AMACHER, 1996)

2.7 STATE OF THE ART

Assessing the HM total concentration within the soil and adjacent compartments may be the most obvious approach to evaluate the associated hazard. Guidelines based on that are currently in use in many countries, as presented in Section 2.5. This approach reflects the contribution of both the pedogeochemical background and eventual anthropogenic inputs into the soil (RAO et al., 2008).

Legros et al. (2013) investigated the Cu and Zn fate in the water–soil–plant system after five PS applications into a Cambisol over a 3-year period. Total HM concentrations were measured within the soil 0–20, 20–40 and 40–60 cm layers, in the soil solution at 60 cm depth, and in the stems and leaves of *S. dimidiatum* grass. Moreover, a HM mass balance considering the HM inputs and its detected concentration in each system was carried out. The overall exogenous Cu was stored in the 0–20 cm soil layer, as confirmed by the absence of either plant uptake or leaching at 60 cm depth. Authors suggested that the Cu speciation in the PS (Cu sulfide) was imperative for the observed behavior. All of the Zn, however, accumulated within the 20–60 cm soil layer. Authors suggested that reversible sorption phenomena took place in the tropical soil analyzed, as contrasted to the common findings of Zn in upper layers, especially in temperate soils. In this case, Zn could leach in the long term.

Leaching was observed by Novak et al. (2004), who found a significant increase in total Cu and Zn concentrations until the 90 cm soil horizon after 4 years of PS application. A loamy sand soil (89% sand, 8% silt, and 3% clay) was object of study, under a very high PS application rate: 4330 m^3 ha^{-1} $year^{-1}$. The dominant sandy texture of the soil and the unusually high PS dose could possibly explain the observed HM leaching.

Negligible Cu and Zn plant uptake observed by Legros et al. (2013) was also confirmed in other studies. Del Castilho et al. (1993) determined the assimilation of potentially bioavailable Cu in a sandy loam soil by wheat cultivars at approximately 0.3%. Mallmann et al. (2012) calculated 0.05–0.12% and 0.33–1.13% removal of the total Cu and Zn mass, respectively, in the 0–60-cm soil layer after an 8-year harvesting period in a PS-amended Alfisol.

The detection of a quantifiable concentration of an element in a given system, above its natural level, may indicate contamination. However, total HM content is a poor indicator of potential mobility or bioavailability. Further investigation should be considered in order to assess and predict HM fate. A useful concept when dealing with contaminant behavior in the environment is speciation. It refers to aspects of the chemical and physical forms of an element such as element identity, isotopic composition, oxidation or electronic state, stoichiometry, physical state, coordination, association with other phases and molecular structure (REEDER et al., 2006).

The ability to identify and distinguish species in practical problems depends on the applied technique (SCHEINOST et al., 2002). Investigation thus presuppose a balance between the information provided and the associated limitations. It is not surprising in this context that a detailed description on the mode of occurrence, availability, mobilization and transport of HM within soils may require strategies combining analytical approaches more sophisticated than the determination of total HM concentration (FERNÁNDEZ-CALIANI et al., 2013; LEGROS et al., 2010a; DOELSCH et al., 2006). Three of these approaches are presented hereafter, along with a review on published works that used them in the context of HM fate investigation within organically amended soils.

2.7.1 Chemical sequential extractions

Sequential extraction procedures have been extensively used to generate information on HM chemical fractionation within soils and other matrices, therefore highlighting their potential impacts due to release into neighboring environmental compartments (BACON & DAVIDSON, 2008). Reagents of different chemical strengths are used, thus leaching the elements according to extractant and target phase properties (ABOLLINO et al., 2011).

The five-step Tessier protocol (TESSIER et al., 1979), the three-stage BCR protocol (URE et al., 1993) and its subsequent four-stage modification (URE & DAVIDSON, 2002) are the most extensively applied sequential extraction schemes. Common fractions denominations and the respective target features include “exchangeable”, which corresponds to HM readily available for plant uptake or mobilization by merely changing the ionic strength of the medium; “bound to carbonates”, which might be sensitive to pH changes; “bound to Fe–Mn oxides” and “organic matter”, which exhibit a stronger interaction with their target phase, but can be mobilized with increasing reducing or oxidizing conditions; and “residual”, which can only be mobilized as a result of weathering (FILGUEIRAS et al., 2002).

Sequential extraction, however, fractionates HM into portions soluble in particular reagents under particular conditions. Although reagents are selected aiming to target defined phases, specificity is not guaranteed. Moreover, phenomena such as HM re-adsorption and redistribution among phases during the extraction may occur. Interpretation of sequential extraction results in terms of binding of trace metals to specific minerals is thus unjustifiable (BACON & DAVIDSON, 2008; ALBORÉS et al., 2000). Therefore, sequential extraction protocols might not be universally applied to all varieties of contaminants and soils, *i.e.* site-by-site based assessments are required. Furthermore, comparing results from different sequential extraction protocols is troublesome (LA FORCE & FENDORF, 2000; ZIMMERMAN & WEINDORF, 2010; HLAVAY et al., 2004).

For instance, the vast majority of studies focusing on trace element contamination in soils were conducted in temperate soil–climate conditions (LEGROS et al., 2013). It was found that the Tessier protocol and the modified BCR procedure underestimated the proportion of HM bound to Fe and Mn oxyhydroxides fractions in

tropical soils (DOELSCH et al., 2008; SILVEIRA et al., 2006). The modified GSC procedure, first proposed by the Geological Survey of Canada (HALL et al., 1996) and later modified (BENITEZ & DUBOIS, 1999; DOELSCH et al., 2006), seemed more suitable for analyzing soils which typically contain high levels of Fe and Mn oxyhydroxides (DOELSCH et al., 2008).

Comprehensive reviews on the available sequential extraction schemes can be found elsewhere. Filgueiras et al. (2002) discussed reagent selectivity and extraction ability amongst protocols. Validation, harmonization and comparison between different schemes were also addressed. Bacon & Davidson (2008) focused on nomenclatures, data presentation and interpretation, and discussed the sequential extractions typical applications. Abollino et al. (2011) and Giacomino et al. (2011) presented and discussed the application of chemometrics in studies involving single and sequential extractions. Of note, investigation of Cu and Zn behavior in soils following organic amendments represent to date a minor contribution for the overall context of sequential extractions usage. Moreover, studies covering long-term field-scale experiment designs are even fewer.

Examples of Cu and Zn chemical fractionation assessment within soils following organic inputs under controlled bench scale and short-term conditions can be found in Guan et al. (2011), Plekhanova (2012), Qiao et al. (2003) and Hseu (2006). Although slightly different approaches were used, results converge to show that OM (or oxidizable fractions) represented a major Cu pool, whereas Zn tended to adsorb into or bound to Fe–Mn oxyhydroxides (or reducible fractions). Controlled conditions are useful for highlighting the effect of single, specific characteristics influencing HM behavior. Nevertheless, the lack of long-term, field-variable environment and soil profile-based sampling pose limitations on predicting HM trends, thus restricting its reliability for practical scenarios.

Guan et al. (2011) examined the Cu availability and uptake by wheat in a Mollisol amended with Cu-enriched livestock manure, by means of pot experiments. Livestock manure was spiked with a series of Cu^{2+} concentrations to simulate soil Cu contamination. Moreover, two levels of manure application were considered: 1% and 3% to bulk soil by weight. Sequential extractions indicated that Cu was predominately distributed in the fraction bound to OM, while the most rapidly concentration increase was found in the reducible fraction, according to the Cu dose. Nevertheless, the acid-extractable fraction was determinant for controlling the potential mobility and

bioavailability of Cu. The application of livestock manure at 1% level reduced the mobility of Cu, whereas that at 3% level exhibited the opposite effect. Authors suggest that the latter was due to more competitive Cu complexation than adsorption. The amount of Cu uptake by wheat was very low.

Plekhanova (2012) studied a loamy sandy agrosoddy-podzolic soil contaminated with sewage sludge, previously applied as an organic fertilizer for 5–10 years. The sampled soil was incubated under two wetting levels – 60 and 100% of the total moisture capacity – and HM were sequentially extracted. Copper behavior depended on the soil wetting and redox conditions and was closely bound to OM and Fe and Mn compounds. Zinc little depended on the soil wetting and redox conditions and was characterized by a low affinity for either organic or Fe and Mn compounds.

Qiao et al. (2003) conducted an incubation experiment to evaluate the chemical speciation and extractability of HM in a clayey paddy soil and a clayey red soil incubated with biosolids. The oxidisable fraction was the major fraction for Cu in both biosolid-amended soils and the acetic acid–soluble and reducible fractions accounted for most of the Zn.

Hseu (2006) evaluated the changes in chemical fractionation of Zn in three biosolid-amended tropical soils of Taiwan. Sequential extraction was applied after a one-year incubation period. Following the incubation, large amounts of Zn within the soils were identified as soluble and were adsorbed by Fe–Mn oxides. According to the author, this is an important way of fixation of Zn when it is released from biosolids. The organically bound Zn was detected in limited amounts within the studied soils.

Other works, however, report results from long-term field experiments (L'HERROUX et al., 1997; ASADA et al., 2012; GIROTTO et al., 2010). Under such experimental conditions, soil-climate characteristics are commonly the main measurable factors influencing HM long-term trends. Moreover, soil sampling in defined layers may improve the interpretation on HM mobility, although the commonly used 20 cm layer resolution may not be sufficiently narrow, because of the usual slow HM migration. Due to the wide range of soils and climates occurring worldwide, there is a common acknowledgment on the lack of surveys covering such variety.

L'Herroux et al. (1997) performed numerous PS applications, over 5 years, on an experimental hydrologically-isolated field equipped to recover all the leachate. The applications corresponded to the amount which might have been spread over one century. The soil was a brown silt loam with 14% of clay, 23% of sand and 63% of silt.

Copper and Zn mainly accumulated in the surface layer: 0–20 cm. Eighty percent of Cu was initially in the residual fraction. After 5 years, an enrichment of the Cu fraction bound to OM was observed, followed by a minor enrichment of the Cu fraction bound to Fe-Mn oxides. Soil natural Zn was also mainly found in the residual fraction. After the PS amendments, the most important variation was noticed in the Zn fraction bound to Fe-Mn oxides: from 25% to 40% in the 0–20 cm layer. A 15% increase was also observed in the Zn fraction bound to carbonates.

Asada et al. (2012) evaluated HM mobility after 13 years of swine manure application into a sandy loam soil (21% clay, 29% silt, and 50% sand), in a field-scale experiment. A standard and a high application rate were tested. Disturbed soil samples were taken at 10 cm intervals from 0 to 30 cm depth. The exchangeable fraction of Zn and the HM–organic complex fractions of Cu and Zn increased their concentration as a result of greater manure application rates. The Cu and Zn fractions bound to OM in the heavily manured plot were likely affected by the soil redox conditions and released into higher-mobility fractions.

Girotto et al. (2010) evaluated the Cu and Zn accumulation and speciation in a sandy loam soil (17% clay, 30% silt, and 53% sand) after 17 PS applications over a 6-years period. The Cu and Zn pseudo-total contents accumulated within surface layers, with migration observed until 12 cm and 10 cm depths, respectively. The Cu accumulated in the soil was preferentially associated with the OM fraction, while Zn was mainly associated with the mineral fraction.

Despite the useful information that sequential extractions may provide, important limitations were previously presented. Inherent features such as lack of specificity and the resulting operationally defined nature, or the absence of a standard and universally suitable protocol should be considered. Sequential extractions provide ultimately macroscopic observation. It may thus mask or underevaluate the actual binding mechanism of HM to soil species (MANCEAU & MATYNIA, 2010). In these sense, microscale analysis may provide further information on HM–soil interactions and therefore improve the understanding of previously assessed macroscopic HM behavior.

2.7.2 Density fractionation

Density fractionation is a physical separation technique used to reduce the bulk matrix heterogeneity and complexity. It thus provide a direct approach for soil-phase separation, which may be convenient for its spectroscopic identification. Consequently, assessment of HM linkage among fractionated phases is possible (EL-MUFLEH et al., 2014; DOELSCH et al., 2006). This fractionation approach has been used to study organic–mineral interactions in marine sediments (ARNARSON & KEIL, 2001) and soils (WAGAI et al., 2015), the distribution and speciation of Cu and Zn in biosolids (DONNER et al., 2012), the distribution of Cu within contaminated lake surface sediment (ZOU et al., 2006), and the distribution of polycyclic aromatic hydrocarbons and trace metals in urban stormwater sediments (EL-MUFLEH et al., 2014).

Few studies, however, deal with contaminant distribution in soils, notably HM and persistent organic pollutants. Krauss & Wilcke (2005) determined the concentration and water partition coefficients of 20 polycyclic aromatic hydrocarbons and 12 polychlorinated biphenyls in bulk samples and three density fractions of 11 urban topsoils in Germany. The concentrations of all pollutants decreased in the order light > medium > heavy fraction. However, the studied failed to identify relationships between sorption strength and distribution among density fractions. According to the authors, it indicated that density fractionation is not a suitable tool to distinguish among differently persistent organic pollutants pools in soils.

Doelsch et al. (2006) studied the natural Cr speciation within an Andosol from the volcanic island of Réunion. Authors fractionated the 40–50 cm soil layer into five density fractions as a previous step to X-ray absorption spectroscopy (XAS) analysis. It was found that most of the Cr was within chromite-type primary minerals. Lesser amounts of Cr were found either coprecipitated as mixed Fe–Cr oxyhydroxides or precipitated as Cr oxyhydroxides. Moreover, 13% of the Cr was bound to organic matter, which was complexed with mineral phases to form organomineral complexes with densities ranging from 1.9 to 2.6 g cm^{-3}. According to authors, the density fractionation-based sample preparation allowed identification of the role of organic matter in Cr speciation and overcoming the difficulties of XAS to detect light elements (carbon) in the vicinity of heavy elements. They recommended that this sample

preparation procedure could be applied to other complex matrices for HM speciation analyses.

However, any study has been reported to date assessing the associations of Cu and Zn with the soil organic/mineral phases by means of soil density fractionation. More broadly, the feasibility of this soil-phase separation approach has not been tested for investigating the fate of HM from an exogenous source (*e.g.* PS) after spreading it into the soil, as compared to the natural HM occurrence.

2.7.3 X-ray absorption spectroscopy

Extended X-ray absorption fine structure (EXAFS) corresponds to a region in the X-ray absorption spectroscopy (XAS) spectrum of a given element. It is one of the most applied tools on the investigation of local structure within amorphous and crystalline materials. At a given energy, an X-ray is absorbed by an atomic core-level with binding energy, and a photo-electron is created and propagates away from the atom, resulting in an abrupt increase in the absorption coefficient. At energies higher than the sharp absorption edge, the X-ray absorption coefficient varies according to the interactions between the ejected photo-electron and neighboring atoms, as the former returns to the absorbing atom (NEWVILLE, 2004).

Because the absorption coefficient strongly depends on the atomic number and the X-ray energy, a good contrast between different materials can be achieved. It renders EXAFS a very selective tool to assess the local environment of essentially every element on the periodic table, even within complex matrices. It provides information on interatomic distances between the central atom and its neighbors, as well and their number and nature. Other materials or impurities in the sample, which either do not contain the absorber or are far from the absorber, do not interfere (TAVARES, 2002; TEO, 1981).

One possible inconvenience associated with this technique is the need of an intense polychromatic X-ray source, available only at expensive and not easily available synchrotron facilities. Moreover, the use of simulation and best-fit procedures to obtain structural parameters may lead to ambiguous or unreliable results, therefore data interpretation should be done critically (VLAIC & OLIVI, 2004).

Nevertheless, XAS has been successfully applied for structural analyses of chemical or biological systems where conventional diffraction methods are not applicable. Study fields include physics, materials science, chemistry (catalysis and coordination chemistry), biology, geochemistry and environmental science (LEBEDEV, 1999). In the environmental sciences, EXAFS has been used to identify chemical species *in situ* with minor or no pretreatment. Local structural information extracted by multishell fitting is typically used to determine the atom coordination in complex structures. Other common approach, more suitable for low concentrated elements in natural samples, is based on fitting linear combinations (LCF) of reference spectra to an unknown sample spectrum, allowing the identification of the main species present in the sample. Principal component analysis (PCA) may be used in combination with LCF in order to avoid doubts concerning whether all fitted species have actually been found in the sample and whether the fit gives a unique solution (SCHEINOST et al., 2002).

Manceau et al. (2005), combining X-ray diffraction and powder and polarized EXAFS spectroscopy, found a predominance of natural Zn bound to hydroxy-Al interlayers sandwiched between 2:1 vermiculite layers in the argillic horizon of an Ultisol with no exogenous Zn contamination (pH = 5.6, total Zn = 42 mg kg^{-1}). According to authors, “this binding environment for zinc is probably the main mechanism by which zinc is sequestered in acidic to near-neutral aluminum-rich clayey soils”, as also suggested by other studies (PANFILI et al., 2005; MANCEAU et al., 2004; MANCEAU et al., 2003). More recently, it was proposed that Zn in naturally metal-enriched soils was preferentially residing in the crystal structure – *i.e.* the octahedral positions – of vermiculite, rather than in the interlayer exchange sites. This would further reduce its mobility in soils under ambient conditions (FERNÁNDEZ-CALIANI et al., 2013).

Scheinost et al. (2002) recorded the Zn EXAFS spectra of samples after each of 6 chemical sequential extraction steps, and then analyzed them by multishell fitting, PCA and LCF, in order to determine the Zn speciation in a heavily smelter-contaminated, strongly acidic soil. Authors found that Zn was predominately associated with the smelter-emitted minerals franklinite and sphalerite in the topsoil, and lesser amounts as aqueous or outer-sphere Zn^{2+}. In the subsoil, aqueous or outer-sphere Zn^{2+} prevailed, but a substantial amount of Zn was incorporated by hydroxy-Al interlayers of phyllosilicates. Although formation of Zn-containing phyllosilicates had been previously observed in slightly acidic to neutral soils, authors reported for the first

time such association in an acidic soil, suggesting an important mechanism for reducing Zn mobility within contaminated soils.

Indeed, Jacquat et al. (2009), determining the speciation of Zn in field soils that had been contaminated since several decades by inputs of aqueous Zn with runoff-water from galvanized power line towers, observed Zn in hydroxy-interlayered minerals (Zn-HIM) in acidic soils. Furthermore, Zn-HIM was only observed in soils containing less than 2000 mg kg^{-1} of Zn, reflecting the high affinity but limited sorption capacity.

As well as the studies of Scheinost et al. (2002) and Jacquat et al. (2009), the majority of other EXAFS studies on the subject focused in soils receiving smelter contamination, *i.e.* containing Zn concentrations far above natural levels. Juillot et al. (2003) found Zn bound to organic matter or goethite, Zn-phyllosilicates and Zn-layered double hydroxides (LDH) in a smelter-contaminated tilled Luvisol (pH = 7.5; total Zn = 571 mg kg^{-1}). Sarret et al. (2004) found Zn bound to organic matter, aqueous Zn, franklinite, Zn sorbed apatite/Zn-phytate and Zn sorbed ferrihydrite in a smelter-contaminated organic soil (pH = 6.2; total Zn = 21,078 mg kg^{-1}). Nachtegaal et al. (2005) found Zn-LDH, hemimorphite and gahnite in a non-remediated, smelter-contaminated sandy soil (pH = 6.4; total Zn = 20,476 mg kg^{-1}). Within the same soil, after remediation (pH = 6.7; total Zn = 13,144 mg kg^{-1}), authors found Zn-kerolite, hemimorphite and Zn-reacted kaolinite.

Kirpichtchikova et al. (2006) investigated the Zn speciation in an agricultural sandy loam soil (pH = 6.5–7.0; total Zn = 1,103 mg kg^{-1}) that had received untreated sewage water irrigation for one hundred years. Zinc was mainly found as Zn sorbed ferrihydrite, Zn phosphate dehydrate, $Zn_{0.45}Mg_{0.55}$-kerolite and willemite.

It should be highlighted that EXAFS studies assessing the speciation of Zn within soils following PS applications are lacking. This might be attributed to either the scarcity of long-term field experiments or the low HM concentration increase within the soil (when compared to more concentrated Zn sources as smelter runoff), which makes the approach more complex. Nevertheless, Zn speciation in PS was assessed by Legros et al. (2010a). Authors found in such matrix a combination of 49% Zn bound to organic matter, 37% amorphous Zn hydroxides [$Zn(OH)_2$], and 14% sphalerite.

Concerning Cu, it has been demonstrated that natural OM has high sorption capacity and selectivity for Cu(II) relative to other divalent cations, over a large concentration range (GAO et al., 1997; COVELO et al., 2004). Hence, the biogeochemistry of Cu is considered largely controlled by its interactions with natural

OM (MANCEAU & MATYNIA, 2010). Nevertheless, investigation on Cu interactions with minerals has also been pursued. Several works used EXAFS to understand the Cu reactivity in natural environments by means of sorption experiments in single minerals (STRAWN et al., 2004; MORTON et al., 2001) or multicomponent systems (LEE et al., 2005; HEIDMANN et al., 2005).

Flogeac et al. (2004) used electron paramagnetic resonance (EPR) and EXAFS to investigate Cu sorption on calcareous soils spiked with Cu in the laboratory. Samples were pre-treated in order to obtain a quasi-insoluble solid adsorbent. It contained silica, illite and smectite, kaolinite, goethite and rutile for the mineral phase. The organic fraction represented 5% of the composition of the soil particles. Authors concluded that the Cu was bonded to OM coated onto the mineral fraction of soil particles, as held in inner-sphere surface complexes in an octahedral coordination.

Liu & Wang (2004) used XAS to analyze a Cu-contaminated soil collected near recycling plants of printed circuit board waste recycling plants. The main minerals in the soil were kaolinite and mica. Authors proposed that the Cu in the soil existed predominantly as Cu-humic substances, with lesser amounts of $CuCO_3$, Cu_2O, and CuO.

Strawn & Baker (2008) used bulk and microscopically focused X-ray absorption near edge structure (XANES) and EXAFS to investigate Cu speciation in a calcareous soil (pH = 7.1; OM = 6.75%; Cu = 4,167 mg kg^{-1}) containing calcite, dolomite, quartz, feldspar (albite), chlorite, jacobsite, and illite. The soil received long-term contamination presumably from $CuSO_4$, which was used as a fungicide in the first half of the 20^{th} century. Results indicated that the Cu was predominantly adsorbed on soil OM, as complexed via bidentate inner-sphere coordination with carboxyl or amine ligands.

Studies investigating the Cu fate and local structure within soils following PS applications by applying X-ray absorption spectroscopy, as previously underlined for Zn, are also lacking.

2.7.4 Remarks

The literature review pointed out that different types of information may be acquired depending on the investigation approach used. Methods have advantages and disadvantages, and a critical evaluation on their capabilities and limitations is imperative.

Sequential extractions have been extensively applied and are well consolidated as a mean of assessing the linkage strength between HM and the associated matrix. Their experimental functioning allows comparing soil samples collected at different depths or under distinct regimes, making it useful to assess HM mobility or bioavailability, *i.e.* the macroscopic behavior. Since sequential extractions lack specificity, results should be interpreted in the sense of extractability, as opposed to a straight association with a given mineral or organic species.

Soil density fractionation reduces the bulk matrix heterogeneity, allowing the identification of discrete soil phases and, as a result, their associations with HM of interest. Nevertheless, its use is still very restricted in the literature and it has never been used in the context of HM investigation within soils following organic amendments.

Synchrotron-based X-ray absorption spectroscopy, on the other hand, provides a direct approach for the analysis of the HM local environment, *i.e.* the structural composition of minerals and organics binding the element of interest. However, high-energy X-ray sources are available only at synchrotron facilities and their somewhat restrict availability may limit the number of samples or scenarios to be evaluated.

In the present study, the capabilities of sequential extractions, density fractionation and X-ray absorption were thought as complementary among each other. Therefore, an analytical approach designed to assess the HM behavior within the soil from the macroscopic towards the molecular scale was pursued.

Moreover, the results reported to date on the HM fate in soils following PS applications are incomplete or inconclusive. Particularly, it was noticed a lack of long-term studies under field conditions. Hence, the proposed macroscopic, microscopic and molecular scale investigation was applied to an experimental field that had received 22 PS applications, at different doses, over 11 years.

3 MATERIALS AND METHODS

"An experiment is a question which science poses to Nature, and a measurement is the recording of Nature's answer."

(Max Planck)

A graphical synthesis of materials and methods used in this study is presented in the diagram of Figure 3.1.

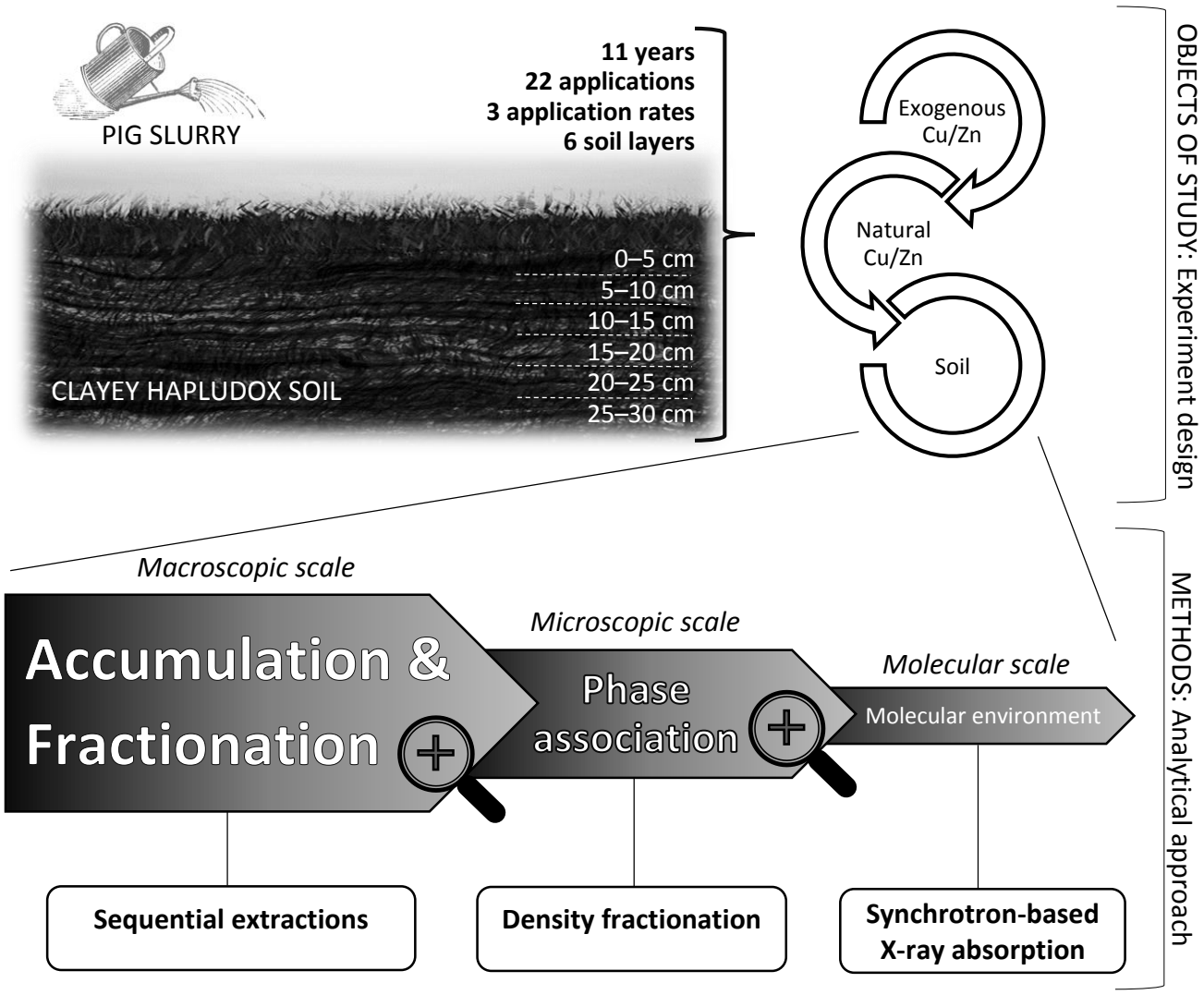

Figure 3.1 – Materials and methods diagram.

Briefly, the soil object of this study consisted of 12 field plots, sampled in six layers, that had received three different PS application rates over 11 years (SECTION 3.1). Chemical sequential extractions were used to assess Cu and Zn accumulation, fractionation and profile distribution (SECTION 3.2). Soil density fractionation was applied to identify possible HM phase associations (SECTION 3.3). Synchrotron-based X-ray absorption was used to analyze the Cu and Zn molecular environment (SECTION 3.4). The detailed description of the objects of study and analytical methods is given hereafter.

3.1 OBJECTS OF STUDY

3.1.1 Experiment location and design

The experimental site was located in Campos Novos, Santa Catarina State, southern Brazil (FIGURE 3.2). The experiment was conducted at the experimental field of the *Cooperativa Regional Agropecuária de Campos Novos* (Copercampos), at 27°22'59" S and 51°15'33" W and 896 m elevation. The area has a humid mesothermal climate, with mild summers, classified as a Cfb type according to the Köppen classification. The annual precipitation ranges from 1460 to 1820 mm, whereas annual average temperature ranges from 15.8 to 17.9 °C (PANDOLFO et al., 2002).

The study area had been continuously fertilized with PS since the year 2000. It consisted of a total of twelve 6 m by 5 m plots, arranged sequentially in three replicated blocks, from lowest to highest PS application rate: control (no PS application), 50, 100 and 200 m^3 ha^{-1} $year^{-1}$ of PS (denoted CT, PS50, PS100 and PS200 treatments, respectively). The PS rates of 50 and 100 m^3 ha^{-1} $year^{-1}$ are in the range commonly applied by local farmers (PINTO et al., 2014) and recommended by the Brazilian Society of Soil Science (SBCS, 2004). The PS rate of 200 m^3 ha^{-1} $year^{-1}$ represented thus an extrapolation of the rates usually applied. In the CT plot, the amounts of P and K exported through harvests were replaced using triple superphosphate (42% P_2O_5) and potassium chloride (60% K_2O), respectively. The first half of the PS dose (or P and K fertilizer) was manually applied before the winter crops

were sown, and the other half before the summer crops were sown. Seeding was performed by direct drilling and followed a 3 year crop rotation scheme: black oat (*Avena strigosa* Schreb.) + common vetch (*Vicia sativa* L.)/corn (*Zea mays* L.) during the first year; black oat/soybean (*Glycine max* L. Merr.) during the second year; and black oat/common bean (*Phaseolus vulgaris* L.) during the third year. The scheme was repeated in the fourth, seventh and tenth years.

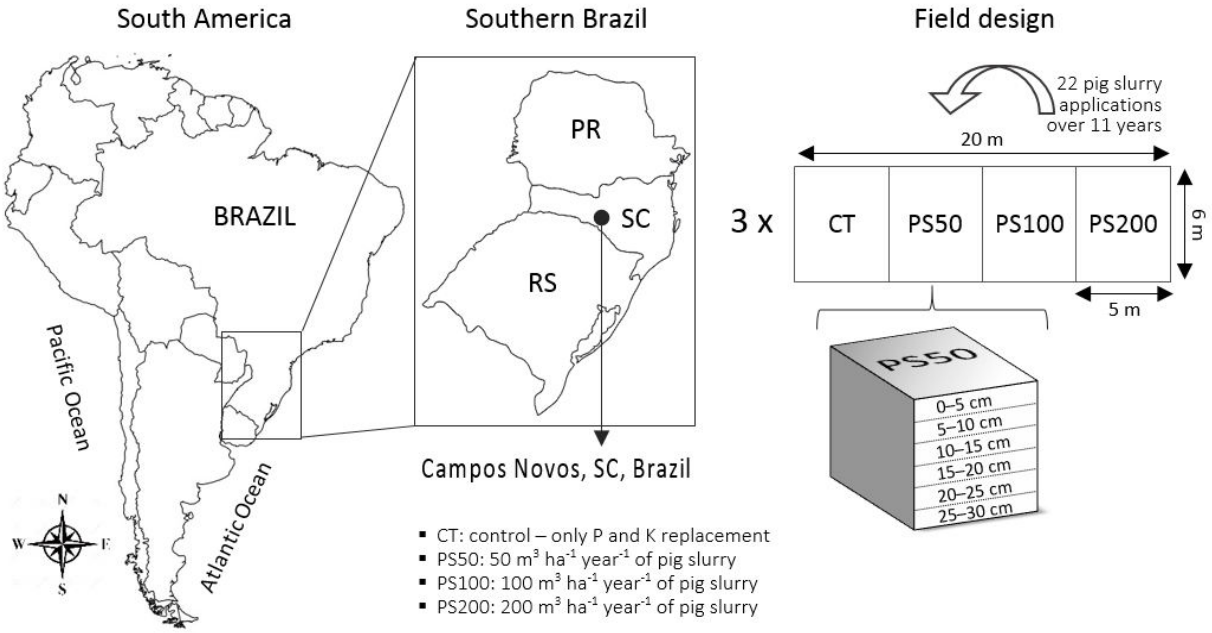

Figure 3.2 – Experiment location and design.

Disturbed soil samples were collected in June of 2011, after 11 years of soil amendment and 22 PS applications (two per year over the 2000–2010 period). Six soil layers were selected from each of the twelve field plots, as follows: 0–5, 5–10, 10–15, 15–20, 20–25 and 25–30 cm depth (FIGURE 3.2), yielding a total of 72 soil samples. One trench per plot was excavated, measuring 25 cm by 25 cm each, and the whole amount of soil within each layer (3125 cm³) was used for the sample composition. After air-drying, the soil samples were crushed, sieved through a 2.0 mm mesh plastic sieve and stored in plastic containers prior to analysis.

3.1.2 Soil and PS characteristics

The soil was a Rhodic Hapludox soil (USDA, 2003), also referred to as *Latossolo Vermelho distroférrico típico* in the Brazilian system of soil classification (EMBRAPA, 2004). It was developed from intermediate effusive rock saprolites of Serra Geral formation. At the beginning of the experiment, the 0–20 cm soil layer exhibited a very clayey texture (USDA, 2013), with 67.8% clay, 30.8% silt and 1.4% sand (MALLMANN, 2013), and the following chemical characteristics: 5.8 pH in water (1:1 v/v); 45 g kg^{-1} organic matter; 0.0, 0.5, 4.7 and 2.9 $cmol_c$ dm^{-3} of exchangeable Al, K, Ca and Mg, respectively (VEIGA et al., 2012); and 8.0 $cmol_c$ dm^{-3} of CEC (assessed independently, according to TEDESCO et al., 1995).

After 22 PS applications, Mallmann (2013) reported the total Cu and Zn concentrations within the soil 0–5, 5–10, 10–15, 15–20, 20–25 and 25–30 cm layers of the CT, PS50 and PS200 plots. Gubiani et al. (2012) reported the organic C concentrations for the same layers of the CT, PS50, PS100 and PS200 plots. The results of Mallmann (2013) and Gubiani et al. (2012) are summarized in Table 3.1.

Table 3.1 – Total Cu, Zn and organic C concentrations within the soil 0–5, 5–10, 10–15, 15–20, 20–25 and 25–30 cm layers of the CT, PS50, PS100 and PS200 plots, after 22 PS amendments.

Soil layer (cm)	Total Cu[(1)]			Total Zn[(1)]			Organic C[(2)]			
	(mg kg^{-1})			(mg kg^{-1})			(g kg^{-1})			
	CT	PS50	PS200	CT	PS50	PS200	CT	PS50	PS100	PS200
0—5	113.2	136.2	173.8	101.5	157.0	214.7	39.4	43.7	45.3	45.2
5—10	110.3	123.4	145.3	99.1	117.2	146.0	34.6	36.4	35.7	37.1
10—15	110.3	114.8	125.6	95.6	99.9	115.5	32.3	33.1	32.5	33.4
15—20	113.1	116.3	122.8	99.6	98.8	108.2	31.4	32.2	31.9	32.4
20—25	115.9	117.7	120.0	100.3	100.5	107.0	30.7	31.7	31.4	31.5
25—30	118.7	119.1	121.4	98.5	98.2	103.7	29.2	29.8	29.6	29.9

[(1)]Determined by Mallmann (2013), no PS100 data available. [(2)]Determined by Gubiani et al. (2012).

Variations in soil pH through the soil profile, after 9 years of PS amendments, were assessed by Veiga et al. (2012). No statistically significant differences in pH were found below the 10 cm soil layer, comparing amended and non-amended plots. Even

in the topmost layers, the difference was as low as 0.4 pH unit, when comparing the PS200 plot with the CT plot.

Pig slurry was obtained from an anaerobic lagoon reservoir located on a pig finishing farm in Campos Novos, Santa Catarina State, Brazil. Average physico-chemical characteristics, determined according to Tedesco et al. (1995), were: 7.3 pH; 2.25% dry mass content; 3.7, 0.6 and 1.7 g kg^{-1} of N, P and K, respectively; 21.0 ± 19.0 g m^{-3} of Cu; and 43.0 ± 37.8 g m^{-3} of Zn.

3.2 ACCUMULATION AND FRACTIONATION METHODS

The sequential extraction procedure and the statistical analysis and calculations applied to assess the Cu and Zn accumulation and fractionation in the field experiment presented in Section 3.1 are described below. The experiments comprised in this step were performed in the Laboratory of Soil Chemistry and Fertility, at the Soil Department of the Federal University of Santa Maria (UFSM), Brazil, from October 2013 to February 2014. Data treatment was initiated during the experiments and continued until January 2015, mainly at the *Centre Européen de Recherche et d'Enseignement des Géosciences de l'Environnement* (CEREGE), Aix-en-Provence, France.

3.2.1 Sequential extraction procedure

In this step, the whole 72-samples set was subjected to analysis. The sequential extraction scheme used in this work, denoted *m*GSC, was first proposed by the Geological Survey of Canada (HALL et al., 1996) and later modified (BENITEZ & DUBOIS, 1999; DOELSCH et al., 2006). It seemed more suitable for analyzing tropical soils which typically contain high Fe and Mn oxyhydroxides levels (DOELSCH et al., 2008). The protocol considers six different HM fractions: exchangeable, adsorbed, bound to organic matter, bound to amorphous oxyhydroxides, bound to crystalline oxides and bound to residual mineral matrix.

One gram of soil was shaken with 30 ml of reagent for 90 min, using a rotary shaker at 70 revolutions per minute (rpm). The mixture was centrifuged (20 min, 2500 rpm) and the supernatant retained. The shaking and centrifugation steps were repeated on the centrifugation residue after adding 30 ml of fresh reagent and, finally, using 30 ml of ultrapure water (MegaUP, Megapurity Inc.). The three collected supernatants were then mixed. This procedure was repeated for the first five fractions. The shaking steps for fractions 4 and 5 were conducted in a water bath (60 and 90 °C, respectively). The final residue was dried and subjected to microwave-assisted acid digestion according to the EPA 3051A protocol (USEPA, 2007). The whole method was performed in three replicates per sample with two reagent blanks per batch for an internal check of the results. The reagents used to extract each fraction and the operating conditions are summarized in Table 3.2. All reagents were Merck analytical grade, with all solutions prepared in ultrapure water. All glass and plastic ware used were previously soaked overnight in a 5% (v/v) nitric acid bath and rinsed with ultrapure water.

Copper and Zn concentrations were determined on each fraction extract, after dilution with ultrapure water when necessary. Measurements were performed using an inductively coupled plasma–optical emission spectrometer (ICP–OES Optima 7000 DV, PerkinElmer Inc.) with an axially viewed plasma system. The spectrometer signal was checked by analyzing the calibration standards every 18 samples (corresponding to an entire field plot) and corrected if necessary.

Table 3.2 – Operating conditions for the *m*GSC sequential extraction procedure for 1.0 g of air-dried soil.

Fraction	Nominal target phase	Reagent	Shaking time and temperature
1	Exchangeable	2 x 30 ml of 0.1 mol l^{-1} $NaNO_3$	90 min at 25 °C
2	Adsorbed	2 x 30 ml of 1.0 mol l^{-1} CH_3COONa at pH = 5.0 with CH_3COOH	90 min at 25 °C
3	Organic matter	2 x 30 ml of 0.1 mol l^{-1} $Na_4P_2O_7$	90 min at 25 °C
4	Amorphous oxyhydroxides	2 x 30 ml of 0.25 mol l^{-1} $NH_2OH{\cdot}HCl$ in 0.05 mol l^{-1} HCl	90 min at 60 °C
5	Crystalline oxides	2 x 30 ml of 1.0 mol l^{-1} $NH_2OH{\cdot}HCl$ in 25% CH_3COOH	90 min at 90 °C
6	Residual	10 ml of concentrated HNO_3	USEPA 3051A

3.2.2 Statistical analysis and calculations

Average Cu and Zn concentrations and standard deviations were calculated for all HM fractions and soil layers, considering the three replicated plots per PS application rate. The data were tested for normality using the Shapiro-Wilk test and for homoscedasticity using Hartley's test. When the data were found to meet the normal distribution and similar variance assumptions (~95% of the dataset), an analysis of variance (one-way ANOVA) was applied. When ANOVA revealed the presence of significant differences between treatments, a *post hoc* multiple mean comparisons test (Tukey's HSD) was used to further assess these differences. Otherwise, nonparametric statistics were used. Significant effects of treatments were tested using Kruskal−Wallis ANOVA followed by pairwise comparison using the Mann-Whitney U Test. Statistical tests were conducted at the 95% probability level.

The sum of the six considered fractions, for all treatments and soil layers, was computed and is hereafter denoted SUMF. The extraction recovery (Rec) was estimated by comparing the SUMF-Cu and SUMF-Zn concentrations (SUMF-HM) to the total Cu and Zn concentrations (total HM) in Table 3.1 (MALLMANN, 2013), as follows:

$$Rec = \frac{SUMF - HM}{total\ HM}\ x\ 100 \quad (1)$$

The accumulated exogenous HM contents in the soil 0–30 cm profile were determined based on the soil bulk density and on the differences in the SUMF-HM concentration between amended and non-amended plots. The HM inputs to each field plot during the whole experimental period were calculated using the PS application rates and the average PS-Cu and PS-Zn concentrations available from 7 out of the 22 applications. Accumulated and applied HM amounts were compared using the two-sample Student's t-test at the 95% probability level.

The exogenous HM distribution among fractions was calculated for the topsoil layer (0–5 cm) and for the deepest layer in which SUMF-Cu and SUMF-Zn concentrations were found to be significantly different from the CT plot. For this purpose, the sum of the fractions that had significantly increased their HM

concentrations within the soil layer under consideration were compared to the sum of the corresponding fractions within the CT plot.

Statistical analysis and calculations were performed using StatSoft Statistica 7.0 and Microsoft Excel 2013 software.

3.3 PHASE ASSOCIATION METHODS

The density fractionation procedure, followed by fractions characterization, chemical analysis and calculations applied to assess the Cu and Zn phase association within selected samples from the field experiment presented in Section 3.1 are described below. The experiments comprised in this step were performed in the laboratories of CEREGE, Aix-en-Provence, France, from August 2014 to January 2015. Data treatment was initiated during the experiments and continued until September 2015, at the Environmental Engineering Graduate Program (PPGEA) of the Regional University of Blumenau (FURB), Brazil.

3.3.1 Density fractionation procedure

Two soil samples were subjected to analysis in this step: the CT 0–5 cm sample (denoted CT sample) and the PS200 0–5 cm sample (denoted PS200 sample). The sample selection was based on HM concentration criteria, in order to provide the most marked contrast between the CT sample and the sample that had presented the highest increase in Cu and Zn concentration among the amended plots.

The procedure here applied was slightly modified from El-Mufleh et al. (2014). Density thresholds were selected according to the theoretical density of minerals previously identified via X-ray diffraction spectroscopy in bulk soil samples. The chosen thresholds – 1.9, 2.25, 2.5, and 2.7 g cm^{-3} – resulted in five soil density fractions: $d<1.9$, $1.9<d<2.25$, $2.25<d<2.5$, $2.5<d<2.7$, and $d>2.7$ g cm^{-3} (hereafter, density thresholds are reported without stating g cm^{-3}).

Density of a given sodium polytungstate (LST Fastfloat ($Na_6[H_2W_{12}O_{40}]$)) solution was obtained by mixing the commercial solution (d = 2.82 g cm^{-3}) with demineralized water. The required dilutions were calculated and performed by mass basis and the resulting densities of solutions were checked with a hydrometer. During the solution preparation stage, sodium hydroxide was added to rise the pH from around 2.0 (pH of the sodium polytungstate solution) to 5.8 (pH of the studied soil), a requirement to reduce HM losses to the solution. El-Mufleh et al. (2014) used d = 2.8 g cm^{-3} as the highest-density threshold and reported difficulty for increasing the pH of the sodium polytungstate solution toward neutrality. The choice of d = 2.7 g cm^{-3} as the highest-density threshold in the present study was thus based on the mentioned setback.

Six grams of finely ground soil were weighed into 50 ml centrifuge tubes and first mixed with 30 ml of d = 1.9 g cm^{-3} sodium polytungstate solution. In order to destroy soil aggregates, the centrifuge tubes were placed in an ice bath and sonicated. Sonication was performed using a Bioblock Scientific® Vibracell sonicator with a 0.5 in probe tip, operating at 70% output for 1 min and 35% output for 8 min. The samples in LST were then centrifuged and two density fractions were separated. The centrifuge time was adapted according to Stokes' law, setting 0.2 µm as the smaller theoretical particle size to settle. The 0.2 µm threshold was selected to provide reasonable centrifuge times.

The supernatant, containing the soil density fraction below 1.9 g cm^{-3} (d<1.9) was sucked off and stored. The remaining sample was then mixed with 30 ml of the next denser sodium polytungstate solution, according to the selected thresholds. The sonication, centrifugation and sucking off steps were repeated for each density threshold.

Demineralized water was added to the stored supernatants in order to decrease the density of the solution below the lowest density of soil in the concerned fraction (*e.g.*: LST solution density decreased down to 1.8 to collect the 1.9<d<2.25 fraction). After centrifugation, the diluted LST was sucked off. Finally, the soil fractions were rinsed three times with demineralized water, centrifuged and the supernatant was retained to determine HM contents that eventually dissolved during the rinsing steps. Samples were then freeze-dried and weighed, resulting in five density fractions for each soil sample. The whole procedure was performed in three replicates per sample.

3.3.2 Characterization and chemical analysis of soil density fractions

The mineral composition of soil density fractions was identified with an X-ray diffractometer (X'Pert Pro, Panalytical) running at 40 kV and 40 mA, using a Co Kα radiation (λ=1.79 Å) with a linear detector (X'Celerator) and a secondary flat monochromator. Samples were ground in an agate mortar and placed on zero background silicon sample holders with a few drops of ethanol. For each sample, a counting time of 5.5 s per 0.033° step was used for 2θ in the 4-80° range. Phase identification was performed using XRD data analysis software (X'pert PRO Highscore plus) and its powder diffraction database (ICDD-PDF2).

For HM analysis, soil bulk samples and density fractions were subjected to microwave-assisted acid digestion, according to the EPA 3051A protocol (USEPA, 2007) and then diluted in 2% HNO_3 (PlasmaPure Plus 69% HNO_3, SCP Science; Milli-Q Reference Ultrapure Water, Millipore). Concentrations were measured by inductively coupled plasma mass spectrometry (ICP-MS, NexION 300X, PerkinElmer) with online addition of Rh-103 as internal standard element. Accuracy of ICP-MS measurements was checked using certified reference samples [SLRS-5 River water, Canada; GBW07402 (GSS-2) and GBW07403 (GSS-3) soils, China]. All results presented good agreement with the certified values (*i.e.* in the range between 85 and 115% of certified values).

Organic C and N contents of dry and homogenized soil samples (bulk and density fractions) were measured using an elemental analyzer (NA 1500, Fisons). Previous acid treatment was not necessary because the soils were carbonate-free. The elemental analyzer was calibrated with standard acetanilide (Säntis analytical). Reproducibility was checked with lab-internal marine and lacustrine standard sediments. The standard deviation was smaller than 2% for organic C and smaller than 5% for N absolute values.

3.3.3 Calculations

The mass recovery of the density fractionation protocol and the mass distribution of density fractions were calculated based on the soil mass obtained in each fraction and the initial mass of bulk sample. The organic C, N, Cu and Zn concentrations within each density fraction were multiplied with mass of soil in the respective fraction. It resulted in the absolute and percentage contribution of organic C, N, Cu and Zn within a given density fraction for the bulk soil sample.

The recoveries of organic C + N and their distribution among fractions were used as a proxy to identify the original host density fraction of the HM amounts lost to the sodium polytungstate solution during the density fractionation steps. It was assumed that:

(i) Organo-mineral particles smaller than 0.2 µm (the selected centrifugation threshold) are a potential HM-bearing phase likely to dissolve or remain in suspension in the sodium polytungstate solution. Their distribution among the density fractions is similar to the non-soluble/non-colloidal OM distribution actually detected and to be presented in Section 4.2.2.

(ii) Soluble, ionic Cu and Zn contents are negligible in the CT sample, but significant in the PS200 sample. Indeed, it will be reported in Section 4.1.3.2 that only 1.4% of the Cu and 1.5% of the Zn were present in readily available fractions (assessed as “exchangeable” and “adsorbed” via sequential extractions) within the CT sample, whereas 6.3% of the Cu and 23.1% of the Zn were found in the same fractions within the PS200 sample.

Therefore, when the Cu and Zn recoveries were either similar to or higher than the organic C + N recoveries (the case for the CT sample), HM losses were ascribed to losses of organo-mineral particles smaller than 0.2 µm. The lost HM content was then accounted in each density fraction according to the actually detected organic C + N distribution, as follows:

$$HM^{di}_{corrected} = HM^{di}_{detected} + \left(HM\ overall\ loss\ x\ [C+N]^{di}_{distribution}\right) \quad (2)$$

When the HM recoveries were lower than the organic C + N recoveries (the case for the PS200 sample), Equation 2 was used to account for the lost HM in each

density fraction until reaching the organic C + N recovery threshold in the same sample. The lost HM content above it was attributed to a new fraction: soluble in LST (denoted s-LST).

3.4 MOLECULAR ENVIRONMENT METHODS

The experimental procedures applied to assess the Cu and Zn molecular environment within selected samples from the field trial presented in Section 3.1 are described below. The synchrotron-based X-ray absorption (XAS) experiments were conducted at the European Synchrotron Radiation Facility (ESRF), Grenoble, France. The first XAS run took place in May 2014, and the second in December 2015. Copper sorption experiments were conducted in the laboratories of CEREGE, Aix-en-Provence, from October to December 2015. Particle size fractionation of pig slurry was also carried out at CEREGE, from October to November 2014. Scanning electron microscopy with X-ray microanalysis (SEM–EDS) was conducted at the *Centre Interdisciplinaire de Nanoscience de Marseille* (CINaM), Aix-Marseille University, Marseille, France, in January 2015.

Data treatment was initiated during the experiments and continued until February 2016, at CEREGE and at the Water Resources and Environmental Engineering Graduate Program (PPGERHA) of the Federal University of Parana (UFPR), Curitiba, Brazil.

3.4.1 X-ray absorption spectroscopy

Two soil samples were subjected to analysis in this step: the CT 0–5 cm sample (denoted CT bulk sample) and the PS200 0–5 cm sample (denoted PS200 bulk sample). The samples were selected in order to provide the most marked contrast in HM concentration between samples, as described in Section 3.3.1. Therefore, these two soil samples coincide with the samples selected for the phase association analysis.

Copper and zinc K-edge X-ray absorption spectra were recorded on the FAME beamline at the European Synchrotron Radiation Facility. Finely ground samples were pressed into pellets, analyzed in liquid He temperature to prevent sample damage by photoreduction, and the signal was acquired in fluorescence mode using a 30 element solid-state Ge detector (CANBERRA Industries Inc.). The spectra are the sum of 5 to 16 scans depending on the HM concentration and the noise level. For spectra normalization and the extraction of the EXAFS spectra, E_0 was fixed at 8992.0 eV for Cu and 9664.6 eV for Zn. The data reduction was performed using the Athena Software (RAVEL & NEWVILLE, 2005).

The EXAFS function $\chi(E)$ is defined as $\chi(E) = [\mu(E) - \mu_0(E)] / \Delta\mu_0(E_0)$, where $\mu(E)$ is the measured absorption coefficient, $\mu_0(E)$ is the absorption of an isolated atom, and $\Delta\mu_0$ is the measured jump in the absorption $\mu(E)$ at the threshold energy E_0. Preedge background subtraction is determined by fitting a linear polynomial to the preedge region and a quadratic polynomial to the postedge region. The difference between these two polynomials extrapolated to the edge energy (E_0) is used as the normalization constant [$\Delta\mu_0(E_0)$]. A spline function is used to approximate $\mu_0(E)$. Then, $\chi(E)$ is converted to $\chi(k)$ with the wave number of the photoelectron (k) (DOELSCH et al., 2006). Pseudo-radial structure functions (RSFs) were obtained by Fourier transforming k^2-weighted $\chi(k)$ spectra to R space using Kaiser–Bessel apodization windows. The resulting distribution is uncorrected from phase shift functions, *i.e.* RDFs peaks are displaced by about 0.3 to 0.4 Å with respect to the crystallographic distances (LEGROS et al., 2010a).

Previously background subtracted and normalized EXAFS spectra were subject to a least-square linear combination fitting (LCF) procedure over the k-range 2–10.3 $Å^{-1}$ for Cu and 2–9.9 $Å^{-1}$ for Zn. A library of Cu and Zn model compounds was used in order to identify and quantify the Cu- and Zn-bearing components in the samples. The percentage contribution of each model spectrum to the best fit is proportional to the amount of Cu or Zn present in that form in the sample. The residual *Res* parameter and visual analysis of the fits were used as the fit criterion. The *Res* parameter is defined as $Res = \Sigma (k^2 \chi_{exp} - k^2 \chi_{model})^2 / \Sigma (k^2 \chi_{exp})^2$, where a lower *Res* value represents a better match between experimental and reference spectra (ISAURE, 2005).

The library of Zn model compounds included (i) primary and secondary Zn minerals and precipitates: sphalerite (ZnS), willemite (Zn_2SiO_4), parahopeite

[$Zn_3(PO_4)_2$•4(H_2O)], zincite (ZnO), franklinite ($ZnFe_2O_4$), zinc hydroxide [$Zn(OH)_2$], smithsonite ($ZnCO_3$), zinc sulphate ($ZnSO_4$), zinc phosphate [$Zn_3(PO_4)_2$], zinc nitrate [$Zn(NO_3)_2$], and zinc aluminate ($ZnAl_2O_4$); (ii) mineral surface sorption complexes at different loadings: Zn-HIM (hydroxy-interlayered mineral), Zn sorbed kaolinite, Zn sorbed ferrihydrite, Zn sorbed goethite, Zn sorbed birnessite, Zn sorbed kerolite, Zn-LDH (layered double hydroxide) and Zn sorbed hydrotalcite; and (iii) Zn-organic complexes: Zn-malate, Zn-cysteine, Zn-acetate, Zn-citrate, Zn-phytate, Zn-oxalate, Zn-malate, Zn-methionine, Zn-histidine, Zn-phthalocyanine, Zn-glycine, Zn-galacturonic acid and Zn-pectin.

The library of Cu model compounds included (i) primary and secondary Cu minerals and precipitates: covellite (CuS), Cu(I) sulfide (Cu_2S), dioptase [$CuSiO_3.H_2O$], cornetite [$Cu_3PO_4OH_3$], chalcopyrite ($CuFeS_2$), Cu(II) oxide (CuO), Cu(I) oxide (Cu_2O), Cu(II) sulfate [$CuSO_4.5H_2O$], Cu(II) carbonate ($CuCO_3$), Cu(II) hydroxide phosphate [$Cu_2(OH)PO_4$], Cu(I) thiophenolate (PhSCu), and Cu(II) hydroxide [$Cu(OH)_2$]; (ii) mineral surface sorption complexes: Cu sorbed goethite and Cu sorbed ferrihydrite; and (iii) Cu-organic complexes: Cu-phenylalanine, Cu-methionine, Cu-gluconate, Cu-phthalocyanine, Cu-phytate, Cu-malate, Cu(I)-cysteine, Cu-thioglycollate, Cu-histidine, Cu-formate, Cu(II)-malonate, Cu(I)-acetate, Cu(II)-acetate, Cu-histidine and Cu-galacturonate. Additionally, two other mineral surface sorption complexes were prepared: Cu sorbed kaolinite and Cu sorbed montmorillonite. Description of the sorption experiments are presented below.

3.4.2 Cu sorption experiments

In order to improve the database of Cu reference materials for EXAFS analysis, two new references were prepared and had their Cu K-edge X-ray absorption spectra recorded: Cu sorbed on kaolinite and Cu sorbed on montmorillonite. The clay minerals were obtained from the Source Clays Repository of the Clay Minerals Society. Georgia kaolinite (K-Ga2) was used as received. Wyoming montmorillonite (SWy-2) was subjected to a purification procedure in order to remove quartz and illite impurities.

Forty grams of raw montmorillonite were shaken in 1 l of demineralized water at 700 rpm for 1 h. The mixture was then centrifuged at 13000 rpm for 45 min. The

supernatant was discarded and the montmorillonite fraction <2 μm was collected at the top of the precipitate pallet. The collected precipitate was subjected once again to the same procedure. The isolated montmorillonite fraction <2 μm was then saturated with Na, by resuspension in 1 l of ~1.0 M NaCl solution at 700 rpm for 3 h. The mixture was then centrifuged at 15000 rpm for 1 h. The precipitate was collected and subjected to the same saturation procedure two more times. Finally, the Na-saturated montmorillonite was rinsed with demineralized water in order to remove the excess of Cl^- ions. For that purpose, a resuspension in 0.5 l of demineralized water at 700 rpm, followed by centrifugation at 15000 rpm for 1 h and collection of the precipitate was repeated six times. The complete removal of Cl^- ions was confirmed by a conductivity measurement in the last centrifugation supernatant solution. The clay was then freeze-dried for 48 h at -53 ºC and considered for X-ray diffraction analysis to verify its purity. The X-ray diffractograms of kaolinite and montmorillonite clays (SUPPORTING INFORMATION SI-3) indicated that no other mineral species were present in the clay composition. Clays were then considered for the Cu sorption experiments.

The Cu sorption experiments were adapted from Schlegel and Manceau (2013). All sorption experiments were performed in 250 ml borosilicate glass beakers thermostated at 25.0 ºC by immersion in a circulating water bath (ED THERM60, Julabo GmbH). Suspensions were stirred with a magnetic bar at 400 rpm, and maintained under inert atmosphere by bubbling through the solution pure N_2 gas (5.0 grade, Linde Gas, France). A ~0.5 M dissolved Na concentration was maintained by using NaCl to prevent Cu adsorption on cation exchange sites. Sorption was performed in 2 g l^{-1} suspensions of kaolinite and montmorillonite.

Sorption experiments were conducted following two complementary approaches. Firstly, the sorption kinetics were evaluated in a 4-day duration sorption reaction at a fixed Cu initial concentration. Secondly, an ideal sorption time (sufficiently close to equilibrium time) was set, based on the first approach, and several Cu initial concentrations were tested in order to obtain HM-clay sorption complexes at different Cu loads.

For the kinetic approach, sorption was initiated by adding aliquots of 0.01 M $CuCl_2$, 0.01 M HCl until a target total Cu concentration of 33.3 μM was attained. Then, the suspension pH was raised slowly to the final pH value of 5.7 by addition of 0.02 M NaOH, 0.48 M NaCl solution. The pH control and base addition were assisted by an

automatic titration unit (785 DMP Titrino, Metrohm AG). The pH electrode was periodically recalibrated with buffers and the base addition was set to 10 μl min^{-1} to minimize local supersaturation and to avoid precipitation of Cu polymers. Copper initial concentration in the suspension was corrected afterwards considering the amount of base solution added to reach the target pH. At given times, 5 ml of suspension were withdrawn with a syringe and immediately filtered by coupling a syringe filter (Whatman 0.1 μm cellulose nitrate). The roughly first filtered ml was discarded to limit Cu losses in the supernatant due to sorption on the filter. Dissolved Cu concentration in the filtered supernatant was measured by ICP-MS (NexION 300X, PerkinElmer), and Cu uptake by clays determined as the difference between the initial Cu concentration and the dissolved Cu concentration at each withdrawing time. Based on the sorption equilibrium curves (SUPPORTING INFORMATION SI-4), further sorption experiments at varying Cu initial concentrations were conducted considering a 4-hours reaction time, *i.e.* a duration deemed sufficiently close to equilibrium time.

The 4-hour sorption experiments were conducted in Cu initial concentrations of 33.3, 100 and 300 μM for kaolinite and 13.3, 33.3, 100 and 300 μM for montmorillonite. The procedure was the same as described above, except that all the suspension volume was collected at the end of the reaction time and centrifuged at 4000 rpm for 45 min. An aliquot of the supernatant solution was filtered (Whatman 0.1 μm cellulose nitrate) and the dissolved Cu concentration was measured by ICP-MS to determine the Cu uptake. The precipitate containing the reacted clay was freeze-dried at -53 ºC for 48 hours, ground in an agate mortar and pressed into pellets to record the EXAFS spectra as described in Section 3.4.1. The resulting Cu uptake by 2 g l^{-1} kaolinite and montmorillonite for different Cu initial concentrations, at pH 5.7, after 4 hours equilibrium time are presented in Supporting information SI-5.

All solutions used for clays purification and sorption experiments were prepared with demineralized water (Milli-Q Reference Ultrapure Water, Millipore) and chemicals of analytical reagent grade.

3.5 COMPLEMENTARY PIG SLURRY ANALYSIS

3.5.1 Particle size fractionation of pig slurry

A PS sample was collected in the anaerobic lagoon at the pig finishing farm that had been providing the PS for spreading on the experimental field over 11 years, in Campos Novos, SC, Brazil. The PS raw sample was tested for its dry matter content by evaporation of 10 g of liquid sample at 60 ºC, for 48 h, in triplicate. The PS dry matter content was at 1.29 ± 0.06% (m/m).

The PS sample was then subjected to particle size fractionation, selecting the filtration thresholds of 20 µm, 0.2 µm and 10 kD. The target particle size fractions were thus: PS > 20 µm, 20 µm > PS > 0.2 µm, 0.2 µm > PS > 10 kD and PS < 10 kD. Forty grams of raw, liquid PS were passed through a 20 µm nylon net filter (Whatman) and the retained solid fraction was dried (60 ºC, 48 h) and weighed, thus accounting for the PS > 20 µm fraction.

The filtrate containing particles smaller than 20 µm was then subjected to tangential flow filtration. The filtration system (KrosFlo, Spectrum Laboratories, Inc.) was first mounted with a 0.2-µm pore size modified polyethersulfone (mPES) hollow filter and fed at 10 ml min^{-1} with the PS sample that had passed through the previous filtration step. The system was adjusted for a filtration flow of 1 ml min^{-1} (10% of the feeding flow), promoting thus the sample recirculation. The permeate end was then closed and the system was fed with 10 ml of demineralized water and allowed to recirculate in order to recover the retentate containing the 20 µm > PS > 0.2 µm fraction. This retentate was dried at 60 ºC for 48 h. The permeate from the previous step (containing particles smaller than 0.2 µm), was then passed through a 10-kD pore size mPES hollow filter, mounted on the filtration system in substitution for the previous filter. The same filtration procedure was applied, and the retentate containing particles in the 0.2 µm > PS > 10 kD range was collected and dried. Lastly, the permeate containing the PS < 10 kD fraction was collected, acidified and stored prior to analysis.

The PS > 20µm fraction was not considered for further analysis due to its low (and therefore insufficient) mass recovery, *i.e.* below 2% of the PS raw dry matter. Dried samples of the raw PS and the 20 µm > PS > 0.2 µm and 0.2 µm > PS > 10 kD

fractions were subjected to acid digestion according to the EPA 3051A protocol (USEPA, 2007). The digested samples were analyzed for their Cu and Zn concentrations using ICP-MS (NexION 300X, PerkinElmer).

The PS dry matter content of 1.29% (m/m) was distributed as follows: 1.9% in the PS > 20 µm fraction, 74.6% in the 20 µm > PS > 0.2 µm fraction, and 17.9% in the 0.2 µm > PS > 10 kD fraction. The dry matter content in the PS < 10 kD fraction was negligible. The recovery of the particle size fractionation procedure was thus of 94.4%. Copper concentrations were at 200.0 mg kg^{-1} of dry fraction in the 20 µm > PS > 0.2 µm fraction, at 5.6 mg kg^{-1} of dry fraction in the 0.2 µm > PS > 10 kD fraction, and at 161.3 mg kg^{-1} of dry PS in the raw PS sample. Zinc concentrations were at 949.9 mg kg^{-1} of dry fraction in the 20 µm > PS > 0.2 µm fraction, at 9.3 mg kg^{-1} of dry fraction in the 0.2 µm > PS > 10 kD fraction, and at 772.1 mg kg^{-1} of dry PS in the PS raw sample.

3.5.2 Scanning electron microscopy with X-ray microanalysis (SEM–EDS)

Because the 20 µm > PS > 0.2 µm fraction contained the vast majority of both the PS-dry matter and the PS-Cu and -Zn content, this fraction was selected to further analysis using scanning electron microscopy with X-ray microanalysis. Portions of non-evaporated samples from the 20 µm > PS > 0.2 µm fraction were analyzed using a scanning electron microscope (Philips XL30 SFEG, North Billerica, MA) equipped with an energy dispersive spectrometer (Oxford Instruments, Oxfordshire, UK).

A small portion of sample was sonicated gently and a droplet was deposited onto a holey-carbon-coated, 200 mesh, Cu-TEM grid. The sample in the grid was allowed to dry for a few hours prior to analysis. The scanning electron microscopy was operated at 15 kV accelerating voltage with a counting time of 60 s per point. Analysis was performed only for Zn, because the grid used contained Cu in its composition.

4. RESULTS AND DISCUSSION

"Science is the acceptance of what works and the rejection of what does not. That needs more courage than we might think."

(Jacob Bronowski)

4.1 ACCUMULATION AND FRACTIONATION

4.1.1 Sequential extraction recoveries and Cu and Zn natural contents

The sequential extraction protocol resulted in a recovery of 109.0 ± 4.9% for Cu and 97.4 ± 5.3% for Zn (TABLE 3.1, TABLE 4.1). Guan et al. (2011) obtained recoveries in the 95–105% range when applying the BCR scheme for Cu extraction in soils amended with Cu-enriched livestock manure. Esakku et al. (2005) achieved recoveries in the 91–110% range for the extraction of Cd, Cr, Cu, Fe, Mn, Ni, Pb and Zn from municipal solid waste using the Tessier protocol. The recoveries obtained in this study using the *m*GSC protocol were thus satisfactory.

There was no influence of the soil depth on the Cu and Zn SUMF concentrations within the CT plot profile. Average SUMF-Cu values ranged from 125.3 to 128.7 mg kg^{-1}, whereas the average SUMF-Zn values ranged from 92.6 to 100.4 mg kg^{-1}. These concentrations were consistent with those found by Pelozato (2008), who set 164.7 ± 11.4 mg kg^{-1} of Cu and 147.5 ± 10.9 mg kg^{-1} of Zn as representative of the pedogeochemical background within Hapludox soils in Campos Novos, SC, Brazil. According to the author, the relatively high HM concentrations were due to the basaltic rock parent material. This was also confirmed by Hugen et al. (2013), who found average Cu and Zn levels of 149.1 and 71.6 mg kg^{-1}, respectively, in different soils derived from basalt in Santa Catarina State.

4.1.2 Cu and Zn accumulation

In a first approach, considering only the SUMF-HM (TABLE 4.1), the analysis of variance indicated no significant difference ($p < 0.05$) in Cu and Zn concentrations between amended and non-amended plots within the three deeper soil layers (15–20, 20–25 and 25–30 cm). Within the three upper layers (0–5, 5–10 and 10–15 cm), however, HM accumulation was influenced by the PS application rate. Within the 0–5 cm layer, the SUMF-Cu concentration increased from 125.3 mg kg^{-1} in the CT plot to 150.7, 154.7 and 180.2 mg kg^{-1} in the PS50, PS100 and PS200 plots, respectively. The SUMF-Zn concentration also increased within the 0–5 cm layer, from 100.4 mg kg^{-1} in the CT plot to 147.8, 163.3 and 188.1 mg kg^{-1} in the PS50, PS100 and PS200 plots, respectively. The *post hoc* test revealed significant increases in both SUMF-Cu and SUMF-Zn concentrations only within the surface soil layer (0–5 cm) of the PS50 and PS100 plots, and up to 10–15 cm in the PS200 plot.

Table 4.1 – SUMF-Cu and SUMF-Zn concentrations (mean ± SD) within the soil layers of the CT, PS50, PS100 and PS200 plots.

HM	Plot	Soil layer (cm)					
		0—5	5—10	10—15	15—20	20—25	25—30
Cu (mg kg^{-1})	CT	125.3 ± 6.5 a	127.5 ± 5.6 a	128.8 ± 1.4 a	125.8 ± 2.3 a	127.9 ± 2.3 a	125.6 ± 1.6 a
	PS50	150.7 ± 3.2 b	137.6 ± 5.1 a	134.7 ± 2.5 a	128.8 ± 0.9 a	122.5 ± 3.8 a	131.4 ± 2.2 a
	PS100	154.7 ± 9.9 b	137.9 ± 6.7 a	134.0 ± 5.6 a	127.1 ± 5.4 a	121.3 ± 4.1 a	128.9 ± 4.7 a
	PS200	180.2 ± 9.5 c	149.3 ± 14.1 b	139.3 ± 2.5 b	127.1 ± 5.3 a	122.2 ± 1.6 a	125.5 ± 3.5 a
Zn (mg kg^{-1})	CT	100.4 ± 5.3 a	96.6 ± 8.4 a	99.0 ± 4.5 a	92.6 ± 5.1 a	98.1 ± 5.1 a	96.9 ± 9.5 a
	PS50	147.8 ± 15.0 b	114.3 ± 7.5 a	106.3 ± 2.1 a	102.6 ± 4.4 a	95.9 ± 8.8 a	103.4 ± 0.6 a
	PS100	163.3 ± 14.6 bc	116.6 ± 11.7 a	108.0 ± 12.8 ab	96.4 ± 6.5 a	93.5 ± 9.1 a	104.1 ± 2.6 a
	PS200	188.1 ± 8.8 c	133.6 ± 9.3 b	117.7 ± 3.8 bc	100.2 ± 9.2 a	96.4 ± 3.7 a	100.9 ± 4.9 a

Values followed by different letters in the same column are significantly different ($p < 0.05$).

To test the hypothesis of overall contaminant accumulation in the topsoil layers, the amounts of Cu and Zn derived from the 22 PS applications were compared with the accumulated Cu and Zn contents detected within the 0–30 cm soil profile after 11 years. The total volume of PS applied to each field plot and the available PS-HM concentration measurements were used to calculate Cu and Zn inputs after all the PS applications. The accumulated HM contents in soils were determined based on the

differences in the SUMF-HM concentrations between amended and non-amended plots, for the whole experimental period. The results are summarized in Table 4.2.

Depending on the PS application rate, HM accumulation within the soil ranged from 22.6 to 43.4 kg ha^{-1} for Cu and from 45.4 to 80.5 kg ha^{-1} for Zn. The applied amounts ranged from 11.6 to 46.2 kg ha^{-1} for Cu and from 23.7 to 94.6 kg ha^{-1} for Zn. Despite the uncertainties involved in the PS-HM inputs, a consistent association between the average HM contents applied via PS and the amounts accumulated within the 0–30 cm soil profile was observed.

Table 4.2 – Cu and Zn quantities (mean ± SD) applied via 22 PS amendments and accumulated within the 0–30 cm profile of PS50, PS100 and PS200 plots after 11 years.

Plot	Cu (kg ha^{-1})		Zn (kg ha^{-1})	
	Applied	Accumulated	Applied	Accumulated
PS50	11.6 ± 10.4 a	23.6 ± 6.5 a	23.7 ± 20.8 a	45.4 ± 13.3 a
PS100	23.1 ± 20.9 a	22.6 ± 9.5 a	47.3 ± 41.6 a	51.7 ± 15.8 a
PS200	46.2 ± 41.8 a	43.4 ± 10.8 a	94.6 ± 83.1 a	80.5 ± 12.4 a

Values followed by the same letter in the same line are not significantly different ($p < 0.05$).

The observation of (a) significant HM concentration increase only until 10-15 cm depth and (b) matching applied/accumulated HM amounts within the 0–30 cm soil profile thus support the hypothesis that most exogenous Cu and Zn tend to accumulate within the topsoil layers, with assimilation by crops and transference via the soil solution virtually negligible in the overall contaminant balance. Indeed, for the same field experiment in the present work, Mallmann (2013) estimated the Zn concentration in the soil solution at 25–30 cm depth as only 0.05 and 0.1 mg l^{-1}, respectively within the PS50 and PS200 plots after 11 years of PS applications, as compared to 0.04 mg l^{-1} within the same layer of the CT plot. The Cu concentration in the soil solution within the 25–30 cm layer remained unchanged within the CT, PS50 and PS200 plots at 0.004 mg l^{-1}.

Del Castilho et al. (1993) determined the assimilation of potentially bioavailable Cu in a sandy loam soil by wheat cultivars at approximately 0.3%. Legros et al. (2013) found negligible Cu (0.005 kg ha^{-1}) and null Zn uptake by *Stenotaphrum dimidiatum* grass, and no significant differences in Cu and Zn flows at 60 cm depth for an Andic Cambisol fertilized for 5 years with PS. Mallmann et al. (2012) calculated 0.05–0.12%

and 0.33–1.13% removal of the total Cu and Zn mass, respectively, in the 0–60-cm soil layer after an 8-year harvesting period in a PS-amended Alfisol.

The influence of PS addition only within upper soil layers was also in close agreement with the results obtained by Girotto et al. (2010). The authors applied ~200 m^3 ha^{-1} $year^{-1}$ of PS, for 78 months, in a sandy loam Ultisol under a no-tillage system and observed an increase in the total Cu and Zn content to depths of 12 and 10 cm, respectively. After applying PS at rates between 68 and 163 m^3 ha^{-1} $year^{-1}$, Legros et al. (2013) assessed the total accumulation of Cu within the 0–20 cm depth soil layer. Surprisingly, Zn accumulation was observed only in the 20–40 and 40–60 cm layers. Regardless of the lower layer resolution (20 cm) and the uncertainty concerning the Zn mass balance, the authors suggested the occurrence of reversible sorption mechanisms that allowed gradual element transfer to deeper layers, associated with the presence of soluble Zn forms within the applied PS.

Novak et al. (2004) observed a significant increase in total Cu and Zn concentrations until the 90 cm horizon after 4 years of PS application. However, the 4330 m^3 ha^{-1} $year^{-1}$ application rate was considerably higher than that used in the present work. Besides, the soil had a sandy texture (89% sand) and pH 4.5 within the surface layer.

The lower HM mobility obtained in the present study compared to those obtained by Novak et al. (2004) for Cu and Zn, and by Legros et al. (2013) for Zn could be explained by the different soil characteristics. Soil texture, pH, organic matter (OM) and Fe and Mn oxyhydroxides have a marked influence on Cu and Zn retention. Both elements may bind to soil OM, or also be adsorbed onto clay minerals and Fe and Mn oxyhydroxides, especially at higher pH values (YIN et al., 2002; MARTINEZ & MOTTO, 2000; ALLOWAY, 1995). The contribution of each of these soil-HM fractions may then be assayed by sequential extraction and this will be further discussed below.

4.1.3 Cu and Zn fractionation

Copper and Zn distribution (in percentage) among the six fractions, within the deepest (25–30 cm) and topmost (0–5 cm) soil layers, for CT and PS treatments is presented in Figure 4.1. Within the CT 25–30 cm layer, Cu fractionation followed the

order: F6 >> F3 > F5 ~ F4 > F2 > F1. Within the CT 25–30 cm layer, Zn was distributed in the following sequence: F6 >> F5 ~ F3 > F4 ~ F2 ~ F1. For both Cu and Zn, none of the 50, 100 and 200 m^3 ha^{-1} $year^{-1}$ treatments altered the fraction order observed in the CT 25–30 cm layer.

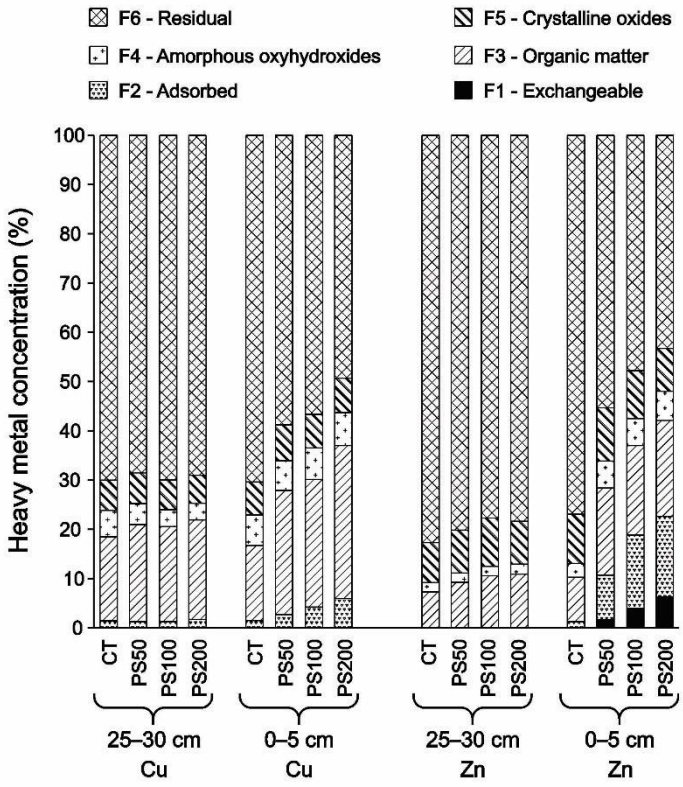

Figure 4.1 – Cu and Zn fractionation among the six fractions within the CT, PS50, PS100 and PS200 deepest (25–30 cm) and topmost (0–5 cm) soil layers.

Within the CT 0–5 cm layer, Cu fractionation followed the order: F6 >> F3 > F5 ~ F4 > F2 > F1. This order did not change in the PS50, PS100 and PS200 treatments. Within the CT 0–5 cm layer, Zn was distributed in the following sequence: F6 >> F5 ~ F3 > F4 > F2 > F1. The PS input of 50 m^3 ha^{-1} $year^{-1}$ modified the previous sequence. The F3 concentration became greater than F5 and F2 greater than F4, resulting in: F6 >> F3 > F5 > F2 > F4 > F1. In the PS100 plot, F2 became more concentrated than F5. Finally, in the PS200 plot, F1 quantities were equivalent to F4, resulting in: F6 >> F3 > F2 > F5 > F4 ~ F1.

The results revealed a major contribution of the residual fraction (F6) in HM partitioning. Compared to Cu, the most labile Zn fractions (F1 and F2) showed a more marked increase in their contribution to HM fractionation in the topsoil as the applied

PS dosage increased. For both HM, however, the organically bound fraction (F3) represented the second most concentrated fraction. Nevertheless, examining the patterns of each fraction individually, before and after PS amendments is essential to assess the exogenous HM distribution.

4.1.3.1 Residual fraction

The analysis of variance indicated that Cu and Zn accumulation in the residual fraction (F6) did not occur at any depth, even when the higher PS dose was applied (SUPPORTING INFORMATION SI-1 and SI-2). Among all treatments and soil layers considered, the average Cu and Zn concentration in this fraction was 88.6 ± 4.5 and 78.3 ± 5.7 mg kg^{-1}, respectively. As a consequence of the overall HM accumulation described in section 4.1.2, the contribution of the residual fraction to Cu partitioning – originally 70.5% within the CT plot profile – decreased to 59.0, 56.8 and 49.3% within the PS50, PS100 and PS200 0–5 cm layers, respectively. Similarly, the residual fraction showed a 76.9% contribution to Zn partitioning within the CT plot profile, and then it dropped to 55.6, 48.0 and 43.5% within the PS50, PS100 and PS200 0–5 cm layers, respectively (FIGURE 4.1).

The residual fraction is considered to be the most stable fraction. Trace metals found in this fraction are generally related to the parent material. Metals arising from anthropogenic sources tend to be distributed among the other fractions, as this distribution is dependent on the source and soil characteristics (RATUZNY et al., 2009; WILCKE et al., 1999; ZIMMERMAN & WEINDORF, 2010). Metals associated with the residual fraction may only be mobilized due to weathering, causing long-term consequences (FILGUEIRAS et al., 2002). Likewise, the incorporation of anthropogenic HM input within more stable structures may occur over an extended period of time, resulting in less mobile fractions (BRÜMMER et al., 1986; RATUZNY et al., 2009). All the Cu and Zn amounts added via PS were likely incorporated within the first five fractions.

4.1.3.2 Fractions influenced by PS amendments and the exogenous Cu and Zn distribution

The soil profile distribution (in mg kg^{-1}) of Cu and Zn in the first five fractions, as well as the corresponding maximum depth at which each PS application rate was significantly different ($p < 0.05$) from the CT plot, are reported in Figure 4.2. The analysis of each fraction individually indicated that the deepest soil layer at which a significant increase in Cu and Zn concentration was observed was distinct for each fraction, when comparing amended and non-amended plots. The behavior also differed as compared to the influence of the PS dose on SUMF-Cu and SUMF-Zn (TABLE 4.1), reflecting the different affinity of exogenous HM for the fractions.

The Cu concentrations in the exchangeable (F1) and adsorbed (F2) fractions were originally the smallest among all fractions in the CT plot. Within the CT 0–5 cm layer, F1-Cu and F2-Cu concentrations were 0.23 and 1.5 mg kg^{-1}, representing 0.2 and 1.2% of SUMF-Cu, respectively. Within the PS200 0–5 cm layer, F1-Cu and F2-Cu concentrations increased to 1.0 and 10.2 mg kg^{-1}, representing 0.6 and 5.7% of SUMF-Cu.

It is noteworthy that, even containing low Cu amounts, the F1-Cu and F2-Cu concentrations showed a statistically significant increase until deep soil layers in the PS-amended plots, compared with the CT plot. The influence on the F1-Cu concentration was observed up to 15–20 cm in the PS50 plot, 20–25 cm in the PS100 plot, and 25–30 cm in the PS200 plot. Similarly, F2-Cu levels were significantly affected until 5–10, 10–15, and 15–20 cm depth in the PS50, PS100 and PS200 plots, respectively.

The concentration of Cu bound to OM (F3) – originally 19.4 mg kg^{-1} within the CT 0–5 cm layer – increased up to 55.5 mg kg^{-1} within the same layer in the PS200 plot. This represents an increase from 15.5% (CT) to 30.8% (PS200) in the contribution of this fraction to SUMF-Cu. The OM-bound fraction exhibited the most marked increase in Cu concentration after PS addition, and it was the only fraction influenced by the three PS application rates until the deepest soil layer (25–30 cm).

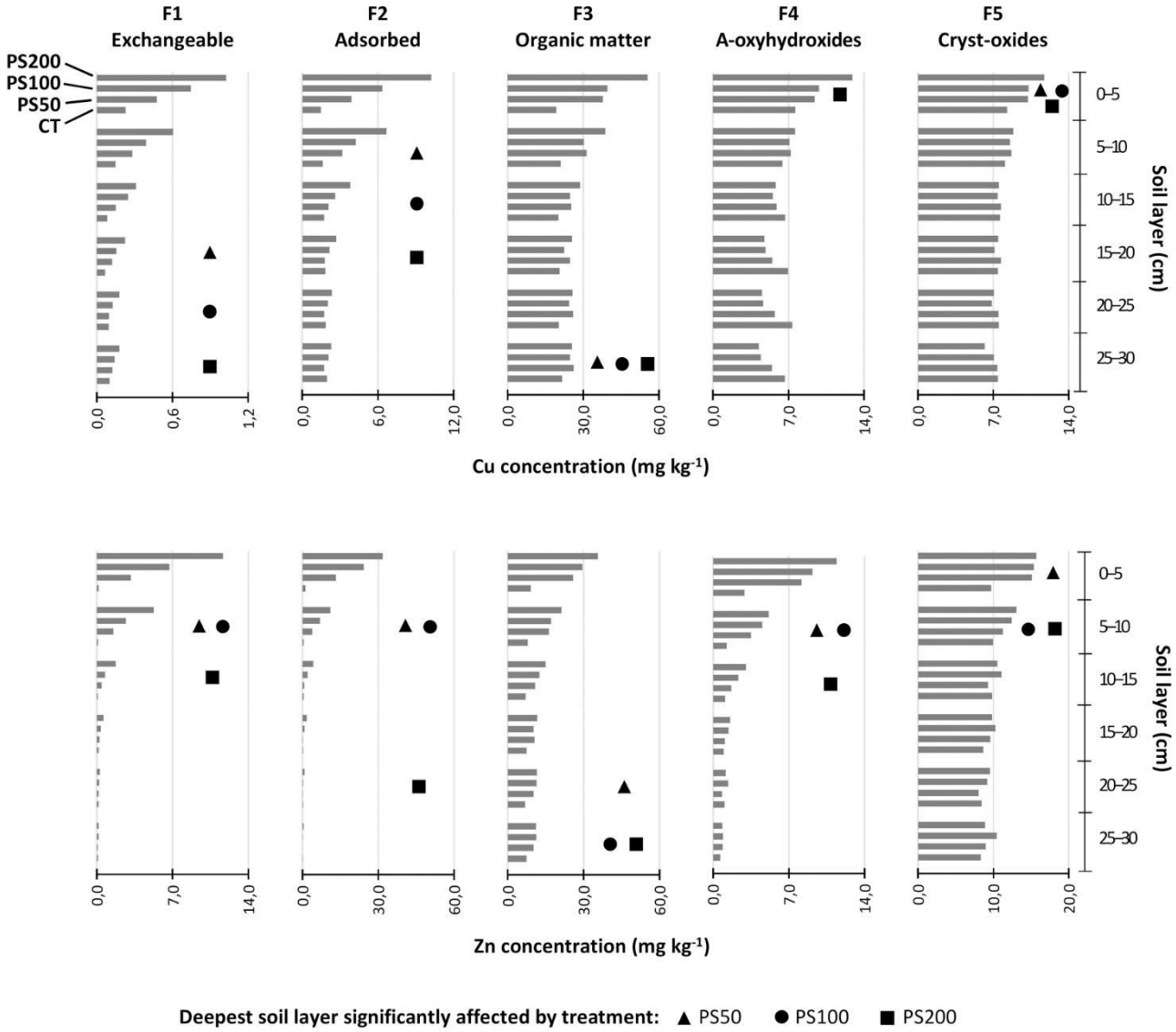

Figure 4.2 – Soil profile distribution of Cu and Zn concentrations associated with the first five fractions and the deepest soil layer significantly affected ($p < 0.05$) by the PS application rate, comparing PS50, PS100 and PS200 with the CT plot.

Copper concentration associated with amorphous oxyhydroxides (F4) increased from 7.6 to 12.9 mg kg^{-1} within the 0–5 cm layer of the CT and PS200 plots, respectively. A similar trend was observed for the Cu concentration associated with crystalline oxides (F5). It increased from 8.3 to 11.7 mg kg^{-1} within the 0–5 cm layer of the CT and PS200 plots, respectively. For both fractions (F4 and F5), it was observed a significant increase in Cu levels within the surface soil layer (0–5 cm) of the PS amended plots compared to the CT plot.

The increased F3-Cu concentration within the upper layers of the amended plots (FIGURE 4.2) was correlated with the higher levels of organic C (TABLE 3.1; GUBIANI et al., 2012), and resulted in the SUMF-Cu distribution profile (FIGURE 4.3).

Within the PS200 0–5 cm layer, exogenous Cu [only the fractions significantly influenced by the PS200 dose within this layer were considered, *i.e.* Σ(PS200-F1 to -F5) – Σ(CT-F1 to -F5)] was distributed as follows: F3 = 66.4%; F2 = 16.1%; other fractions = 17.5%. At 10–15 cm, the deepest layer in which SUMF-Cu was significantly influenced by the PS200 dose (TABLE 4.1), the exogenous Cu distribution [Σ(PS200-F1 to -F3) – Σ(CT-F1 to -F3)] was F3 = 79.1%, F2 = 18.9% and F1 = 2.0%. This indicated that OM fraction was the main factor controlling exogenous Cu partitioning through the soil profile.

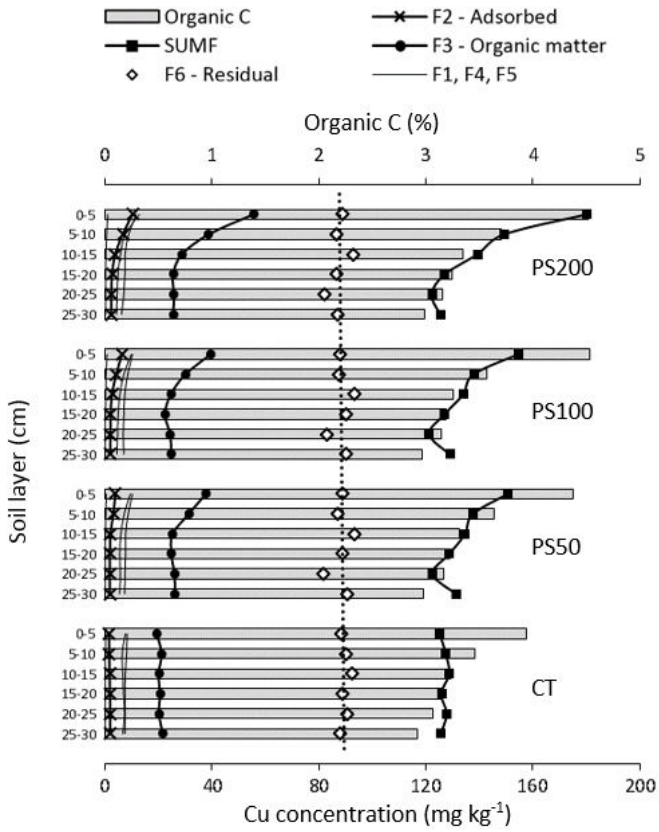

Figure 4.3 – Cu fractions, SUMF and soil organic C profile within CT, PS50, PS100 and PS200 plots.

Asada et al. (2012) and Girotto el al. (2010) found most of the Cu added via PS spreading on the soil in the OM fraction. Several studies reported the same influence of OM functional groups, especially phenyl and carboxyl groups, on Cu adsorption and complexation (GARCIA-MINA, 2006; HAN et al., 2000; L'HERROUX et al., 1997).

The observed OM dominance could be explained by two different (but not mutually exclusive) hypotheses:

(i) Cu in PS was originally distributed in the OM fraction (F3) and, after PS amendments, Cu-sorbed OM was subsequently mobilized through the soil to deeper layers. Indeed, F3-Cu was the only fraction in which significant differences in Cu concentration were found until the deepest layer evaluated, and for all PS application rates – 50, 100 and 200 m^3 ha^{-1} $year^{-1}$ –, as compared to the CT plot (FIGURE 4.2). Moreover, different studies showed that OM is the main fraction associated with Cu in PS effluents (HSU & LO, 1999; L'HERROUX et al., 1997) and Cu bound to dissolved OM can be mobile in the soil profile (GUAN et al., 2011).

(ii) Mobile Cu in PS was in the exchangeable (F1) and adsorbed (F2) fractions. These fractions might have been subject to leaching by solute transport and then immobilized by the soil OM in deeper layers. This assumption is supported by the fact that, besides the low concentrations and minor contribution of F1 and F2 for the exogenous Cu partitioning (FIGURE 4.3), these fractions exhibited a relatively high mobility through the soil profile. Moreover, the deeper layer at which a significant increase in F1-Cu and F2-Cu concentrations was observed, as compared to the CT plot, was clearly influenced by the PS application rate (FIGURE 4.2). Therefore, continuous Cu transfer from the more labile F1 and F2 fractions to the more stable F3 fraction should have taken place.

These two hypotheses are also supported by the findings of the study of Guan et al. (2011). They reported, based on bench experiments, that livestock manure addition to a level of 1% (to bulk soil by weight), spiked with different Cu^{2+} concentrations, induced a decrease in Cu extraction by weak acids (exchangeable and weakly adsorbed fractions), leading to an increase in the less mobile OM-Cu fraction. An increase in the livestock manure addition to 3%, however, enhanced Cu mobility. According to authors, this could be explained by the increment in the amount of soluble organic ligands, which favors complexation of Cu with ligands instead of adsorption to soil OM.

The Zn concentration associated with the exchangeable (F1) and adsorbed (F2) fractions within the CT plot, similar to Cu, were less than 2 mg kg^{-1}. However, the comparison of the 0–5 cm layers of the CT and PS200 plots showed an increase in the F1-Zn concentration from 0.15 to 11.7 mg kg^{-1}, respectively, *i.e.* almost 80-fold higher. Similarly, F2-Zn concentrations increased from 1.3 to 31.8 mg kg^{-1}, *i.e.* a 25-fold

increase. Therefore, the first two fractions respectively represented 6.2 and 16.9% of the SUMF-Zn within the PS200 topsoil layer, jointly accounting for a larger portion than the organically bound fraction. Interestingly, this substantial contribution within the surface layer was not transferred through the soil profile to deeper layers. A significant difference in F1-Zn concentration between amended and non-amended plots was observed only until 5–10 cm depth in the PS50 and PS100 plots, and to 10–15 cm in the PS200 plot. Likewise, the F2-Zn concentration increased significantly until 5–10 cm in the PS50 and PS100 plots, and up to 20–25 cm in the PS200 plot.

The Zn fraction bound to OM (F3) was the only fraction significantly influenced by PS amendments until the deepest layer (25–30 cm), except for the 50 $m^3 ha^{-1} year^{-1}$ dose. The F3-Zn concentration increased from 9.1 mg kg^{-1} (CT) to 35.7 mg kg^{-1} (PS200) within the 0–5 cm layer, corresponding to 9.0 and 19.0% of the SUMF-Zn, respectively.

The Zn concentration associated with amorphous oxyhydroxides (F4) increased from 2.9 mg kg^{-1} (CT) to 11.4 mg kg^{-1} (PS200) within the 0–5 cm layer, *i.e.* a 4-fold increase. The influence of PS spreading was observed until 5–10 cm depth for both PS50 and PS100 plots, and up to 10–15 cm for the PS200 plot. The Zn concentration associated with crystalline oxides (F5) slightly increased from 9.7 mg kg^{-1} (CT) to 15.7mg kg^{-1} (PS200) within the 0–5 cm layer. PS amendments influenced F5-Zn amounts only within the 0–5 cm layer for the lowest PS dose (50 m^3 ha^{-1} $year^{-1}$), and up to 10–15 cm for the highest doses (100 and 200 m^3 ha^{-1} $year^{-1}$).

The correlation between the increased F3-Zn concentration within the upper layers of the amended plots (FIGURE 4.2) and the higher levels of organic C (TABLE 3.1; GUBIANI et al., 2012) was also followed by the increased F2-Zn concentration, both resulting in the SUMF-Zn distribution profile (FIGURE 4.4). Within the PS200 0–5 cm layer, exogenous Zn [Σ(PS200-F1 to -F5) – Σ(CT-F1 to -F5)] was distributed as follows: F2 = 36.7%; F3 = 32.0%; other fractions = 31.3%. At 10–15 cm, the deepest layer in which SUMF-Zn was significantly influenced by the PS200 dose (TABLE 4.1), the exogenous Zn distribution [Σ(PS200-F1 to -F4) – Σ(CT-F1 to -F4)] was: F2 = 24.6%; F3 = 52.0%; other fractions = 23.4%.

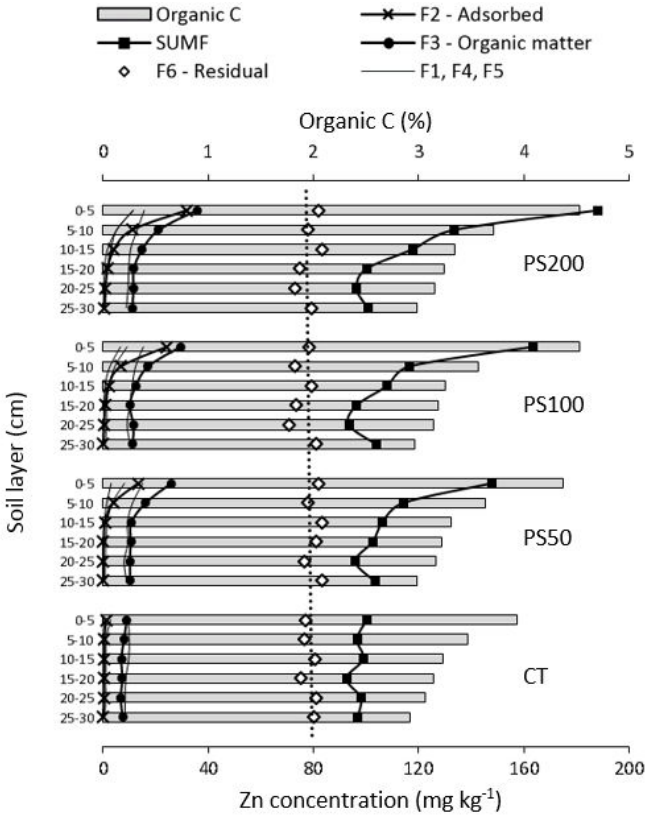

Figure 4.4 – Zn fractions, SUMF and soil organic C profile within CT, PS50, PS100 and PS200 plots.

In addition to the OM pool, Zn was also found in more labile fractions (mainly adsorbed, F2) within the upper soil layers. Since this affinity was not observed in deeper layers, and considering the marked influence of PS amendments (especially the 200 m^3 ha^{-1} $year^{-1}$ dose) on Zn accumulation in F4 (amorphous oxyhydroxides), two hypotheses were put forward:

(i) Exogenous Zn was primarily weakly adsorbed in the exchangeable (F1) and adsorbed (F2) fractions, and subsequently retained via stronger interaction mechanisms such as surface complexation or precipitation. This is supported by the fact that F1-Zn and F2-Zn exhibited a considerable increase in their concentrations – 80-fold and 25-fold, respectively, when comparing the PS200 0–5 cm layer with the CT plot – and F2 accounted for the largest part of the exogenous Zn distribution – 36.7% – within the 0–5 cm layer. However, the PS application rates of 50 and 100 m^3 ha^{-1} $year^{-1}$ led to a significant increase in F1-Zn and F2-Zn only until the 5–10 cm soil layer. Moreover, Zn associated with amorphous oxyhydroxides (F4) increased its concentrations until the same 5–10 cm layer, within the PS50 and PS100 plots (FIGURE 4.2). Clay minerals and amorphous oxyhydroxides (part of the soil clay

fraction, almost 70% in the present soil) were likely involved in these processes, by complexing or precipitating previously adsorbed Zn.

The adsorption affinity of exogenous Zn by clay minerals is well documented in the literature (ISAURE et al., 2005; MANCEAU et al., 2004; SCHEINOST et al., 2002), and has been confirmed by many studies (ASADA et al., 2012; BORGES & COUTINHO, 2004; GIROTTO et al., 2010; KABALA & SINGH, 2001; L'HERROUX et al., 1997). Several authors have reported a major transformation of Zn present in labile and readily available fractions to more stable fractions, such as OM and Fe and Mn oxyhydroxides in soils amended with an exogenous Zn source (NASCIMENTO et al., 2002; SCHUMAN, 1986; SIMS & PATRICK, 1978; XIANG et al., 1995).

(ii) Part of the Zn added was already associated with metal oxyhydroxides in the PS. This is supported by the fact that concentrations of Zn bound to amorphous oxyhydroxides (F4) and crystalline oxides (F5) significantly increased within the upper soil layers of PS-amended plots, as compared to the CT plot (FIGURE 4.2). Results from L'Herroux et al. (1997) and Hsu & Lo (2001), that found a preponderance of Zn bound to Fe and Mn oxides (67% and 35–49%, respectively) in PS effluents, reinforce this hypothesis.

4.1.4 Remarks

Five extractable fractions and a residual fraction in which Cu and Zn occurred within the soil profile were assessed, comparing natural contents with plots subjected to long-term PS spreading as fertilizer, at different rates, for 11 years. The *m*GSC protocol proved to be suitable for the tested soil, providing reproducible data and satisfactory HM recovery rates. This allowed comparing the HM concentration between the control and the three PS-amended soils, as well as assessing the HM migration through progressively deeper layers within each particular plot. The OM fraction played a leading role in exogenous Cu and Zn fractionation, consistent with the high accumulation of SUMF, F3 and the organic C in the soil. The results also indicated that the adsorbed fraction (F2) was important for exogenous Zn fractionation within upper soil layers.

The background HM concentration within the soil was relatively high due to its basaltic rock parent material. Over 70% of the original Cu and Zn contents were found in the residual fraction, not susceptible to mobilization. After PS spreading, exogenous HM were distributed entirely among the first five fractions of the protocol: exchangeable, adsorbed, OM, amorphous oxyhydroxides and crystalline oxides. Since these fractions are considered to be subject to mobilization through the soil profile, one would expect to find increased Cu and Zn concentrations at deeper layers as a consequence of the increased PS doses. However, this influence was observed only to a certain extent. Pig slurry rates of 50 and 100 m^3 ha^{-1} $year^{-1}$ influenced the SUMF-Cu and SUMF-Zn concentrations only within the topmost soil layer (0–5 cm), while the 200 m^3 ha^{-1} $year^{-1}$ treatment induced a significant concentration increase until the 10–15 cm soil layer, as compared to the CT plot. Moreover, the mass balance between the HM amounts added with the 22 PS applications and the HM concentration found within the soil 0–30 cm profile after 11 years was evidence that accumulation within the surface soil profile was the main fate of exogenous Cu and Zn.

Nevertheless, Figure 4.2 indicates that migration of the readily available HM exchangeable (F1) and adsorbed (F2) fractions to deeper soil layers is dependent on the PS application rate. Moreover, the HM fraction bound to OM (F3) significantly increased its concentration until the deepest layer evaluated (25–30 cm), for both Cu and Zn under the 50, 100 and 200 m^3 ha^{-1} $year^{-1}$ PS treatments (except for Zn within the PS50 plot), as compared to the CT plot. Therefore, increasing PS additions – overdose or over time – may lead to groundwater contamination.

The studied soil profile (0–30 cm) coincides with the plant root zone. The highest available HM concentrations were found within the PS200 0–5 cm soil layer: F1-Cu + F2-Cu = 11.3 mg kg^{-1} (FIGURE 4.2; FIGURE 4.3; SUPPORTING INFORMATION SI-1) and F1-Zn + F2-Zn = 43.5 mg kg^{-1} (FIGURE 4.2; FIGURE 4.4; SUPPORTING INFORMATION SI-2). Based on field observations, the Cu and Zn concentrations considered to be phytotoxic to most agronomic crops were 60 and 120 mg kg^{-1}, respectively for Mehlich-3 extractable Cu and Zn (HARDY et al., 2008). The field study results investigated here were thus consistent with the absence of Cu- and Zn-related phytotoxic problems.

4.2 PHASE ASSOCIATION

4.2.1 Mass distribution and mineral characterization of soil density fractions

The mass recovery of the soil density fractionation protocol was at 88.5 ± 5.3% for the CT sample and 85.5 ± 0.6% for the PS200 sample, as compared to the initial 6.0 g of bulk sample. The losses may be attributed to (a) sample direct contact with the sonication probe, resulting in noticeable leftover soil on probe after each sonication step and (b) dissolution/suspension of particles smaller than 0.2 μm (the adopted threshold for centrifugation) in the sodium polytungstate solution.

Figure 4.5a presents the distribution (in percentage, normalized to 100%) of the soil mass among density fractions of the CT and PS200 samples. In the CT sample, the three lightest fractions – d<1.9, 1.9<d<2.25 and 2.25<d<2.5 – accounted for 12.1% of the mass distribution (4.1, 3.7 and 4.3%, respectively). Most of the soil mass – 81.2% – was found in the 2.5<d<2.7 fraction. The d>2.7 fraction represented 6.6% of the mass distribution. In the PS200 sample, as compared to the CT sample, the contribution of the lightest fractions – d<1.9, 1.9<d<2.25 and 2.25<d<2.5 – to the soil mass distribution slightly increased to 16.5% (7.2, 2.7 and 6.6%, respectively). Conversely, the contribution of the 2.5<d<2.7 fraction slightly decreased to 76.9%. The d>2.7 fraction accounted for 6.6% of the mass distribution.

The X-ray diffractograms of density fractions from the CT and PS200 samples were very similar (data not shown). Therefore, Figure 4.5b presents only the mineral composition of the CT density fractions. The heaviest fraction – d>2.7 – contained the heavy Fe and Ti oxides anatase (d = 3.89 g cm^{-1}), hematite (d = 5.26 g cm^{-3}), ilmenite (d = 4.79 g cm^{-3}), rutile (d = 4.25 g cm^{-3}) and some inosilicate mineral from the pyroxene group. The 2.5<d<2.7 fraction contained quartz (d = 2.66 g cm^{-3}), the phyllosilicates kaolinite (d = 2.63 g cm^{-3}) and vermiculite (d = 2.50 g cm^{-3}), but also the iron oxide hematite. The 2.25<d<2.5 fraction contained cristobalite (d = 2.33 g cm^{-3}) and the hydroxide mineral gibbsite (d = 2.44 g cm^{-3}), as well as kaolinite, vermiculite and hematite. The latter minerals were also present in the 1.9<d<2.25 and d<1.9 fractions. Moreover, except for the heaviest d>2.7 fraction, the diffractograms were characterized by a large diffusion band centered around 24º (2θ), which may be

attributed to the presence of either OM or low-crystallized mineral phases (BONNARD et. al, 2012).

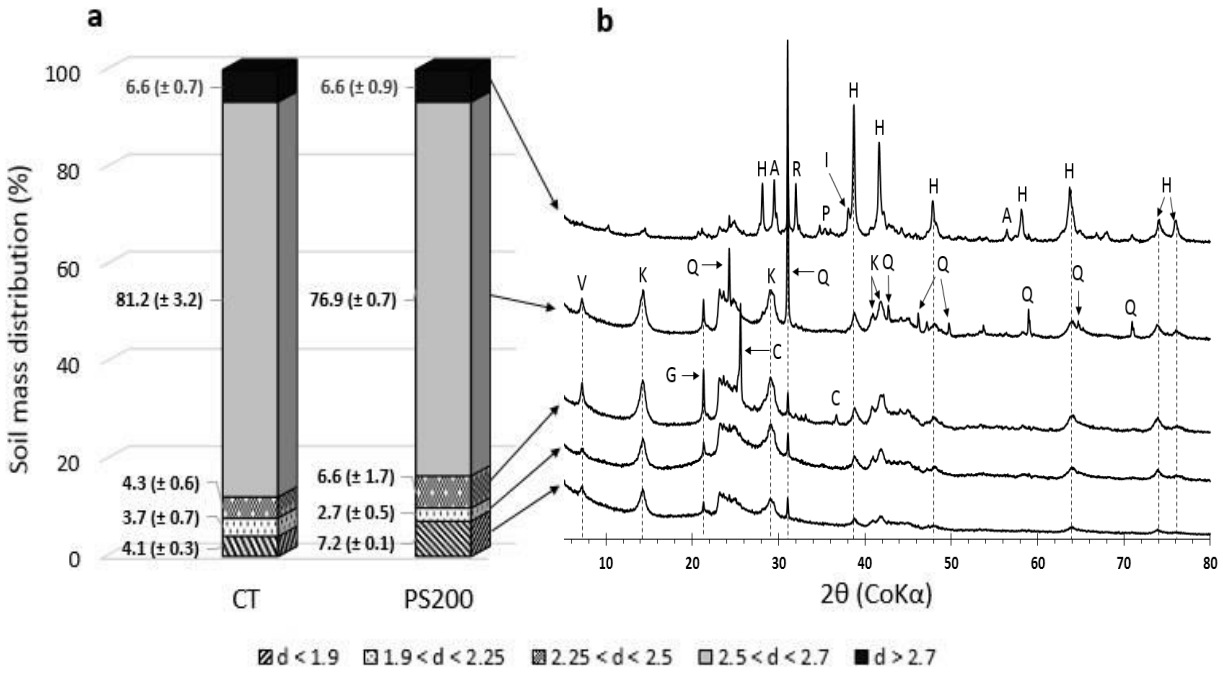

Figure 4.5 – Soil mass distribution (in percentage) among density fractions and X-ray diffraction characterization. C=Cristobalite, G=Gibbsite, V=Vermiculite, K=Kaolinite, Q=Quartz, A=Anatase, R=Rutile, P=Pyroxene, I=Ilmenite, H=Hematite.

The phyllosilicates kaolinite and vermiculite were detected in the most abundant density fraction (2.5<d<2.7), but also in the lighter 2.25<d<2.5, 1.9<d<2.25 and d<1.9 fractions, *i.e.* outside of their expected density range. The same occurred for hematite, detected mainly in the d>2.7 fraction, but also presenting diffraction peaks of lower intensity in lighter density fractions (dashed lines, FIGURE 4.5b). This may be explained by the incomplete breaking of soil aggregates during the sonication step. Such organo-mineral aggregates within light-density fractions were previously observed by SEM-EDX analyses (EL-MUFLEH et al., 2014) and OM oxidation and laser particle size analyses (BADIN et al., 2009) in stormwater sediments. Moreover, the theoretical density of organo-phyllosilicates complexes associated with different OM contents can be as low as ~2 g cm^{-3} (BONNARD et. al, 2012).

Nevertheless, the minerals detected primarily in the 2.5<d<2.7 fraction – quartz, kaolinite and vermiculite – are likely the most abundant minerals in the soil and were detected mainly in its target density fraction: 2.5<d<2.7. This was supported by

the following observations: (i) the large contribution of the 2.5<d<2.7 fraction to the bulk soil mass (FIGURE 4.5a); (ii) the small contribution of lighter fractions to the bulk soil mass (FIGURE 4.5a); (iii) the low organic C and N concentration in the 2.5<d<2.7 fraction (FIGURE 4.6); (iv) the high organic C and N concentration in lighter fractions (FIGURE 4.6); and (v) the very clayey texture of the soil (67.8%, SECTION 3.1.2).

It is worth noting that hematite was also detected in the 2.5<d<2.7 fraction, though some of the diffraction peaks attributed to this mineral in the d>2.7 fraction are absent in the diffractogram of the 2.5<d<2.7 fraction, and other peaks are clearly at lower intensity (dashed lines in FIGURE 4.5b, diffractograms of different fractions were recorded under the same experimental configuration). Thus, hematite may have occurred at minor or residual proportion in the composition of the 2.5<d<2.7 fraction. Nevertheless, this iron oxide is acknowledged for a high HM sorption capacity (GIRIJA et al., 2013) and its presence in the 2.5<d<2.7 fraction, even likely at low concentration, must not be neglected in the discussion of Cu and Zn linkage to be presented.

4.2.2 Organic C and N

The organic C concentration (in mg g^{-1} of fraction) within the five density fractions of the CT sample were: d<1.9 = 241.9 mg g^{-1}, 1.9<d<2.25 = 101.4 mg g^{-1}, 2.25<d<2.5 = 53.3 mg g^{-1}, 2.5<d<2.7 = 20.4 mg g^{-1} and d>2.7 = 0 mg g^{-1}. The CT bulk sample presented organic C concentration at 43.2 mg g^{-1}. In the PS200 sample, the organic C concentration within the same fractions were: d<1.9 = 228.3 mg g^{-1}, 1.9<d<2.25 = 98.3 mg g^{-1}, 2.25<d<2.5 = 39.0 mg g^{-1}, 2.5<d<2.7 = 18.3 mg g^{-1} and d>2.7 = 0 mg g^{-1}. The PS200 bulk sample presented organic C concentration at 50.5 mg g^{-1}. Figure 4.6a shows the decreasing in the organic C concentration as a result of the increase in the density range of each fraction.

The N concentration (in mg g^{-1} of fraction) within the density fractions of the CT sample were: d<1.9 = 15.5 mg g^{-1}, 1.9<d<2.25 = 7.4 mg g^{-1}, 2.25<d<2.5 = 4.4 mg g^{-1}, 2.5<d<2.7 = 1.4 mg g^{-1} and d>2.7 = 0.01 mg g^{-1}. The CT bulk sample presented N concentration at 3.1 mg g^{-1}. In the PS200 plot, the N concentration within the same fractions were: d<1.9 = 15.9 mg g^{-1}, 1.9<d<2.25 = 7.5 mg g^{-1}, 2.25<d<2.5 = 3.2 mg g^{-1}, 2.5<d<2.7 = 1.3 mg g^{-1} and d>2.7 = 0.01 mg g^{-1}. The PS200 bulk sample presented N

concentration at 3.8 mg g^{-1}. Therefore, the N concentrations within each density fraction followed the same trend observed for the organic C, *i.e.* a decrease in the concentration as a result of the increase in the density range of each fraction (FIGURE 4.6b).

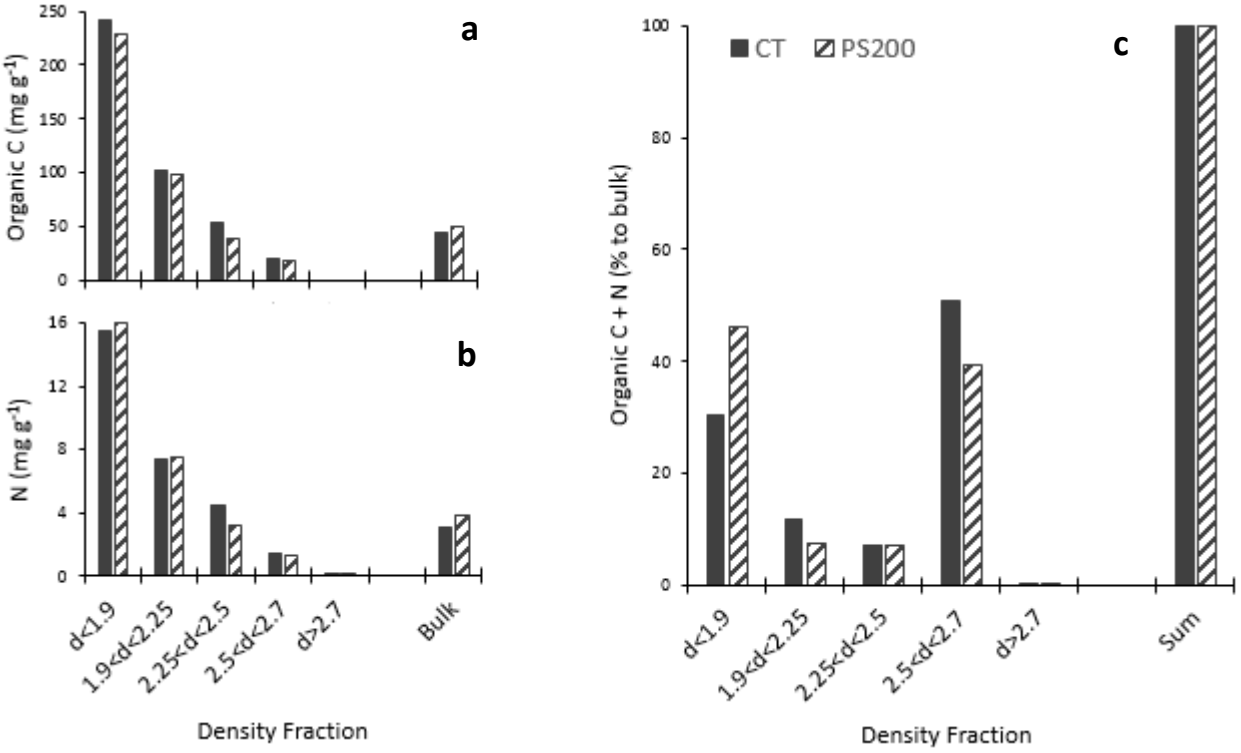

Figure 4.6 – (a) Organic C and N concentrations (in mg g^{-1} of fraction) within the five density fractions of CT and PS200 samples. (b) Percentage distribution of organic C + N amongst density fractions of CT and PS200 samples (recoveries normalized to 100%).

Comparing the sum of organic C + N concentrations within each density fraction to the organic C + N concentrations detected in the bulk samples, the recovery of organic C + N after the fractionation protocol was at 75.3% for the CT sample and at 70.7% for the PS200 sample. The organic C + N concentration within each density fraction was multiplied with the mass of soil detected in the respective fraction, and finally normalized to 100%. Therefore, the amounts of organic C + N detected in the d<1.9 fraction represented 30.4% of the total organic C + N in the CT bulk sample, and 46.0% of the total organic C + N in the PS200 bulk sample. Likewise, the organic C + N detected in the 2.5<d<2.7 fraction represented 50.8% of the total organic C + N in the CT sample, and 39.2% of the of the total organic C + N in the PS200 sample. Other

density fractions accounted together for 18.8% (CT) and 14.8% (PS200) of the total organic C + N (FIGURE 4.6c).

Despite the high organic C and N concentrations detected in the d<1.9 fraction, as compared to the other fractions and bulk samples (FIGURE 4.6a and 4.6b), the distribution of organic C + N (in percentage to the bulk soils) was roughly split between the d<1.9 and 2.5<d<2.7 fractions (FIGURE 4.6c). This was due to the large contribution of the 2.5<d<2.7 fraction to the bulk soil mass, nearly 20 times more abundant than the d<1.9 fraction (FIGURE 4.5a). Moreover, the organically amended soil (PS200) contained a higher percentage of organic C + N in the light d<1.9 fraction, as compared to the percentage of organic C + N in the same fraction of the non-amended soil (CT). The opposite trend was observed in the percentage distribution of organic C + N in 2.5<d<2.7 fraction, *i.e.* the PS200 sample presented a lower organic C + N proportion in this fraction, as compared to the CT sample.

4.2.3 Cu and Zn

The HM concentration detected within each density fraction and bulk samples of CT and PS200 are presented in Table 4.3. The Cu concentration in the CT bulk sample was at 122.4 ± 16.7 mg kg^{-1}, whereas the Cu concentration in the PS200 sample was at 174.1 ± 9.5 mg kg^{-1}. It represented thus a Cu enrichment of 51.7 ± 19.2 mg kg^{-1}, explained by the continued application of PS on the soil at the rate of 200 m^3 ha^{-1} $year^{-1}$ over 11 years. The Zn concentration in the CT bulk sample was at 105.8 ± 12.3 mg kg^{-1}, and at 206.6 ± 10.7 mg kg^{-1} in the PS200 bulk sample. It represented thus a Zn enrichment of 100.8 ± 16.3 mg kg^{-1} after 11 years of PS application. These results are in close agreement with the HM concentrations found by Mallmann (2013; reproduced in TABLE 3.1) and in the present study via sequential extractions (TABLE 4.1).

The Cu and Zn concentrations within each density fraction were found at levels slightly lower than within their corresponding bulk samples (TABLE 4.3), likely due to HM losses during the fractionation protocol. Indeed, the HM recoveries, *i.e.* the sum of the HM contents detected within each density fraction as compared to the bulk sample,

were at 76.8% (Cu) and 88.3% (Zn) in the CT sample, and at 60.3% (Cu) and 57.5% (Zn) in the PS200 sample.

Table 4.3 – Cu and Zn concentrations within the density fractions and bulk soil of the CT and PS200 samples.

	Density Fraction	Cu (mg kg^{-1} of fraction or bulk)			Zn (mg kg^{-1} of fraction or bulk)		
		Solid sample	Rinsing water	Total	Solid sample	Rinsing water	Total
CT sample	d<1.9	92.7 ± 3.1	2.6 ± 0.8	95.3 ± 3.2	62.4 ± 3.1	<LoQ*	62.4 ± 3.1
	1.9<d<2.25	67.3 ± 5.1	2.7 ± 1.4	70.0 ± 5.3	60.2 ± 6.3	<LoQ	60.2 ± 6.3
	2.25<d<2.5	89.2 ± 10.0	0.8 ± 0.1	90.0 ± 10.0	86.6 ± 14.0	<LoQ	86.6 ± 14.0
	2.5<d<2.7	92.5 ± 7.2	0.9 ± 0.1	93.4 ± 7.2	95.8 ± 12.4	0.2 ± 0.2	96.1 ± 12.4
	d>2.7	116.2 ± 11.1	1.2 ± 0.1	117.4 ± 11.1	102.5 ± 3.2	<LoQ	102.5 ± 3.2
	Bulk	122.4 ± 16.7	-	122.4 ± 16.7	105.8 ± 12.3	-	105.8 ± 12.3
PS200 sample	d<1.9	133.5 ± 2.2	2.9 ± 0.1	136.4 ± 2.2	89.0 ± 3.8	1.3 ± 2.2	90.3 ± 4.4
	1.9<d<2.25	78.5 ± 5.9	7.6 ± 0.8	86.2 ± 6.0	73.6 ± 4.7	1.1 ± 1.9	74.7 ± 5.1
	2.25<d<2.5	105.0 ± 5.3	1.4 ± 0.6	106.4 ± 5.3	124.8 ± 8.8	0.7 ± 1.3	125.5 ± 8.9
	2.5<d<2.7	99.6 ± 6.4	2.9 ± 0.1	102.4 ± 6.4	122.9 ± 9.0	2.6 ± 0.2	125.5 ± 9.0
	d>2.7	104.2 ± 13.5	3.5 ± 0.3	107.7 ± 13.5	118.7 ± 20.4	<LoQ	118.7 ± 20.4
	Bulk	174.1 ± 9.5	-	174.1 ± 9.5	206.6 ± 10.7	-	206.6 ± 10.7

* LoQ: Limit of quantification.

The contribution of the HM concentration within each fraction to the bulk soil (as opposed to the HM concentration within the fraction itself) was assessed in order to evaluate the fate of the exogenously added Cu and Zn. Heavy metal losses to the LST solution in the CT sample were ascribed to the losses of organo-mineral particles or aggregates smaller than 0.2 µm (the centrifugation threshold), and their distribution calculated according to Equation 2. In the PS200 sample, Equation 2 was used to account for HM losses in each density fraction until reaching the organic C + N recovery threshold in this sample (70.6%). The HM losses above it were attributed to a new fraction: soluble in LST (s-LST) (SECTION 3.3.3).

The HM amounts computed in each density fraction (expressed in mg of HM per kg of bulk sample), before (CT) and after (PS200) the PS inputs, are presented in Figures 4.7a (Cu) and 4.8b (Zn). Moreover, the Cu and Zn enrichment (*i.e.* the increase in concentration: HM–PS200 - HM–CT) within each density fraction and the resulting percentage distribution of exogenous HM amongst the five density fractions are presented in Figures 4.7b (Cu) and 4.8b (Zn).

The Cu concentration in the CT bulk sample (122.4 mg kg^{-1}) was mainly accounted within the 2.5<d<2.7 fraction, at 90.2 mg kg^{-1} of bulk sample. The d<1.9 fraction exhibited a Cu concentration at 12.5 mg kg^{-1} of bulk sample, while the Cu

concentrations in other fractions were below 8 mg kg^{-1} each. In the PS200 bulk sample (Cu total = 174.1 mg kg^{-1}), the 2.5<d<2.7 fraction also contained most of the Cu, at 98.8 mg kg^{-1} of bulk sample. However, as compared to the CT sample, the s-LST and d<1.9 fractions of the PS200 sample markedly increased their concentrations, to 17.9 mg kg^{-1} and 33.4 mg kg^{-1} of bulk sample, respectively. As a result, the exogenous Cu was distributed as follows: 34% in the s-LST fraction, 40% in the d<1.9 fraction, 1% in the 1.9<d<2.25 fraction, 9% in the 2.25<d<2.5 fraction, 16% in the 2.5<d<2.7 fraction and 0% in the d>2.7 fraction.

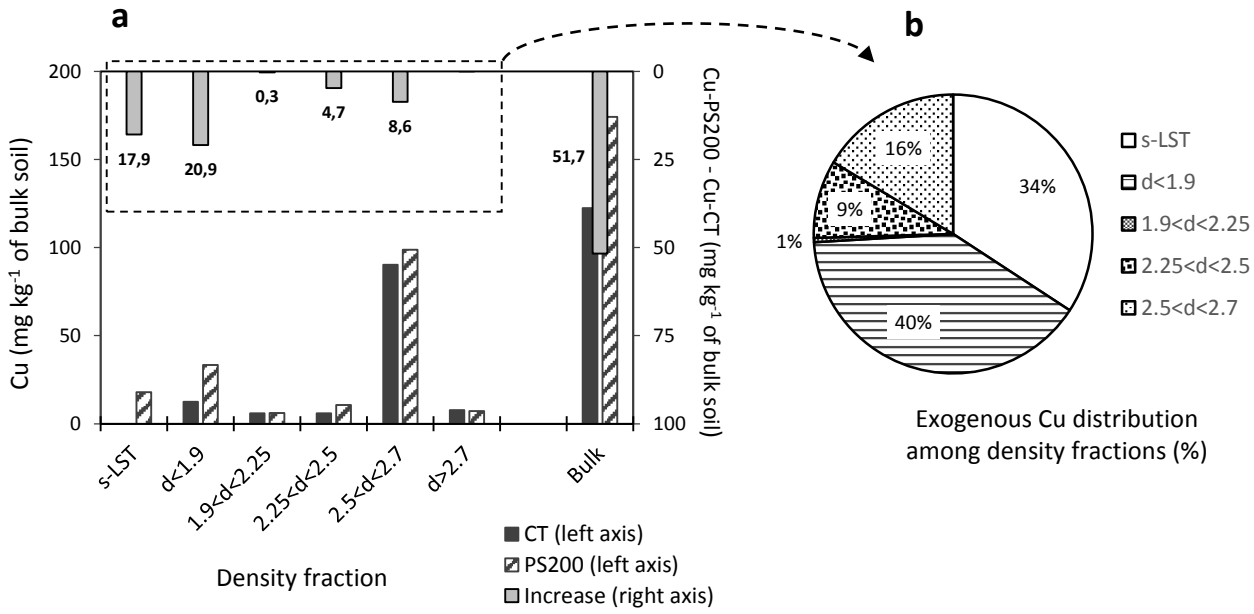

Figure 4.7 – (a) Cu concentration within soil density fractions (relative to the bulk soil mass) in the CT and PS200 samples and Cu concentration increase within each fraction (PS200 - CT). (b) Resulting exogenous Cu distribution.

The Zn concentration in the CT bulk sample (105.8 mg kg^{-1}) was mainly accounted within the 2.5<d<2.7 density fraction, at 84.3 mg kg^{-1} of bulk sample. The contribution of other density fractions to the Zn concentration in the bulk sample was below 7 mg kg^{-1} each. In the PS200 sample (Zn total = 206.6 mg kg^{-1}), marked increases in the Zn concentration within density fractions, as compared to the CT sample, were observed in the s-LST (27.2 mg kg^{-1} of bulk sample), d<1.9 (34.3 mg kg^{-1} of bulk sample) and 2.5<d<2.7 (118.2 mg kg^{-1} of bulk sample) fractions. As a result, the exogenous Zn was distributed as follows: 27% in the s-LST fraction, 28% in the

d<1.9 fraction, 3% in the 1.9<d<2.25 fraction, 8% in the 2.25<d<2.5 fraction, 33% in the 2.5<d<2.7 fraction and 1% in the d>2.7 fraction.

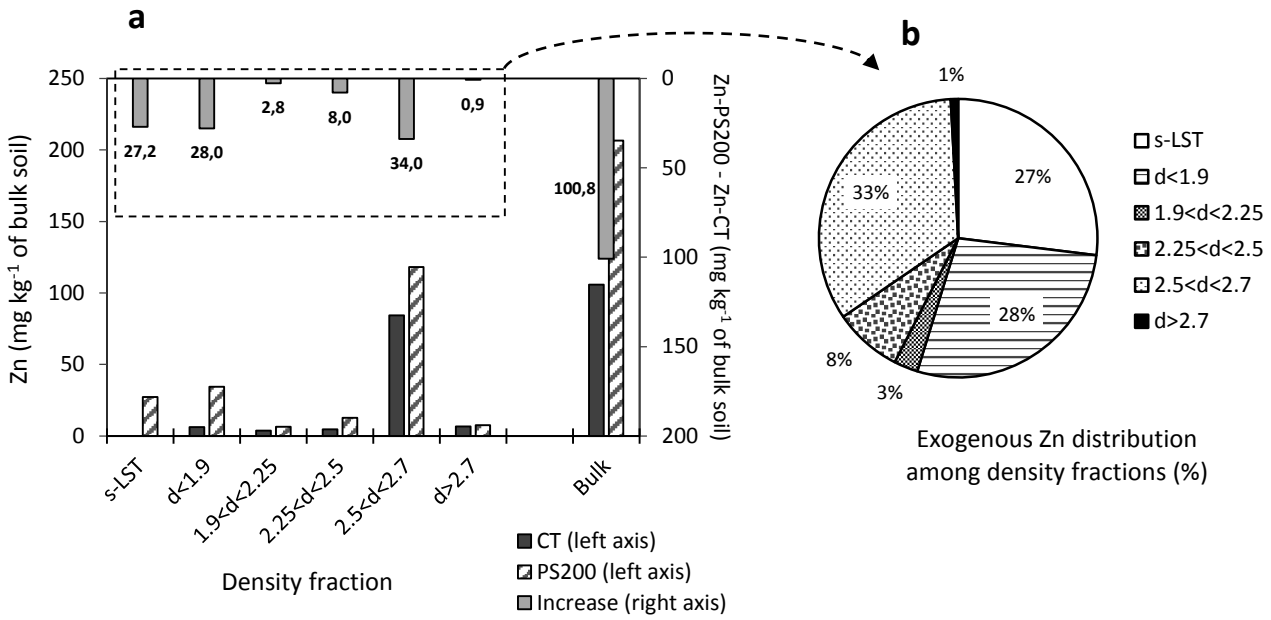

Figure 4.8 – (a) Zn concentration within soil density fractions (relative to the bulk soil mass) in the CT and PS200 samples and Zn concentration increase within each fraction (PS200 - CT). (b) Resulting exogenous Zn distribution.

4.2.4 Discussion

4.2.4.1 Cu and Zn natural occurrence

The 2.5<d<2.7 fraction contained 73.7% of the Cu (90.2 mg out of 122.4 mg kg^{-1} of bulk sample) and 79.7% of the Zn (84.3 out of 105.8 mg kg^{-1} of bulk sample) detected within the CT sample. Conversely, only 10.2% of the Cu (12.5 mg out of 122.4 mg kg^{-1} of bulk sample) and 6.0% of the Zn (6.3 out of 105.8 mg kg^{-1} of bulk sample) were found within the d<1.9 fraction of the CT sample (FIGURES 4.7 and 4.8). Therefore, two main trends were observed when comparing the HM concentration with the soil mass and organic content detected in each density fraction of the CT sample:

(i) the mass of soil detected in the 2.5<d<2.7 fraction of the CT sample (81.2% of the bulk; FIGURE 4.5a) nearly matched the distribution of the natural Cu and Zn within this same fraction (73.7% and 79.7% of the total, respectively);

(ii) the organic C + N distribution within the d<1.9 fraction (30.4% of the bulk, FIGURE 4.6c) did not match the Cu and Zn distribution within this same fraction (10.2% and 6.0% of the total, respectively). In other words, the OM enrichment towards the light d<1.9 fraction, resulting from the density fractionation protocol, did not lead to a HM enrichment towards this fraction.

These trends display together evidence that most of the soil pedogenic Cu and Zn were associated with the minerals present in the 2.5<d<2.7 fraction: kaolinite, vermiculite and hematite. Quartz was deliberately omitted because it is acknowledged for being relatively inert and therefore for holding very low HM contents in soils (GAMBLE et al., 2000).

It was reported via sequential extractions that 70.5% of the Cu and 76.9% of the Zn of natural occurrence (CT plot, 0–5 cm) were found in the residual fraction of the *m*GSC protocol (FIGURE 4.1, SUPPORTING INFORMATION SI-1 and SI-2). These percentages are in close agreement with the 73.7% of Cu and 79.7% of Zn of natural occurrence detected in the 2.5<d<2.7 density fraction. The residual fraction in sequential extractions represents the most stable HM fraction, tightly bound to or incorporated into the crystal structures of primary and secondary minerals and thus accounting for HM related to the parent material (RATUZNY et al., 2009). The results obtained via soil density fractionation and the comparison with sequential extractions display thus evidence that kaolinite, vermiculite and hematite are the likely the main pools for the Cu and Zn of natural occurrence within the studied soil.

The result for Cu is rather unexpected, because its biogeochemistry is considered mainly controlled by its interactions with natural OM (MANCEAU et al., 2010). However, the majority of investigations asserting OM as the main Cu pool within soils were conducted in polluted soils (*e.g.* JACOBSON et al., 2007; STRAWN & BAKER, 2008), differently from the CT sample analysed in the present study. Nevertheless, It has been observed that Cu in soils may be sorbed onto clay minerals, particularly in soils with low organic matter content (FURNARE et al., 2005). Moreover, inner-sphere sorption of Cu onto phyllosilicates have been observed by distinct mechanisms consistent with reduced exchangeability (CHEAH et al., 2000; STRAWN et al., 2004, FURNARE et al., 2005). There is no evidence to reject that such low-

exchangeability mechanisms of natural Cu incorporation onto phyllosilicates occurred in the soil here studied.

The results for Zn, on the other hand, are in line with several previous observations on its natural occurrence within soils. Manceau et al. (2005) showed that Zn natural contents were most likely incorporated in the gibbsitic interlayer of vermiculite in a clayey paddy soil. According to the authors, this incorporation in interlayered minerals would be a significant geochemical process for Zn sequestration in Earth's near-surface environments, as suggested by other studies (PANFILI et al., 2002; MANCEAU et al., 2003; MANCEAU et al., 2004). More recently, it was proposed that Zn was preferentially located at the octahedral positions of vermiculite in naturally metal-enriched soils (FERNÁNDEZ-CALIANI et al., 2013).

However, the possible mechanisms of Cu and Zn incorporation into the mineral matrix of the soil here investigated may be further analysed and discussed, at the molecular level, via synchrotron-based X-ray absorption techniques. This will be pursued in Section 4.3.

4.2.4.2 Cu and Zn exogenous distribution

The comparison between the Cu and Zn amounts detected within each density fraction, before (CT) and after (PS200) the PS amendments, indicated that exogenous Cu and Zn distributed mainly among the s-LST, d<1.9 and 2.5<d<2.7 fractions. Nevertheless, the distribution followed different trends for each HM, revealing their distinct affinities for the soil phases following PS applications.

The distribution of exogenous Cu indicated a great affinity for the OM-rich d<1.9 fraction, as suggested by its 40% contribution. Conversely, the mineral-rich 2.5<d<2.7 fraction accounted for only 16% of the exogenous Cu, in spite of the major contribution of this fraction for the bulk soil mass and for the Cu of natural occurrence. In addition, the s-LST fraction accounted for 34% of the exogenous Cu distribution.

The exogenous Cu distribution reported via sequential extractions indicated 66.4% in the OM fraction and 16.1% in the adsorbed fraction of the *m*GSC protocol (SECTION 4.1.3.2). The latter (adsorbed = 16.1%) may be directly compared to the exogenous Cu share of the 2.5<d<2.7 density fraction (16%), since it contained

minerals well known for their HM adsorption characteristics. On the other hand, the contribution of the sequentially extracted OM fraction to the exogenous Cu distribution (66.4%) was higher than the exogenous Cu distribution detected in the OM-rich d<1.9 density fraction (40%), though both approaches pointed out that OM was the main exogenous Cu pool.

The distribution of exogenous Zn indicated a great affinity for the 2.5<d<2.7 density fraction, as suggested by its 33% contribution. Nevertheless, the contribution of the s-LST fraction, at 27%, and the OM-rich d<1.9 fraction, at 28%, were also important for the exogenous Zn distribution.

The exogenous Zn distribution reported via sequential extractions indicated 32.0% in the OM fraction and 36.7% in the adsorbed fraction of the *m*GSC protocol (SECTION 4.1.3.2). Therefore, there was a close agreement between the amounts of exogenous Zn detected in the *m*GSC OM fraction (32.0%) and in the OM-rich d<1.9 density fraction (28%), as well as between the *m*GSC adsorbed fraction (36.7%) and the 2.5<d<2.7 density fraction (33%).

It is noteworthy that the 2.5<d<2.7 density fraction was asserted as the main pool for Zn of both natural (FIGURE 4.8a) and exogenous (FIGURE 4.8b) occurrence. It was hypothesized in Section 4.1.3.2 that clay minerals and oxyhydroxides are involved in exogenous Zn sorption mechanisms such as adsorption, surface complexation and precipitation, ultimately reducing Zn mobility trough the soil profile. These mechanisms may differ from mechanisms of natural Zn incorporation, discussed in Section 4.2.4.1. In both cases, the major importance of the minerals detected in the 2.5<d<2.7 fraction, *i.e.* the phyllosilicates kaolinite and vermiculite and the Fe-oxide hematite, in attenuating the mobility of PS-added Zn within the studied soil was remarkable.

4.2.5 Remarks

The use of a density fractionation protocol allowed decreasing the soil heterogeneity, resulting in soil fractions with contrasting characteristics. The light d<1.9 fraction was characterized by a high organic content and a minor contribution to the bulk soil mass, consequently hosting a very low mineral content. Conversely, the

2.5<d<2.7 fraction concentrated most of the soil mass and mineral composition (notably the phyllosilicates kaolinite and vermiculite, but also the Fe oxide hematite), while its organic concentration was very low. Based on that contrasting characteristics, it was possible to identify the soil main constituents as well as their most likely associations with the Cu and Zn of natural and exogenous occurrence.

Kaolinite, vermiculite and hematite were the main mineral phases accounting for the Cu and Zn of pedogeochemical origin, as indicated by their matching predominance within the 2.5<d<2.7 density fraction of the CT sample. These same minerals also played an important role on the immobilization of PS-added HM, notably Zn, whereas exogenous Cu was likely mainly associated to the soil OM. Finally, supported by sequential extractions results, soil density fractionation confirmed and provided further insights on the mechanisms previously proposed to control the exogenous HM fate through the soil profile.

The main drawback of the density fractionation protocol here applied were the HM losses to the LST solution, together with the unfeasibility of further analysis in this solution due to its heavy matrix characteristics (EL-MUFLEH et al., 2014). For this reason, soil density fractionation may not stand alone for a complete overview on the rather complex interactions between HM and soil constituents. Improvements to avoid or control such HM losses are strongly encouraged by the present study.

Nevertheless, the association of soil density fractionation with additional analytical approaches (*e.g.* chemical sequential extractions, X-ray diffraction and X-ray absorption spectroscopies) may certainly provide useful insights on HM behavior and associations within the soil matrix. For instance in the case of the present study, which successfully applied this approach for the first time in the context of agricultural soils that had received PS amendments over an extended period of time, *i.e.* in a “before and after” scenario.

4.3 MOLECULAR ENVIRONMENT

The k^2-weighted Cu K-edge EXAFS and Fourier transform (FT) spectra of bulk soil samples, pig slurry and Cu-containing or Cu sorbed on selected references are presented in Figure 4.9. The EXAFS spectra of the CT and PS200 soil samples

presented a distinct shoulder in the left side of the first oscillation, at 3.45 $Å^{-1}$ (vertical dashed line), as well as a deep in the second oscillation, at 6.1 $Å^{-1}$. These two well-defined spectral features were also present in both the Cu-kaolinite and Cu-vermiculite references, but absent in either the Cu-montmorillonite or the organic references Cu-acetate and Cu-thioglycol.

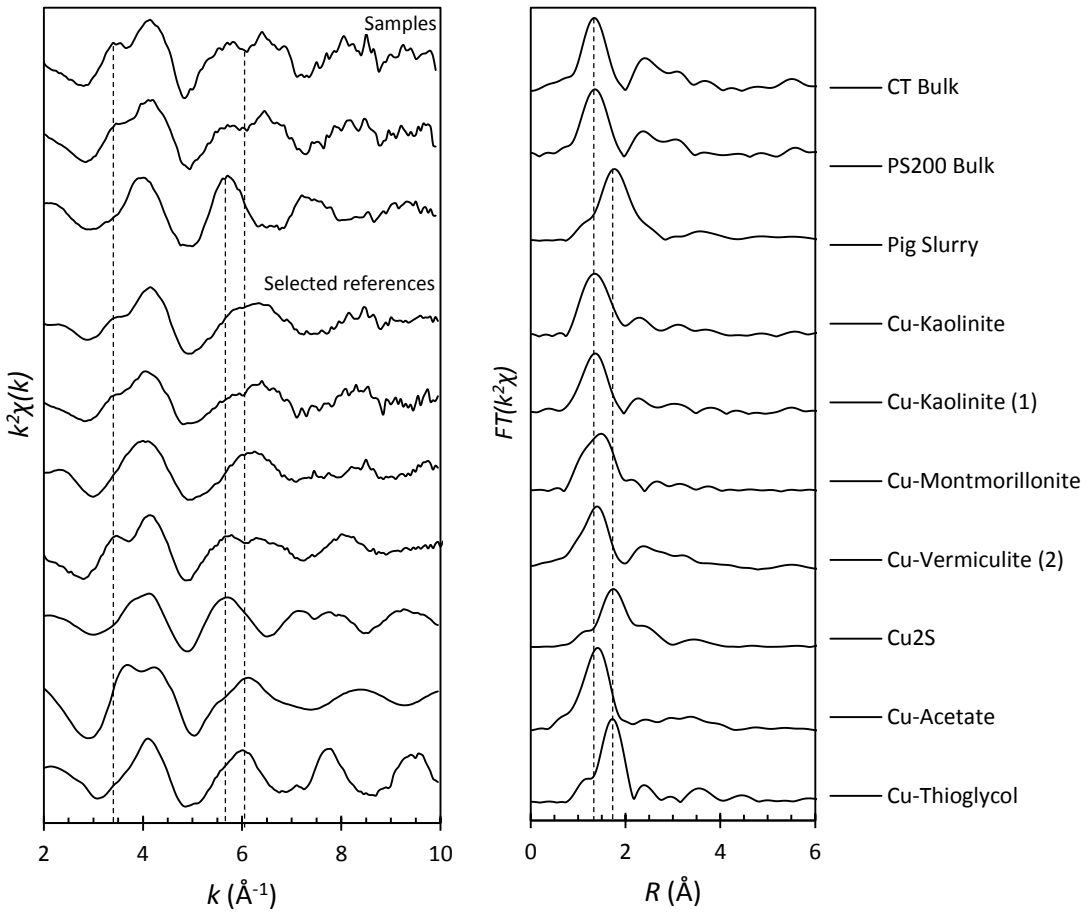

Figure 4.9 – k^2-Weighted Cu K-edge EXAFS and Fourier transform (FT) spectra of CT, PS200 and pig slurry samples as compared to Cu-containing or Cu sorbed on selected mineral and organic references. (1) Reference from Schlegel & Manceau (2013). (2) Reference from Furnare et al. (2005).

The beat features near k = 6.1 A^{-1} for Cu–kaolinite are indicative of backscatterer(s) from higher atomic shells. In this reference, Cu was shown to be sorbed in an inner-sphere, sharing edges with Al/Mg octahedra and corners with Si/Al tetrahedra. Moreover, Cu presented an irregular square bipyramidal coordination, with four equatorial oxygens at about 1.93 Å and two axial oxygens (SCHLEGEL & MANCEAU, 2013).

In the Cu-vermiculite reference, Cu was surrounded by 4 O atoms at 1.95 Å and 8 second shell O atoms at 3.14 Å. It was suggested that the Cu atoms were adsorbed above the hexagonal cavities of the clay mineral, forming multinuclear complexes (dimers) in the interlayer, as opposed to inner-sphere complexation in the Cu-kaolinite reference (FURNARE et al., 2005).

The spectrum of the pig slurry sample may be distinguished by its second EXAFS oscillation, centered at 5.85 $Å^{-1}$ (vertical dashed line), which is also present in the Cu_2S reference. Moreover, analysis of the *R*-space spectra showed that Cu nearest neighboring atom was S, as indicated by the FT peak representing the Cu first coordination shell at 1.85 Å (not phase-shifted, vertical dashed line). This same first coordination distance was present in the Cu/S containing references Cu_2S and Cu-thioglycol, as opposed to the Cu-O first neighbor in other samples and references, whose first FT peak was centered around 1.4 Å (not phase-shifted).

Figure 4.10 presents the k^2-weighted Zn K-edge EXAFS and Fourier transform (FT) spectra of bulk soil samples, pig slurry and Zn-containing or Zn sorbed on selected references. The EXAFS spectra of the bulk soil samples (CT and PS200) showed a distinct splitting in the first oscillation, at 3.75 $Å^{-1}$ (vertical dashed line). The same splitting was also found in the references containing Zn sorbed on phyllosilicates: Zn-kaolinite and Zn-HIM (hydroxy-interlayered mineral).

The origin of this splitting is discussed elsewhere, suggesting that Zn in Zn-HIM was octahedrally coordinated and mainly incorporated in the dioctahedral vacancies of gibbsitic layers, with 6 Al atoms in the second coordination shell, as reflected by the FT peak at 2.75 Å (not phase-shifted, vertical dashed line). This molecular arrangement was also reflected by the FT peak at 5.5 Å (vertical dashed line), originated from multiple scattering along the 6 collinear Zn–Al-Al axes.

In contrast, it was suggested that Zn uptake into the kaolinite reference might have occurred partly due to incorporation into vacant dioctahedral sites and partly due to substitution for Al. In the latter, the number of Al atoms in the second shell is reduced to 3. This was phenomenological reflected by the lower amplitude of FT peaks at 2.75 Å and 5.5 Å, as compared to the corresponding peaks in the Zn-HIM reference (JACQUAT et al., 2009a; JACQUAT et al., 2009b; SCHLEGEL & MANCEAU, 2007).

Moreover, the EXAFS spectra of Zn-kaolinite presented a shoulder in the left side of the second oscillation, at 5.2 $Å^{-1}$ (vertical dashed line), which was absent in the Zn-HIM reference. This curvature was also observed in the spectra of bulk soil

samples, being more pronounced in the CT sample. In addition, the FT peak at 5.5 Å slightly shifted to a shorter distance in the Zn-HIM reference, as opposed to Zn-kaolinite and the soil samples. Therefore, despite the strong resemblance between Zn-kaolinite and Zn-HIM references, a comprehensive comparison of the spectra suggested that Zn-kaolinite presented characteristics more in agreement with the soil samples than Zn-HIM.

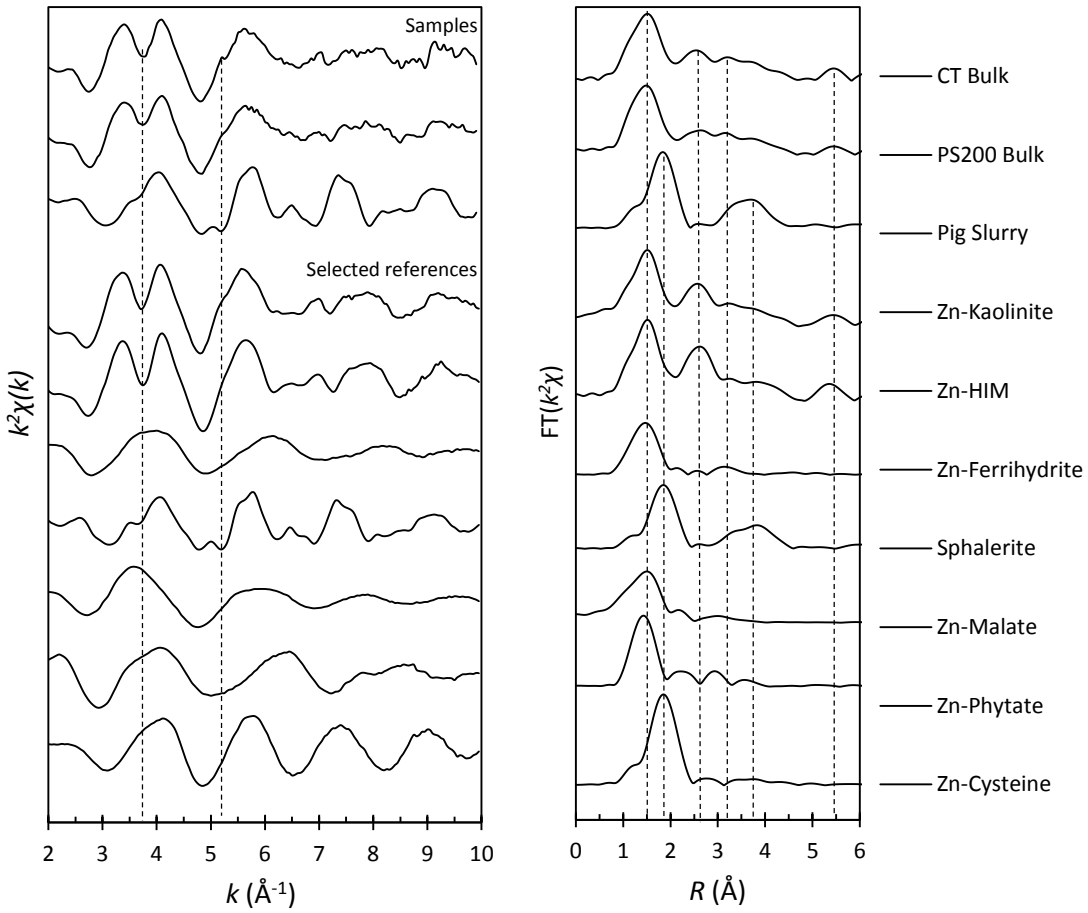

Figure 4.10 – k^2-Weighted Zn K-edge EXAFS and Fourier transform (FT) spectra of CT, PS200 and pig slurry samples as compared to Zn-containing or Zn sorbed on selected mineral and organic references.

The EXAFS spectra of the pig slurry sample presented oscillation patterns in close agreement with the sphalerite (ZnS) reference. Observation of the *R*-space showed that Zn first neighbor in the pig slurry sample was S, as indicated by the FT peak at 1.9 Å (not phase-shifted, vertical dashed line). This peak was coincident and therefore indicative of the Zn local environment in both the sphalerite and the cysteine references, *i.e.* Zn surrounded by four S atoms located 2.34 Å from the central atom in

the first coordination shell. In contrast, the Zn-O binding lengths varying from 1.95 to 2.07 Å (depending on the coordination) in other references and samples gave rise to the peak around 1.5 Å (not phase-shifted, vertical dashed line) (LEGROS et al., 2010a).

The wide oscillation in *R*-space centered at 3.7 Å (vertical dashed line), noticed in the ZnS reference, but absent in the Zn-cysteine reference, originated from the Zn-Zn interaction in the second coordination shell, with a bonding distance of 3.87 Å and a coordination number of 12 (ROBERTS et al., 2002). Because this peak was also present in the FT spectrum of the pig slurry sample, sphalerite was the reference with spectral features more in agreement with the pig slurry sample.

Out-of-phase oscillations were observed in the EXAFS spectra of the organic references Zn-malate and Zn-phytate, reflecting the different local environment of Zn in these references. Moreover, Zn-phytate displayed a rather intense FT peak at 3.0 Å, most likely due to Zn-P second shell interaction in this cyclic polyphosphate, which is absent in the Zn-malate reference. In the Zn-malate complex, Zn-O first coordination shell is octahedral, and the second shell is composed of C and O atoms. Because Zn-malate is a common organic acid present in plant roots and soils, and it presents structural characteristics common to a broad range of organic compounds, it was used as LCF proxy to account for Zn bound to organic matter (Zn-OM) (SARRET et al., 2002; SARRET et al., 2003; JONES et al., 1996).

Finally, the Zn-ferrihydrite reference presented distinct peaks in *R*-space, reflecting the different Zn local environment in this ferric oxyhydroxide mineral. The first FT peak around 1.5 Å (not phase-shifted, vertical dashed line) was slightly shifted to a shorter distance, as compared to Zn-kaolinite and Zn-HIM references. It was shown that complexes on the surface of ferrihydrite had Zn-O distances of around 1.97 Å and coordination numbers consistent with tetrahedral oxygen coordination, as opposed to Zn-O distances of around 2.11 Å in octahedral coordination. Moreover, the FT peak at 3.25 Å (not phase-shifted, vertical dashed line) arises from the Zn-Fe interaction in the second coordination shell, at 3.44 Å distance (WAYCHUNAS et al., 2002). The mineral structure of ferrihydrite is very similar to that of hematite, the main iron oxide detected within the soil via XRD (SECTION 4.2.1 , FIGURE 4.5) (VOEGELIN et al., 2011; TOWE & BRADLEY, 1967). Therefore, Zn-sorbed ferrihydrite was used as a proxy to represent tetrahedrally coordinated adsorbed/complexed Zn on ferric (oxyhydr)oxides.

4.3.1 Linear combination fitting

In order to quantify the amounts of Cu and Zn associated to each mineral or organic species within the samples, the soil and pig slurry EXAFS spectra were analysed by linear combination fitting (LCF). Fits were carried out based on an extensive collection of EXAFS reference spectra described in Section 3.4.1. Scenarios using only one and up to five fitting components were tested and critically evaluated based on the *Res* value (SECTION 3.4.1) and by visual observation on the quality and improvement of the LCF when adding an extra component to previous best fits. Copper and Zn references presented in Figures 4.9 and 4.10 were the most representative components used for the simulations in each case.

The sum of the fitted components used to simulate the spectra of the samples ranged from 111.6% to 122.8% for Cu and from 102.0% to 118.1% for Zn. Deviations from 100% may arise from variations in amplitudes due to overabsorption during spectra recording or from slight differences between the structure of Cu and Zn species existing in the soil samples and in the reference materials (JACQUAT et al., 2009b; MANCEAU et al., 2002). Linear combination results were normalized to 100% for the comparison of the relative speciation between samples.

The k^2-weighted Cu K-edge EXAFS and FT spectra of bulk soil samples and pig slurry, superposed by the respective best LCF using the Cu reference database, are presented in Figure 4.11. The best LCF for the CT bulk sample using two components pointed out the presence of Cu-kaolinite and Cu-vermiculite. Adding a third component (Cu-thioglycol in the best fit) did not lead to a better reproduction of the EXAFS and FT spectra of the sample. Moreover, the three-component fit scenario resulted in using the third component at a very low proportion (below 10%). It reinforced that the two-component fit was the optimal solution.

The LCF for the PS200 bulk sample produced similar results as compared to the CT bulk sample, *i.e.* Cu-kaolinite and Cu-vermiculite as the best references in the two-component scenario, with no noticeable improvement on the fits when adding a third component. Hence, the best spectra reproduction for both the CT and the PS200 bulk samples was attained by using two references of Cu sorbed on phyllosilicates: Cu-kaolinite and Cu-vermiculite.

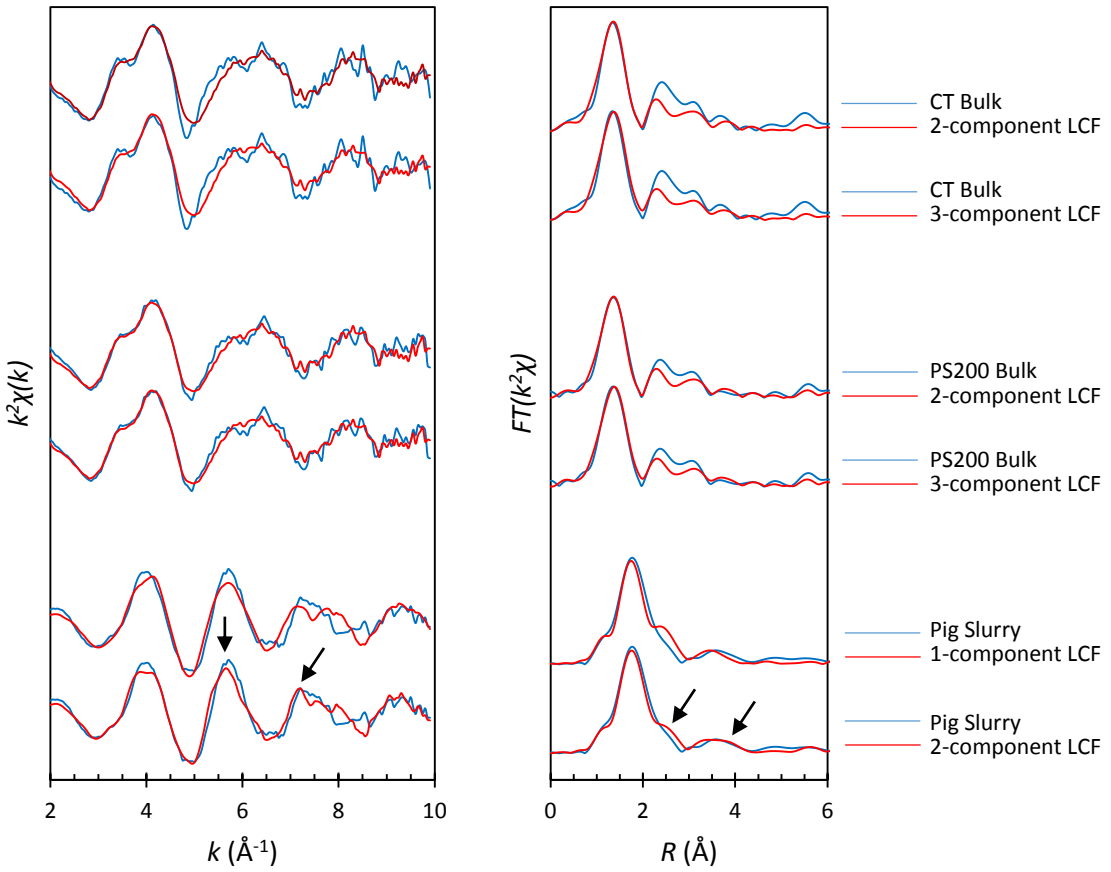

Figure 4.11 – k^2-Weighted Cu K-edge EXAFS and Fourier transform (FT) spectra of CT, PS200 and pig slurry samples (blue), superposed by the best LCF fits for each sample (red).

The LCF using only one component for the pig slurry sample indicated the presence of Cu_2S as the main Cu species. Nevertheless, adding a second component (CuCl) to the fit improved the reproduction of the EXAFS and FT spectra of the sample. Figure 4.11 shows that the magnitude of the second EXAFS oscillation (5.85 Å^{-1}, pointing arrow) and the peak of the third EXAFS oscillation (7.2 Å^{-1}, pointing arrow) were best simulated in the two-component scenario, as compared to the one-component LCF. In the *R*-space, this was reflected in smoothing of the shoulder in the first FT peak (2.6 Å, pointing arrow) and a shift in the second FT peak (centered around 3.6 Å, pointing arrow) to a slightly longer distance. The two-component LCF, containing Cu_2S and CuCl, was deemed the best solution to simulate the spectra of the pig slurry sample.

The resulting Cu speciation using two fitting components for the CT, PS200 and pig slurry samples are summarized in Figure 4.12. Moreover, in order to obtain the concentration of the Cu species, the normalized LCF proportions in each sample were

multiplied with the respective total Cu contents, previously assessed during the soil density fractionation procedure (TABLE 4.3). The CT bulk sample (Cu = 122.4 mg kg^{-1}) contained 60% Cu-kaolinite (73.4 mg kg^{-1}) and 40% Cu-vermiculite (49.0 mg kg^{-1}). The PS200 bulk sample (Cu = 174.1 mg kg^{-1}) contained 69% Cu-kaolinite (120.1 mg kg^{-1}) and 31% Cu-vermiculite (54.0 mg kg^{-1}). Finally, the Cu speciation in the pig slurry sample was 85% Cu_2S and 15% CuCl.

As a result, the distribution of the exogenous Cu arising from the 22 PS applications in the PS200 plot (calculated as Cu–PS200 - Cu–CT = 51.7 mg kg^{-1}) was 90.3% Cu-kaolinite (46.7 mg kg^{-1}) and 9.7% Cu-vermiculite (5.0 mg kg^{-1}). It is worth noting that PS was the only noticeable source of Cu, accounting for the enrichment of 51.7 mg kg^{-1} in Cu concentration within the PS200 plot (Cu = 174.1 mg kg^{-1}), as compared to the CT plot (122.4 mg kg^{-1}). However, the Cu speciation in pig slurry, *i.e.* 85% Cu_2S and 15% CuCl, was not detected at all in the amended soil.

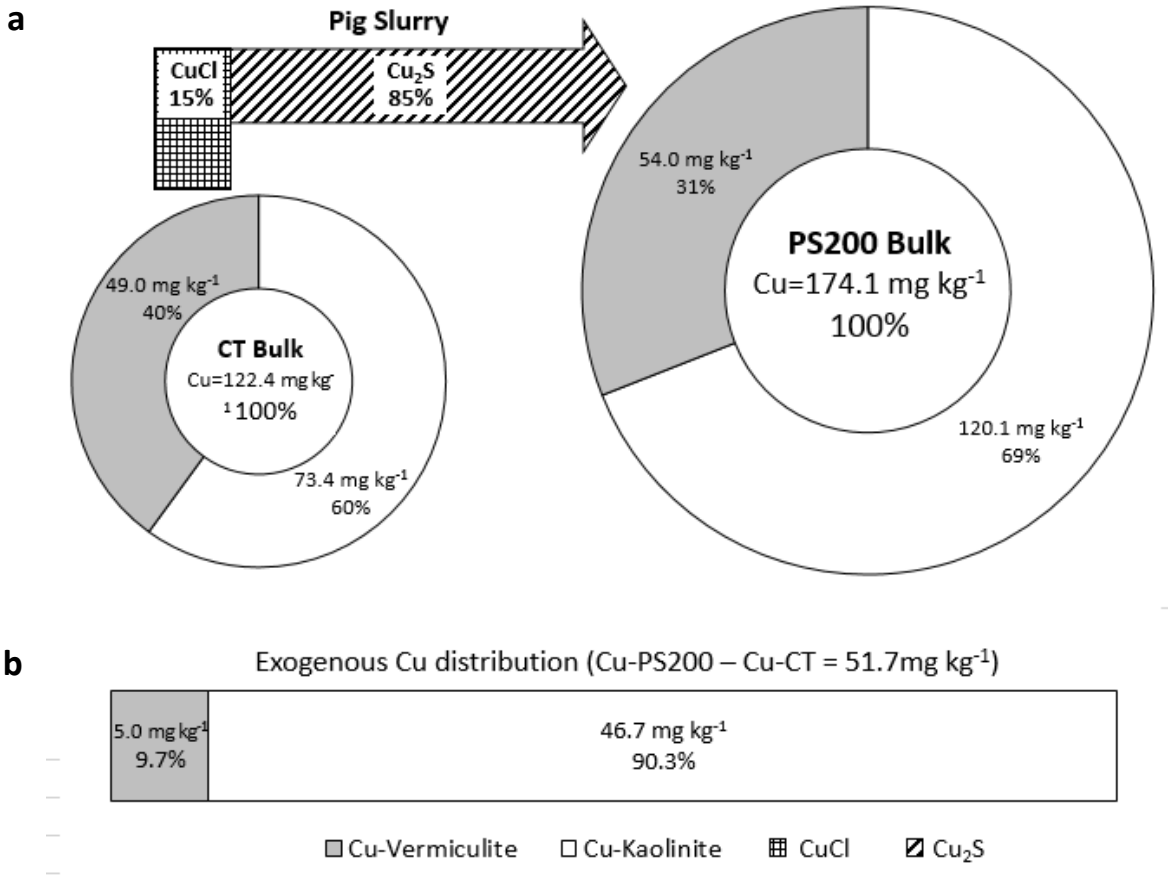

Figure 4.12 – (a) Absolute and percentage distribution of Cu species within CT, PS200 and pig slurry samples. (b) Absolute and percentage distribution of exogenous Cu (PS200 - CT).

Figure 4.13 presents the k^2-weighted Zn K-edge EXAFS and FT spectra of bulk soil samples and pig slurry, superposed by the respective best LCF using the Zn reference database. The best LCF for the CT bulk sample using two components indicated the presence of Zn-kaolinite and Zn-ferrihydrite. The introduction of a third component (Zn-malate in the best fit) did not lead to a better reproduction of the EXAFS spectrum of the sample. In fact, despite the slight increase in the amplitude of the first fitted EXAFS peak, the first deep and the second peak were less satisfactorily reproduced in the three-component scenario. Moreover, no noticeable improvement in the resulting *R*-space was attained by introducing the third component. Hence, the two-component reproduction of the CT spectra was used as the best solution.

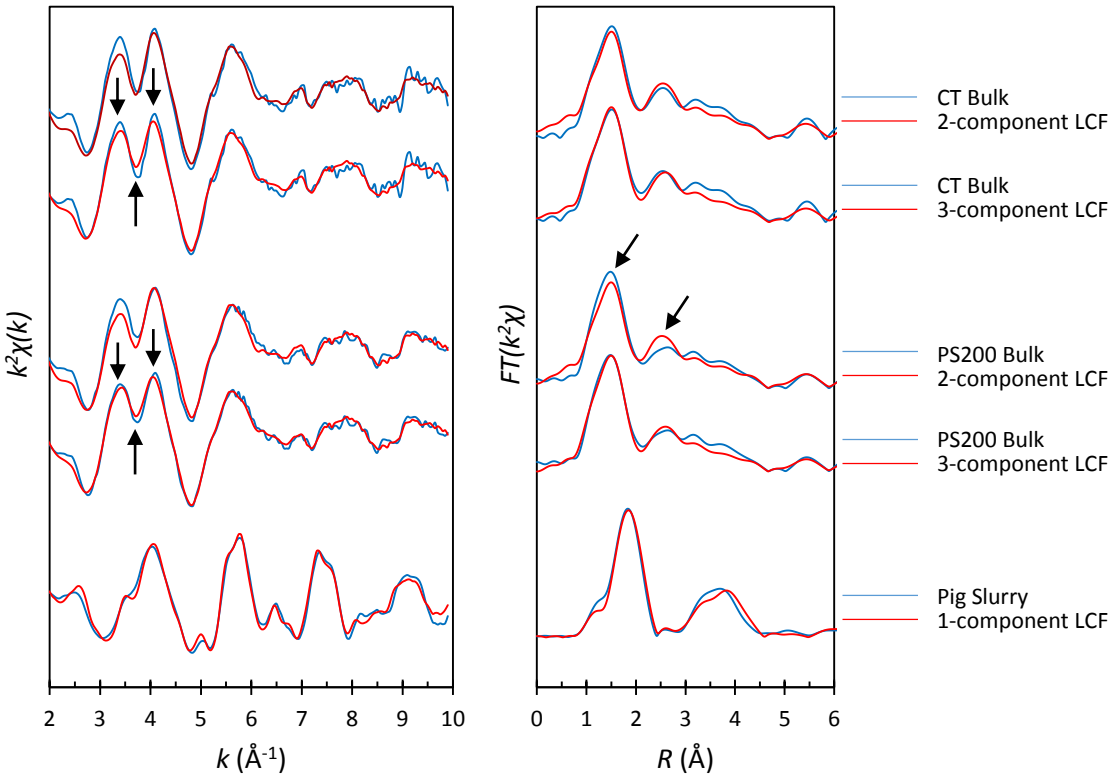

Figure 4.13 – k^2-Weighted Zn K-edge EXAFS and Fourier transform (FT) spectra of CT, PS200 and pig slurry samples (blue), superposed by the best LCF fits for each sample (red).

The best LCF for the PS200 bulk sample when using two components was also achieved by combining Zn-kaolinite and Zn-ferrihydrite. Nevertheless, the introduction of a third component to the fit (Zn-malate) improved the reproduction of the EXAFS spectrum of the sample, notably in the first peak and first deep of the main oscillation (pointing arrows). Moreover, the FT spectrum in the three-component

scenario presented an increase in the amplitude of the first oscillation, followed by a decrease and a shift to a higher distance in the second oscillation, as compared to the two-component scenario (pointing arrows). Hence, the three-component LCF was more in agreement with the PS200 spectra and it was used as the optimal solution.

The LCF for the pig slurry sample using only one component, *i.e.* sphalerite (ZnS), was deemed satisfactory. No combination of two references altered the proportion of the first component (ZnS) to the best fits, which was used at 100% in all scenarios. This can be confirmed by the very good agreement between the sample spectra and the reference spectra in Figure 4.13.

The resulting Zn speciation using one fitting component for pig slurry, two fitting components for the CT bulk sample and three fitting components for the PS200 bulk sample are presented in Figure 4.14. The concentration of each Zn species was obtained by multiplying the normalized LCF proportions with the total Zn content in each sample, previously assessed during the density fractionation procedure (TABLE 4.3). The CT bulk sample (Zn = 105.8 mg kg^{-1}) contained 70% Zn-kaolinite (74.5 mg kg^{-1}) and 30% Zn-Fe-oxide (31.3 mg kg^{-1}). The PS200 bulk sample (Zn = 206.6 mg kg^{-1}) contained 54% Zn-kaolinite (110.6 mg kg^{-1}), 27% Zn-Fe-oxide (56.0 mg kg^{-1}) and 19% Zn-OM (40.0 mg kg^{-1}). Finally, the Zn speciation in the pig slurry sample was 100% composed by sphalerite (ZnS).

As a result, the Zn arising from the 22 PS applications in the PS200 plot was distributed between Zn-bounding species preexisting in the CT plot (Zn-kaolinite and Zn-Fe-oxide) and Zn-OM, which was not detected in the CT sample. The exogenous Zn distribution (Zn–PS200 - Zn–CT = 100.8 mg kg^{-1}) was: 35.8% Zn-kaolinite (36.1 mg kg^{-1}), 24.5% Zn-Fe-oxide (24.7 mg kg^{-1}), and 39.6% Zn-OM (40.0 mg kg^{-1}). It is noteworthy that pig slurry was the only noticeable source responsible for the increase of 100.8 mg kg^{-1} in Zn concentration within the amended soil, from 105.8 mg kg^{-1} (CT) to 206.6 mg kg^{-1} (PS200). However, the Zn speciation in pig slurry, *i.e.* 100% ZnS, was not detected at all in the amended soil.

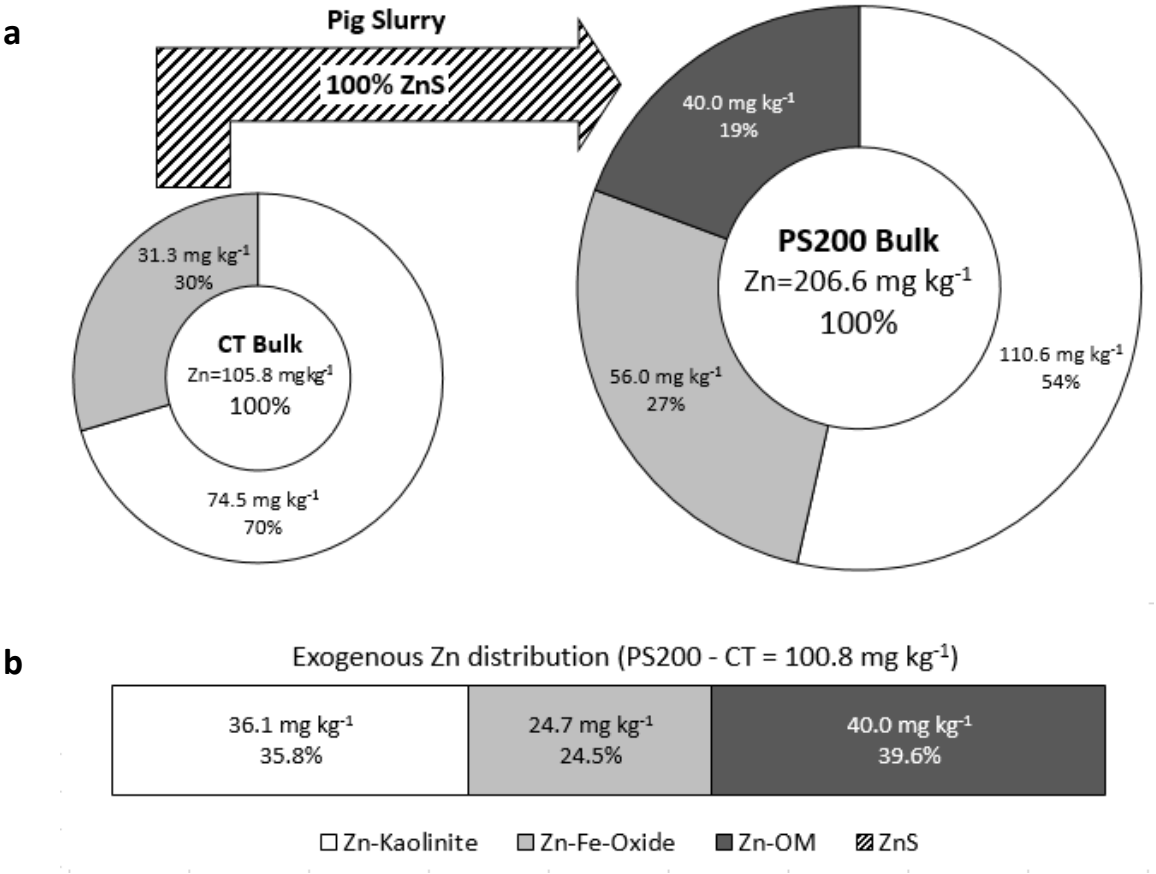

Figure 4.14 – (a) Absolute and percentage distribution of Zn species within CT, PS200 and pig slurry samples. (b) Absolute and percentage distribution of exogenous Zn (PS200 - CT).

4.3.2 Pig slurry SEM–EDS analysis

Scanning electron microscopy with X-ray microanalysis (SEM–EDS) was used to explore the Zn environment in the PS matrix. The 20 µm > PS > 0.2 µm particle size fraction was selected because it contained most of the dry matter and the Zn concentration in the raw PS (SECTION 3.5.1).

After extensive examination, the single region on the analyzed sample surface that contained Zn in the elemental composition was selected and presented in Figure 4.15. The detached area in Figure 4.15a was magnified in Figure 4.15b, and the elemental composition of the two particles indicated by the arrows are presented in Figure 4.15c. The two particles contained mostly Zn and S in their elemental composition, but also low intensity peaks indicating the presence of Ca and K cations. The colocalization of Zn and S may be directly attributed to sphalerite (ZnS), as

confirmed by EXAFS analysis in the pig slurry. The diameter of both particles was of about 1 µm.

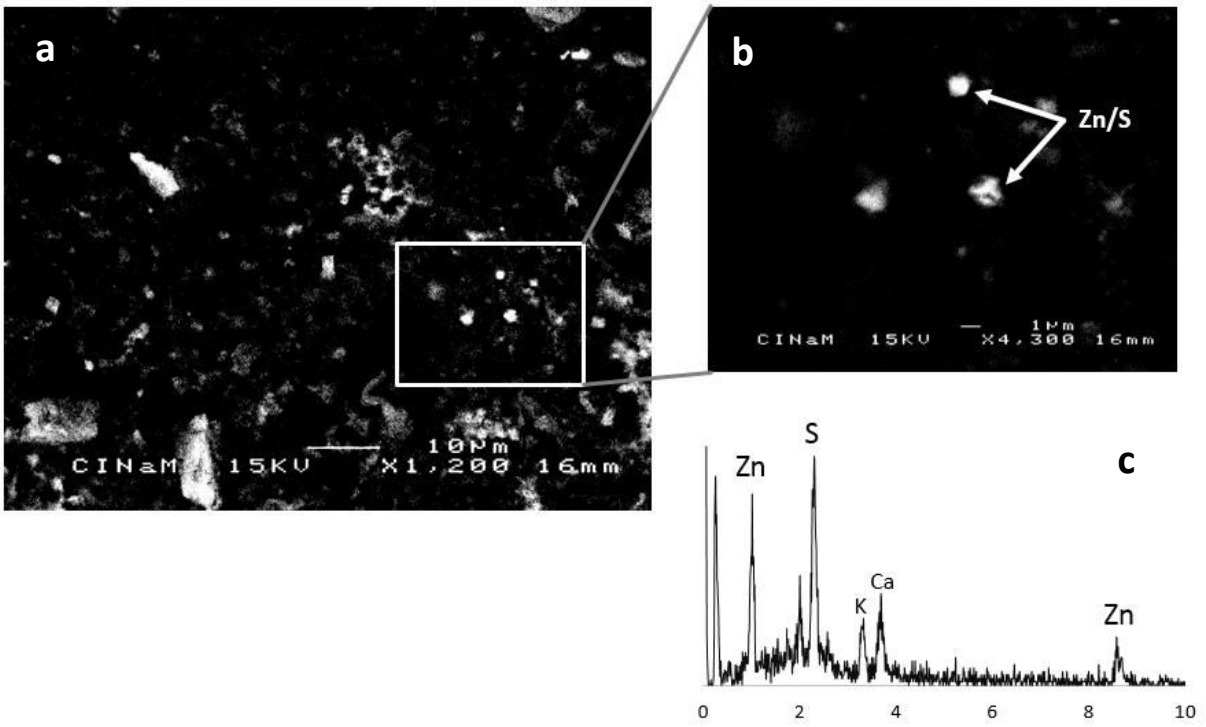

Figure 4.15 – (a, b) Scanning electron microscopy micrograph of the pig slurry 20 µm > PS > 0.2 µm particle size fraction; arrows indicate regions selected for energy dispersive spectrometer spectrum (c).

4.3.3 Discussion

4.3.3.1 Cu and Zn natural occurrence

Linear combination fittings indicated that 100% of the Cu of natural occurrence (CT sample, 0–5 cm layer) was associated to the clay minerals kaolinite and vermiculite. This is essentially in agreement with the results previously reported in this study, which indicated the preponderance of Cu in the residual fraction of the sequential extraction protocol (70.5%; SECTION 4.1) and in the 2.5<d<2.7 density fraction (73.7%; SECTION 4.2).

Similarly, LCF showed that 70% of the Zn of natural occurrence was associated to kaolinite. This is in close agreement with the 76.9% of Zn found in the

residual fraction via sequential extractions (SECTION 4.1) and the 79.7% of the Zn contained in the 2.5<d<2.7 density fraction (SECTION 4.2).

The combination of sequential extractions and soil density fractionation had led to infer that these proportions represented the Cu and Zn fraction tightly bound to or incorporated into the crystal structures of primary and secondary minerals, thus accounting for HM related to the parent material. The use of synchrotron-based X-ray absorption spectroscopy not only confirmed, but allowed detailing on the mode of occurrence of these HM within the mineral matrix.

Copper was sorbed into kaolinite in an inner-sphere and into vermiculite forming multinuclear complexes in the interlayer. It was previously discussed in Section 4.2.4.1 that the finding of Cu incorporated into the soil mineral matrix was rather unexpected, because its biogeochemistry is considered mainly controlled by its interactions with natural OM. It should be noted that sequential extractions and soil density fractionation procedures may not be conclusive in asserting particular mineral/organic species or mechanisms involved in the HM incorporation within the soil. However, the LCF procedure for the CT bulk sample, supported by visual comparison of sample and reference spectra, was unequivocal to show that, indeed, associations between natural Cu and the phyllosilicates kaolinite and vermiculite occurred in the studied soil. The contribution of the soil OM or other mineral species to the Cu speciation should have been minor, if occurred at all.

It was proposed that Cu exhibits a better match in size and bond-angle with carboxyl groups and hydroxyl donors in OM, as compared to the geometrical fit in mineral structures, thus explaining the widespread association of Cu and natural OM in the environment (MANCEAU & MATYNIA, 2010; SCHLEGEL & MANCEAU, 2013). However, different analytical approaches used in the present study confirmed that clay minerals may play a dominant role in the natural Cu speciation within the soil. The most remarkable characteristic of the soil here investigated was its very high clay content, thus consistent with the observed Cu-clay minerals association. It emphasizes the importance of studies under different soil environments and reinforces the need of further field investigations towards a more broadly understanding of Cu behavior in soils.

Zinc was mainly incorporated into the kaolinite mineral structure, either occupying vacant dioctahedral sites or in substitution for Al in this 1:1 clay mineral. Although it was not possible to completely rule out the occurrence of Zn in octahedral

sites of gibbsite-like layers at the basal or interlayer surface of vermiculite (due to the resemblance between Zn-kaolinite and Zn-HIM references), LCF and visual analysis of key-features in the spectra indicated that Zn-kaolinite was the best reference proxy for Zn speciation in the soil sample. The affinity of Zn for gibbsitic layers is well documented and may represent a significant geochemical process for Zn sequestration in Earth's near-surface environments (MANCEAU et al., 2005).

The remaining 30% speciation of Zn in the CT sample was composed of Zn-Fe-oxide. It was reported via sequential extractions (SECTION 4.1, SUPPORTING INFORMATION SI-1 and SI-2) that 2.9% of the natural Zn was associated to the amorphous oxyhydroxides fraction and 9.7% to the crystalline oxides fraction. Thus, both fractions accounted together for a 12.6% share. XRD analysis of density fractions (FIGURE 4.5b) revealed that hematite was the main Fe-oxide composing the heaviest d>2.7 fraction, but also present in lesser amounts within lighter fractions. Therefore, EXAFS results were in line with sequential extractions and density fractionation, since both approaches pointed out the role of iron oxides as a secondary species associated to natural Zn.

The contribution of OM and other minor species to the Zn speciation within the CT soil sample may have been underestimated by the LCF approach. It is worth noting that LCF is less sensitive to species present at low concentration in the sample. According to sequential extraction results, the proportion of natural Zn bound to OM was 9.0%. This proportion was slightly below the accuracy threshold of 10%, conservatively respected for LCF.

4.3.3.2 Cu and Zn exogenous distribution

Copper speciation within the amended PS200 sample (0–5 cm) was composed of 69% Cu-kaolinite and 31% Cu-vermiculite. These mineral species were the same that had accounted for the Cu speciation in the non-amended CT sample. Comparison between the Cu speciation before (CT) and after (PS200) the PS amendments indicated that 90.3% of the exogenous Cu was associated to kaolinite within the amended soil.

This result contrasted with previous observations via sequential extractions and density fractionation, which suggested that the main pool for exogenous Cu was OM, followed by a secondary contribution of clay minerals. Nevertheless, EXAFS results indicating the uptake of exogenous Cu into the kaolinite structure in an inner-sphere was likely the key explanation for the very reduced mobility of this HM in the soil profile after 22 PS applications, as presented in Section 4.1.

Zinc speciation within the PS200 sample (0–5 cm) was composed of Zn-kaolinite (54%) and Zn-Fe-oxide (27%), which had been detected also in the CT sample, plus Zn-OM (19%), which was absent in the CT sample. Comparison between the Zn speciation in the control (CT) and in the amended (PS200) samples resulted in the following contribution to the assimilation of exogenous Zn: 35.8% Zn-kaolinite, 24.5% Zn-Fe-oxide and 39.6% Zn-OM.

The finding of 35.8% of the exogenous Zn as Zn-kaolinite reinforce an hypothesis previously put forward based on sequential extractions and the density fractionation results. That is, clay minerals were the main species accounting for the exogenous Zn detected in the adsorbed fraction via sequential extractions (36.7%, SECTION 4.1) and in the 2.5<d<2.7 density fraction (33%, SECTION 4.2). As previously discussed for the Zn of natural occurrence, LCF and visual analysis of spectra confirmed that Zn-kaolinite was the best reference proxy also for the PS200 sample, in spite of the similar Zn local environment in Zn-kaolinite and Zn-HIM references.

Numerous EXAFS studies so far suggested that the formation of Zn-phyllosilicate associations may be a significant HM pool in slightly acidic to neutral soils contaminated by mining and smelting emissions (MANCEAU et al., 2000; JUILLOT et al., 2003; NACHTEGAAL et al., 2005; VOEGELIN et al., 2005; SCHUWIRTH et al., 2007). Moreover, the incorporation of Zn into the gibbsitic octahedral sheets of Al-hydroxy interlayered clay minerals (Zn-HIM) have been reported within natural and contaminated acidic soils (SCHEINOST et al., 2002; MANCEAU et al., 2004; MANCEAU et al., 2005). Nevertheless, this study reports for the first time that both Zn of natural occurrence and exogenous Zn arising from long-term application of PS into the soil were preferably incorporated into the kaolinite mineral structure rather than into hydroxy-interlayered minerals.

The 39.6% contribution of Zn-OM to the exogenous Zn distribution, determined via EXAFS, were in line with the 32.0% of exogenous Zn found in the OM fraction via

sequential extractions (SECTION 4.1) and the analogous 27% in the OM-rich d<1.9 density fraction (SECTION 4.2). The slightly higher proportion of exogenous Zn-OM detected via EXAFS analysis may be attributed to the absence of this species in the LCF for the CT plot, as discussed previously.

Finally, Zn-Fe-oxide accounting for 24.5% of the exogenous Zn distribution, as indicated by LCF of EXAFS spectra, reinforce the hypotheses that (oxyhydr)oxides play an important role in Zn retention. It constitutes part of the explanation for the low mobility of exogenous Zn through the soil profile, as presented and discussed in Section 4.1.3.2.

4.3.3.3 Cu and Zn in the pig slurry

Copper speciation in the PS was 85% Cu_2S and 15% CuCl, whereas Zn speciation in PS was 100% composed of ZnS, as indicated by LCF of EXAFS spectra (Cu and Zn) and confirmed by SEM–EDS analysis (Zn). The presence of CuCl may be explained by the high concentration of chloride occurring in most animal slurries (BURTON & TURNER, 2003), reported at levels as high as 1400 mg l^{-1} in PS (FEDER & FINDELING, 2007). The anoxic environment within PS lagoons may explain the formation of Cu and Zn sulfides by two possible mechanisms: chemical precipitation or bacteria-assisted sulfate reduction (LEGROS et al., 2010a). The solubility constants for Cu_2S and ZnS are $1.6x10^{-48}$ and 2.93×10^{-36}, respectively. Therefore, both species are expected to be highly insoluble and stable within the soil.

Indeed, Zhou et al. (1999) reported that Cu sulfide solubility was very low in soils under aerobic conditions in the 6.6–7.6 pH range, while Calmano et al. (1993) demonstrated that Cu sulfides were soluble in oxidized sediment only at pH below 4.5. Legros et al. (2010b) reported the presence of Cu_2S in great majority in PS from an anaerobic lagoon. They hypothesized that the solubility of Cu sulfide within soils would be very low, even under aerobic conditions, and this would be the main factor explaining the observed Cu accumulation at the soil surface resulting from intensive PS spreading. However, in the present study, Cu_2S was not present at all within the PS-amended soil, after 22 PS applications over 11 years. Further characterization of

Cu sulfides in the PS, using SEM-EDS, was not possible. Nevertheless, it was performed for Zn, as discussed hereafter.

It has been reported that ZnS can be solubilized within soils by increasing aerobic conditions, at pH 7.0, in a laboratory-controlled incubation of pyrite mine waste suspensions (CARBONELL-BARRACHINA et al., 2004) and after land-disposition of a dredged sediment affected by smelter operations, at pH 8.2–8.3, over an 18-month period (ISAURE et al., 2005). In the latter, however, ZnS was still detected as the main Zn component within the soil 0–10 cm profile, making up ~63% of the Zn speciation. Voegelin et al. (2011) reported 26 to 75% dissolution of spiked ZnS after four years of soil incubation, pointing out that the ZnS dissolution in acidic soils was slower, as compared to a near-neutral and a calcareous soil. Moreover, Legros et al. (2010a) have recently reported for the first time the occurrence of ZnS particles in the PS matrix, although its fate within the soil was not assessed. Sphalerite made up 14% of the Zn speciation in the PS, and scanning electron microscopy micrograph showed that the particles were about 5 µm diameter.

Hence, the present study is the second to report the occurrence of sphalerite in the PS matrix, adding up the following information: (i) sphalerite represented 100% of the Zn speciation in the PS matrix; (ii) the ZnS particles detected via SEM–EDS were approximately 1 µm diameter, therefore smaller than the previous observation; (iii) The sphalerite-containing PS was spread on the soil over 11 years, making up 22 PS applications, and the resulting Zn speciation within the amended soil was analyzed.

It was very surprising that ZnS was not detected within the amended soil, even if PS was the only source responsible for an increase in Zn concentration from 105.8 mg kg^{-1} (CT) to 206.6 mg kg^{-1} (PS200). A scenario comparing how the EXAFS and FT spectra of the amended soil should look like if the Zn speciation in the PS was preserved after spreading on the soil (dotted red line), as compared to spectra of the CT plot (blue line), is presented in Figure 4.16a.

Out-of phase oscillations may be observed due to the hypothetical presence of ZnS at roughly 50% of the Zn speciation in this scenario, when compared to the spectra of the CT soil sample, without ZnS. Moreover, the sphalerite Zn-S bond would cause a shift to a longer distance in the FT peak representing the Zn first coordination shell, and the Zn-Zn bond would give rise to a peak at 3.9 Å (not phase-shifted), absent in the FT spectrum of the CT sample (FIGURE 4.16a). However, the EXAFS and FT spectra actually recorded for the PS200 sample strongly resembles the spectra of the

CT sample (FIGURE 3.16a), indicating the transfer of PS-added Zn mainly towards pre-existing species in the soil.

Based on the observed results, the hypothesis put forward to explain the low stability of ZnS from PS origin after spreading on the soil is that the units of approximately 1 µm diameter observed via SEM–EDS would rather consist of aggregates of ZnS nanoparticles, more susceptible to solubilization. Indeed, analytical grade sphalerite was analyzed for its particle structure and ZnS crystallites were reported to have sizes around 25-40 nm, aggregated into spherical particles with diameters around 1-2 µm that were further coagulated into larger entities (VOEGELIN et al., 2011).

There is no evidence to rule out that this same aggregation mechanism of ZnS nanoparticles took place in the PS matrix analyzed in this study. Moreover, due to analogous characteristics, the hypothesis put forward for ZnS may be also valid to explain the fate in the soil of Cu_2S from PS origin. Therefore, additional investigation is necessary on the structure and stability of Cu and Zn sulfides within PS and other organic wastes, whose fate after spreading on the soil in the present study followed a path not previously reported in the literature.

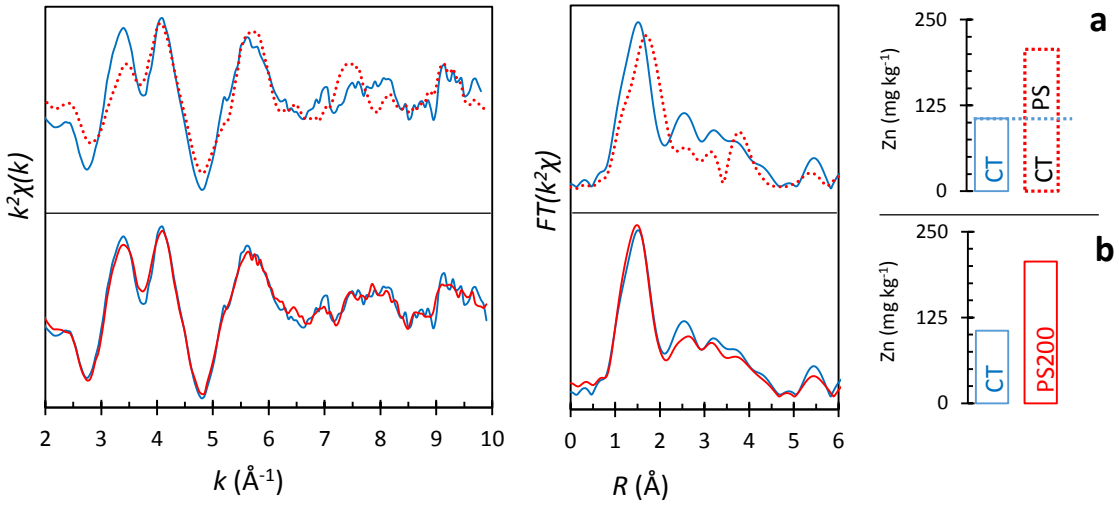

Figure 4.16 – (a) Scenario comparing hypothetical EXAFS and Fourier transform (FT) spectra of the amended plot if the ZnS detected within PS was preserved in the soil (CT + PS, dotted red line) with the spectra of the CT plot (blue line). (b) EXAFS and Fourier transform (FT) spectra actually recorded for the PS200 plot (red line) as compared to the spectra of the CT plot (blue line).

5 CONCLUDING REMARKS

The HM-soil interactions affecting the Cu and Zn transfer within the studied soil were assessed at the macroscopic scale using chemical sequential extractions, at the microscopic scale by means of soil density fractionation and at the molecular scale via synchrotron based X-ray absorption spectroscopy. Moreover, complementary investigation was conducted in the PS matrix, notably to estimate the HM inputs into the soil over the field experiment period and to explore the Zn associations in this matrix via scanning electron microscopy with X-ray microanalysis.

Firstly, results were evaluated in order to identify the macroscopic trends of Cu and Zn accumulation and migration through the soil profile. This approach took into account the HM extractability and total concentration within plots that received different PS application rates, at progressively deeper layers. Exogenous HM accumulated within the soil surface layers.

Subsequently, the HM-soil associations within the control plot, containing natural levels of Cu and Zn, and within the PS200 plot, that received 22 PS applications over 11 years at the rate of 200 m^3 ha^{-1} $year^{-1}$, were further examined. The proposed multi-scale investigation provided a description on the Cu and Zn phase associations and their incorporation into the mineral matrix at the molecular level. It allowed additional understanding on the previously reported trend of HM accumulation.

5.1 THE HM ACCUMULATION WITHIN THE SOIL SURFACE AND THE ENVIRONMENTAL ISSUE

The mass balance conducted to compare the amounts of HM added into the soil via 22 PS applications over 11 years and the increase in HM concentration within the 0–30 cm horizon of PS-amended soils showed that accumulation within the surface horizon was the main fate of exogenous Cu and Zn. Moreover, statistical analysis of HM concentration within individual layers of PS-amended soils, as compared to the same layers in the control soil, showed that migration was even more limited. Pig slurry application rates of 50 and 100 m^3 ha^{-1} $year^{-1}$ resulted in virtually absent mobility of Cu

and Zn through the soil profile, as indicated by the significant increase in HM concentration only in the topmost soil layer (0–5 cm). Within the field plot that received the highest PS application rate, 200 m^3 ha^{-1} $year^{-1}$, a significant migration of Cu and Zn was observed until the 10–15 cm soil layer.

Under natural climate and soil water regime conditions, the investigated soil acted as a strong buffer to exogenous HM, which were damped out in the upper layer of the soil. Moreover, the Cu and Zn concentration detected in readily bioavailable fractions were below the levels considered phytotoxic. Therefore, the 22 PS applications over 11 years did not pose immediate concern related to adjacent systems such as groundwater contamination or plant uptake, even in the scenario receiving the highest PS dose (200 m^3 ha^{-1} $year^{-1}$). Hence, taking into account only the contamination by Cu and Zn, the application of PS waste on the studied soil proved to be a suitable recycling strategy, in line with principles of using waste in an environment-friendly manner. Pig slurry may be an important source of OM and nutrients for crops, at the same time that economic and environmental costs are reduced.

Obviously, the observed capability of the investigated soil for HM retention, as well as the presupposed lack of phytotoxicity, are not unlimited. Likewise, other possible contaminants present in the PS matrix (*e.g.* N, P and persistent organic pollutants) may pose concerns to adjacent systems. The complete assessment of these factors are necessary in order to formulate safe strategies of PS recycling, notably the maximum loads and duration for a given scenario. This assessment is beyond the scope of the present study, but highly recommended for future research.

5.2 TOWARDS A MICROSCOPIC AND MOLECULAR LEVEL EXPLANATION FOR THE MACROSCOPIC OBSERVATION

Soil density fractionation was applied for the first time to assess possible associations between HM and the soil matrix in the context of a long-term field experiment involving PS amendments. It provided a good contrast between OM-rich and phyllosilicate-rich density fractions, allowing the identification of the soil main constituents and the most likely mineral and organic associations of natural containing and exogenously added Cu and Zn.

Synchrotron-based X-ray absorption spectroscopy, on the other hand, provided direct identification of the main species accounting for the natural and exogenous Cu and Zn occurrence in the soil. It underlined the strong influence that clay minerals, abundant in the investigated clayey soil, exert for the HM accumulation in the soil surface. Moreover, it revealed a distinguishing and unexpected divergence between the Cu and Zn speciation in the PS matrix and within the soil following long-term PS amendments. This instigated further analysis in the PS matrix that revealed the occurrence of ZnS particles with characteristics reported for the first time.

5.2.1 A novel application for soil density fractionation: assessing the HM fate within organically amended soils

Analysis of the organic and mineral composition of the soil density fractions, along with assessment of the HM distribution among the same fractions, indicated that the clay minerals kaolinite and vermiculite and the Fe oxide hematite were the most likely hosting phases for the Cu and Zn of natural occurrence. Hence, the new approach permitted the recognition of the mineral species associated to HM. Moreover, this observation was in close agreement with the predominance of natural Cu and Zn found in the residual fraction of sequential extractions. Therefore, the combination of sequential extractions and soil density fractionation provided further insights on the natural HM occurrence within the soil. The dominant Cu and Zn hosting phases were phyllosilicates and Fe oxides, and this linkage was highly stable, not subject to mobilization.

Comparison between the HM distribution within density fractions of the control plot and the amended plot pointed out that the same mineral species associated to Cu and Zn in the natural soil also played an important role on the immobilization of PS-added HM. Again, this observation corroborated an hypothesis previously put forward, *i.e.* that clay minerals and Fe oxides existing in the soil reduced the exogenous HM mobility by adsorption followed by stronger interaction mechanisms such as surface complexation or precipitation. Moreover, soil OM was the most likely phase responsible for the retention of exogenously added Cu, which was also in agreement with previous results obtained via sequential extractions.

Despite the drawback concerning the HM losses to the LST solution used for the soil density fractionation, this approach was successfully applied for the first time in the assessment of the HM fate following long-term organic amendments in the soil. It improved the understanding on the previously observed Cu and Zn macroscopic behavior, by indicating the main soil-phase associations of natural and exogenous HM. Therefore, soil density fractionation may be an important tool to assist similar assessments on contaminant fate within soils. Improvements seeking to avoid or control the HM losses are highly encouraged by the present study.

5.2.2 The Cu and Zn molecular environment: confirming the leading role of clay minerals for HM retention and observing a novel Zn speciation in PS followed by a unique behavior after spreading on the soil

Linear combination fittings of EXAFS spectra for the control soil confirmed that the clay minerals kaolinite and vermiculite were the two species accounting for the speciation of pedogenic Cu. The contribution of each mineral for the Cu speciation was roughly split between both phyllosilicates. Moreover, the same two phyllosilicates also accounted for the uptake of exogenous Cu added to the soil via 22 PS applications over 11 years. Nevertheless, the exogenous Cu detected within the soil surface layer was almost completely inner-sphere sorbed into the kaolinite mineral structure. This was the key observation at the molecular level to explain the low mobility of Cu after the long-term PS amendments.

The phyllosilicate kaolinite and the Fe oxide hematite were the main minerals accounting for the Zn of natural occurrence within the studied soil. After the 11-year period of PS application, exogenous Zn distributed about equally among Zn-kaolinite, Zn-Fe-oxide and Zn-OM. Therefore, the local environment of natural and exogenous Zn was also consistent with the low mobility through the soil profile noticed for this HM.

Several observations regarding the molecular environment of natural and exogenous Cu and Zn within the studied soil were contrasting with results previously reported in other studies. Notably (i) the occurrence of natural Cu into the mineral structure of clay minerals kaolinite and vermiculite, as opposed to the usual observations of Cu mostly associated to OM; (ii) the uptake of exogenous Cu from

organic amendments predominantly by kaolinite, also opposed to the commonly reported Cu-OM association; (iii) the incorporation of natural and exogenous Zn into the mineral structure of kaolinite, as opposed to the uptake by hydroxy-interlayered minerals such as vermiculite, also existing in the studied soil.

These findings reinforce the importance of long-term investigations under field conditions, and highlight the influence of the soil characteristics on the HM fate. It was clear in the present study that the high clay content of the studied soil (composed mainly by the clay minerals kaolinite and vermiculite) was imperative for the strong attenuation of the PS-added HM mobility. Moreover, the clayey texture of the soil may be relevant to explain the lack of Cu and Zn associated to OM in the natural soil, as well as the absence of Cu-OM in the amended soil. It was suggested based on the soil density fractionation that organo-mineral aggregates could have occurred in the soil and, therefore, it may have led to ambiguous interpretation of sequential extractions and density fractionation results. Hence, further studies on the HM behavior within soils, as influenced by the dynamics of OM or organo-mineral aggregates, should be pursued.

Finally, the comparison between the HM speciation in the PS matrix and within the soil following 22 PS applications over 11 years revealed a number of novel and somewhat unexpected evidences. Copper speciation in the PS matrix was composed by 85% Cu_2S, while Zn speciation was composed 100% by ZnS. Though the occurrence of metal sulfides may be explained by the anoxic environment in PS lagoons, it was only the second time that ZnS particles were detected in a PS matrix. Furthermore, this was the first time that this species accounted for 100% of the Zn speciation in PS, and the particle size was nearly 1 μm diameter, considerably smaller than the first observation. This finding is remarkable by itself, because the particle size was close to that of nanoparticles, whose current interest and scientific research is intense.

Nevertheless, Cu_2S and ZnS species were not detected within the PS-amended soil, in spite of their predominance in the PS matrix and their expected very low solubility. These findings launch a new line of investigation, necessary to enlighten the role of soil and contaminant environments, as well as particle structural features on the stability of Cu and Zn sulfides within organic wastes, whose fate after spreading on the soil followed a path never reported previously in the literature. It was here hypothesized that the observed micro ZnS particles would rather consist of nano ZnS

aggregates, more susceptible to solubilization. This hypothesis should be considered as a starting point for future research.

5.3 FUTURE RESEARCH

The new findings of the present study that may directly instigate further research were previously highlighted above. Nevertheless, a more broad context on the geochemical and environmental aspects concerning the recycling of organic wastes via land application should also be considered. Several of these aspects are briefly summarized hereafter, followed by suggestions, comments and questions on how the results here reported could guide upcoming research.

5.3.1 Type of soil

The field experiment exanimated in the present study presented a very clayey texture. Clay sized particles of kaolinite, vermiculite and hematite minerals dominated the uptake of exogenously-added HM. As a result, most of the Cu and Zn arising from PS spreading were retained in the soil surface horizon. Since long-term studies on the subject are scarce in the literature, further long-term, field-design investigations should be pursued in different types of soils, encompassing, for example, distinct textures and mineralogy. Should the same minerals found in the soil here studied, but in a minor proportion to the soil composition, still display a high sorption affinity for Cu and Zn? In the long-term, should Cu and Zn also be retained in the soil surface when a sandy soil is subject to pig slurry application? If not, the HM would leach. In this case, which other factors should play an important role on the speciation and fate of exogenously-added HM? Are climate, water regime, soil structure or soil OM more relevant variables to explain the HM behavior when the latter are weakly associated to the soil mineral matrix? What would be the implications for plant growth and toxicity? And for groundwater contamination?

5.3.2 Scenarios of PS application

The investigation here conducted was among the longest reported field studies on the HM fate within the soil following organic waste application. Different application rates were considered and the soil and PS characteristics were evaluated. However, the soil was sampled several months after the previous PS application. Scenarios taking into account other time-variable aspects should also be pursued. For instance, the soil sampling could be carried out only a few hours or days after spreading PS on the soil. Alternatively, a series of samplings could be conducted, considering short time intervals, after the PS application. Are the Cu and Zn species in the PS matrix rapidly converted to the ones here detected within the soil? How are the dynamics of the PS-borne HM and OM within the amended soil? How this new information could improve the understanding of the HM behavior observed in the present study?

Moreover, scenarios of discontinuity should be tested. What would be the long-term implications of ceasing the PS application on the HM behavior? Would it have an impact on the soil pH, redox potential, and hence in the Cu and Zn mobility and bioavailability? What if the PS dose was 2- or 3-fold increased? Would the same mineral species still be able to account for the immobilization of Cu and Zn? If so, to what extent? The previous questions lead to another key outcome of the present research that should be further explored: modeling.

5.3.3 Modeling

Geochemical transport models may be divided into models with specific chemistry and more general models. Though models with specific chemistry are considered more efficient than general models for a given scenario, they are somewhat restricted to major ions. In this sense, the long-term field experiment exanimated in the present study, as well as the results here reported, may provide useful contribution in improving the modeling scope. An effort should be done aiming to couple the reported results on the Cu and Zn speciation into more specific models of contaminant transport.

It may benefit from the detailed characterization and history report on the soil and PS here studied.

5.3.4 Analytical approach

A novel analytical approach was proposed to assess the fate and behavior of Cu and Zn following long-term PS application into the soil. Of note, soil density fractionation was used for the first time in this context. The integrated analytical approach proved to enhance data interpretation and allowed a detailed description on the macroscopic, microscopic and molecular scale interactions between the soil matrix and the Cu and Zn contaminants. Similar approaches should be tested for other HM contaminants, sources of contamination and types of soil. Is the analytical approach here proposed also suitable for other HM? What are the limitations related to the HM concentration, the contaminant origin, or the solid matrix? Which improvements could be made for a given context? Would it be possible to go towards a standardization of procedures in order to assess the HM fate within soils following land application? What are the advantages and disadvantages of different methods for the same study case?

5.3.5 The big picture

Finally, one must keep in mind that all the analytical efforts dispended to thoroughly understand the mechanistic aspects regulating the fate and behavior of HM contaminants after organic waste recycling in the soil represent only a part of one common major concern: maintaining the quality of soils and adjacent systems, and therefore preserving the Earth's natural resources for sustainable human practices such as food production, water supply and recreational activities. In that regard, the studied long-term field experiment provides a practical and realistic system that have been and should be further explored.

Since the watershed is the basic unit for water and matter circulation, the contaminant transport should be assessed also at the watershed scale. A broader assessment taking into account the production units, the nature of different organic wastes, the soil use and occupation, groundwater mapping, risk assessment, among others, should contribute to enhance the environmental safety of agricultural and recycling practices. Such broad assessment should necessarily reach the political sphere, impacting the concerned legislation and, ultimately, people's lives. For better.

REFERENCES

ABOLLINO, O.; MALANDRINO, M.; GIACOMINO, A.; MENTASTI, E. The role of chemometrics in single and sequential extraction assays: a review: part I. Extraction procedures, uni- and bivariate techniques and multivariate variable reduction techniques for pattern recognition. **Analytica chimica acta**, v. 688, n. 2, p. 104-21, 2011.

ADRIANO, D. C. **Trace Elements in Terrestrial Environments: Biogeochemistry, Bioavailability, and Risks of Metals**. 2nd ed. New York: Springer, 867p., 2001.

ALBORÉS, A. F; CID, B. P.; GÓMEZ, E. F.; LÓPEZ, E. F. Comparison between sequential extraction procedures and single extractions for metal partitioning in sewage sludge samples. **The Analyst**, v. 125, n. 7, p. 1353–1357, 2000.

ALLOWAY, B. J. **Heavy Metals in Soils**. 1st ed. London: Chapman & Hall, 368p., 1990.

ALLOWAY, B. J. **Heavy Metals in Soils**. 2. ed. New York: Springer, 384p., 1995.

ARNARSON, T. S.; KEIL, R. G. Organic–mineral interactions in marine sediments studied using density fractionation and X-ray photoelectron spectroscopy. **Organic Geochemistry**, v. 32, p. 1401–1415, 2001.

ASADA, K.; YABUSHITA, Y.; SAITO, H.; NISHIMURA, T. Effect of long-term swine-manure application on soil hydraulic properties and heavy metal behaviour. **European Journal of Soil Science**, v. 63, n. 3, p. 368-376, 2012.

ATSDR - AGENCY FOR TOXIC SUBSTANCES AND DISEASE REGISTRY. **Toxicological Profile for Copper**. Atlanta, 2004.

ATSDR - AGENCY FOR TOXIC SUBSTANCES AND DISEASE REGISTRY. **Toxicological Profile for Zinc**. Atlanta, 2005.

AZEVEDO, F. A.; CHASIN, A. A. M. **Metais: gerenciamento da toxicidade**. São Paulo: Atheneu, 554p., 2003.

BACH, H.; CHRISTENSEN, N.; KRISTENSEN, P. **The State of the Environment in Denmark, 2001**. Technical Report 409. Roskilde, National Environmental Research, 2002.

BACON, J. R.; DAVIDSON, C. M. Is there a future for sequential chemical extraction? **The Analyst**, v. 133, p. 25-46, 2008.

BADIN, A. L.; MÉDEREL, G.; BÉCHET, B.; BORSCHNECK, D.; DELOLME, C. Study of the aggregation of the surface layer of Technosols from stormwater infiltration basins using grain size analyses with laser diffractometry. **Geoderma**, v. 153, p. 163–171, 2009.

BENITEZ, L. N.; DUBOIS, J. P. Evaluation of the selectivity of sequential extraction procedures applied to the speciation of cadmium in soils. **International Journal of Environmental Analytical Chemistry**, v. 74, p. 289–303, 1999.

BONNARD, P.; BASILE-DOELSCH, I.; BALESDENT. J.; MASION, A.; BORSCHNECK, D.; ARROUAYS, D. Organic matter content and features related to associated mineral fractions in acid loamy soil. **European Journal of Soil Science**, v. 63, p. 625–636, 2012.

BORGES, M. R; COUTINHO E. L. M. Metais pesados do solo após aplicação de biossólido. I – Fracionamento. **Revista Brasileira de Ciência do Solo**, v. 28, p. 543–555, 2004.

BRADY, N. C. **Natureza e propriedades dos solos**. 7.ed. São Paulo: Freitas Bastos, 878p., 1989.

BRÜMMER, G. W.; GERTH, J.; HERMS, U. Heavy metal species, mobility and availability in soils. **Journal of Plant Nutrition and Soil Science**, v. 149, p. 382–397, 1986.

BURTON, C. H.; TURNER, C. **Manure management: treatment strategies for sustainable agriculture.** 2nd ed. Wrest Park, Silsoe, Bedford, UK: Silsoe Research Institute, 490 p., 2003.

CARBONELL-BARRACHINA, A. A.; ROCAMORA, A.; GARCÍA-GOMIS, C.; MARTÍNEZ- SÁNCHEZ, F.; BURLÓ, F. Arsenic and zinc biogeochemistry in pyrite mine waste from the Aznalcóllar environmental disaster. **Geoderma,** v. 122, p. 195–203, 2004.

CEC – COUNCIL OF THE EUROPEAN COMMUNITIES. Council Directive 86/278/EEC of 12 June 1986 on the protection of the environment, and in particular of the soil, when sewage sludge is used in agriculture. **Official Journal**, v. 181, p. 6-18, 1986.

CETESB – COMPANHIA DE TECNOLOGIA DE SANEAMENTO AMBIENTAL. Norma CETESB P4.230/1999: **Aplicação de lodos de sistemas de tratamento biológico em áreas agrícolas – Critérios para projeto e operação.** Manual Técnico. 1999.

CETESB – COMPANHIA DE TECNOLOGIA DE SANEAMENTO AMBIENTAL. Decisão de Diretoria 045/2014/E/C/I: Dispõe sobre a aprovação dos valores orientadores para solos e águas subterrâneas no estado de São Paulo – 2014, em substituição aos valores orientadores de 2005 e dá outras providências. **Diário Oficial do Estado de São Paulo (DOSP)**, v. 124, n. 36, p. 53, 2014.

CHASTAIN, J. P.; CAMBERATO, J. J.; ALBRECHT, J. E.; ADAMS, J. Swine manure production and nutrient content. In: **South Carolina Confined Animal Manure Managers Certification Program**. Clemson University, SC, USA (Chapter 3), 2003.

CHEAH, S. F.; BROWN, G. E.; PARKS, G. A. XAFS study of Cu model compounds and Cu^{2+} sorption products on amorphous SiO2, γ-Al_2O_3 and anatase. **American Mineralogist**, v. 55, p. 118–132, 2000.

CONAMA – CONSELHO NACIONAL DO MEIO AMBIENTE. Resolução nº 375/2006: Define critérios e procedimentos, para o uso agrícola de lodos de esgoto gerados em estações de tratamento de esgoto sanitário e seus produtos derivados, e dá outras providências. **Diário Oficial da União**, n. 167, s. 1, p. 141–146, 2006.

CONAMA – CONSELHO NACIONAL DO MEIO AMBIENTE. Resolução nº 420/2009: Dispõe sobre critérios e valores orientadores de qualidade do solo quanto à presença de substâncias químicas e estabelece diretrizes para o gerenciamento ambiental de áreas contaminadas por essas substâncias em decorrência de atividades antrópicas. **Diário Oficial da União**, n. 249, p. 81–84, 2009.

COVELO, E. F.; COUCE, M. L. A.; VEGA, F. A. Competitive adsorption and desorption of cadmium, chromium, copper, nickel, lead, and zinc by humic umbrisols. **Communications in Soil Science and Plant Analysis**, v. 35, p. 2709–2729, 2004.

DEL CASTILHO, P.; CHARDON, W. J.; SALOMONS, W. Influence of cattle-manure slurry application on the solubility of cadmium, copper, and zinc in a manured acidic, loamy-sand soil. **Journal of Environmental Quality**, v. 22, p. 689–697, 1993.

DEMUELENAERE, R. G. A. **Caracterização de Propriedades de Transporte de metais Pesados em Solos Residuais do Rio de Janeiro**. 113 p. M.Sc. thesis (Mestrado em Engenharia Civil), Pontifícia Universidade Católica do Rio de Janeiro, 2004.

DOELSCH, E.; BASILE-DOELSCH, I.; ROSE, J. BORSCHNECK, D.; HAZEMANN, J. L.; MACARY, H. S.; BOTTERO, J. Y. New combination of EXAFS spectroscopy and density fractionation for the speciation of chromium within an andosol. **Environmental Science & Technology**, v. 40, n. 24, p. 7602-7608, 2006.

DOELSCH, E.; MOUSSARD, G.; MACARY, H. S. Fractionation of tropical soilborne heavy metals – Comparison of two sequential extraction procedures. **Geoderma,** v. 143, n. 1–2, p. 168–179, 2008.

DOELSCH, E.; VAN DE KERCHOVE, V.; MACARY, H. S. Heavy metal content in soils of Reunion (Indian Ocean). **Geoderma**, v. 134, p. 119–134, 2006.

DONNER, E.; RYAN, C. G.; HOWARD, D. L.; ZARCINAS, B.; SCHECKEL, K. G.; MCGRATH, S. P.; DE JONGE, M. D.; PATERSON, D.; NAIDU, R.; LOMBI, E. A multi-technique investigation of copper and zinc distribution, speciation and potential bioavailability in biosolids. **Environmental Pollution**, v. 166, p. 57–64, 2012.

DUBE, A.; ZBYTNIEWSKI, R.; KOWALKOWSKI, T.; CUKROWSKA, E.; BUSZEWSKI, B. Adsorption and migration of heavy metals in soil. **Polish Journal of Environmental Studies**, v. 10, n. 1, p. 1–10, 2001.

EC – EUROPEAN COMISSION. **Making the most of pig manure**. 2014. Available at: <http://ec.europa.eu/programmes/horizon2020/en/news/making-most-pig-manure>. Accessed 2015, June 15th.

EL-MUFLEH, A.; BÉCHET, B.; BASILE-DOELSCH, I.; GEFFROY-RODIER, C.; GAUDIN, A.; RUBAN, V. Distribution of PAHs and trace metals in urban stormwater sediments: combination of density fractionation, mineralogy and microanalysis. **Environmental Science And Pollution Research International,** v. 21, p. 9764–9776, 2014.

EMBRAPA – EMPRESA BRASILEIRA DE PESQUISA AGROPECUÁRIA. **A suinocultura no Brasil.** 2010. Available at: <http://www.cnpsa.embrapa.br/cias/index.php?option=com_content&view=article&id=5:origem-dos-suinos&catid=4:suinos-publico&Itemid=19>. Accessed 2015, June 18th.

ESAKKU, S.; SELVAM, A.; JOSEPH, K.; PALANIVELU, K. Assessment of heavy metal species in decomposed municipal solid waste. **Chemical Speciation and Bioavailability**, v. 17, n. 3, p. 95–102, 2005.

ESSINGTON, M. E. **Soil and Water Chemistry: An Integrative Approach**. 1st ed. Boca Raton: CRC Press, 552p., 2004.

FADIGAS, F. S.; AMARAL SOBRINHO, N. M. B.; MAZUR, N.; ANJOS, L. H. C.; FREIXO, A. A. Proposição de valores de referência para a concentração natural de metais pesados em solos brasileiros. **Revista Brasileira de Engenharia Agrícola e Ambiental**, v.10, p.699–705, 2006.

FAO – FOOD AND AGRICULTURE ORGANIZATION OF THE UNITED NATIONS. **Soil quality considerations in the selection of sites for aquaculture**. Corporate Document Repository, 1987. Available at: <http://www.fao.org/docrep/field/003/ac172e/AC172E00.htm#TOC>. Accessed 2015, June 17th.

FAO – FOOD AND AGRICULTURE ORGANIZATION OF THE UNITED NATIONS. **Statistics Division: FAOSTAT**. 2013. Available at: <http://faostat3.fao.org/home/E> Accessed 2015, June 18th.

FEDER, F.; FINDELING, A. Retention and leaching of nitrate and chloride in an andic soil after pig manure amendment. **European Journal of Soil Science**, v. 58, p. 393–404, 2007.

FERNÁNDEZ-CALIANI, J. C.; TIMÓN, V.; RIVERA, M. B.; GIRÁLDEZ, I.; PÉREZ-LÓPEZ, R. Experimental and theoretical evidence of zinc structurally bound in vermiculite from naturally metal-enriched soils. **Clay Minerals**, v. 48, n. 3, p. 529–541, 2013.

FILGUEIRAS, A. V.; LAVILLA, I.; BENDICHO, C. Chemical sequential extraction for metal partitioning in environmental solid samples. **Journal of Environmental Monitoring**, v. 4, n. 6, p. 823-857, 2002.

FLOGEAC, K.; GUILLON, E.; APLINCOURT, M. Surface complexation of copper(II) on soil particles: EPR and XAFS studies. **Environmental Science & Technology**, v. 38, p. 3098–3103, 2004.

FURNARE, L. J.; VAILIONIS, A.; STRAWN, D. G. Molecular-level investigation into copper complexes on vermiculite: effect of reduction of structural iron on copper complexation. **Journal of Colloid and Interface Science**, v. 289, p. 1–13, 2005.

GAMBLE, D. S.; BRUCCOLERI, A. G.; LINDSAY, E.; LANGFORD, C. H. Chlorothalonil in a quartz sand soil : wetting effects on sorption capacity and bound residue. **Environmental Science & Technology**, v. 34, p. 125–129, 2000.

GAO, S. A.; WALKER, W. J.; DAHLGREN, R. A; BOLD, J. Simultaneous sorption of Cd, Cu, Ni, Zn, Pb, and Cr on soils treated with sewage sludge supernatant. **Water, Air, & Soil Pollution**, v. 93, p. 331–345, 1997.

GARCIA-MINA, J. M. Stability, solubility and maximum metal binding capacity in metal–humic complexes involving humic substances extracted from peat and organic compost. **Organic Geochemistry**, v. 37, n. 12, p. 1960–1972, 2006.

GIACOMINO, A.; ABOLLINO, O.; MALANDRINO, M.; MENTASTI, E. The role of chemometrics in single and sequential extraction assays: a review. Part II. Cluster analysis, multiple linear regression, mixture resolution, experimental design and other techniques. **Analytica Chimica Acta**, v. 688, n. 2, p. 122-39, 2011.

GIRIJA, V. V.; RATTAN, R. K.; DATTA S. P. Adsorption study: A systematic approach to determine zinc availability in soils of divergent characteristics. **International Journal of Agricultural Sciences**, v. 4, n. 2, p. 102–105, 2013.

GIROTTO, E. **Cobre e Zinco no solo sob uso intensivo de dejeto líquido de suínos**. M.Sc. thesis (Mestrado em Ciência do Solo), Universidade Federal de Santa Maria, 2007.

GIROTTO, E.; CERETTA, C. A.; BRUNETTO, G.; SANTOS, D. S.; SILVA, L. S.; LOURENZI, C. R.; LORENSINI, F.; VIEIRA, R. C. B.; SCHMATZ, R. Acúmulo e formas de cobre e zinco no solo após aplicações sucessivas de dejeto líquido de suínos. **Revista Brasileira de Ciências do Solo**, v. 34, n. 3, p. 955-965, 2010.

GUAN, T. X.; HE, H. B.; ZHANG, X. D.; BAI, Z. Cu fractions, mobility and bioavailability in soil-wheat system after Cu-enriched livestock manure applications. **Chemosphere**, v. 82, n. 2, p. 215-22, 2011.

GUBIANI, E.; MALLMANN, F. J. K.; SANTOS, D. R.; BENDER, M. A.; VEIGA, M.; PICCIN, R.; ROSSATO, L. F. R.; GEBERT, F. H., Influência da aplicação continuada de dejeto líquido de suínos nos teores de carbono e nitrogênio do solo. In: **FERTBIO 2012 – A responsabilidade socioambiental da pesquisa agrícola**. SBCS/UFAL, Maceió, 2012.

HALL, G.E.M.; VAIVE, J.E.; BEER, R.; HOASHI, M. Selective leaches revisited, with emphasis on the amorphous Fe oxyhydroxide phase extraction. **Journal of Geochemical Exploration**, v. 56, p. 59–78, 1996.

HAN, F. X.; KINGERY, W. L.; SELIM, H. M.; GERALD, P. Accumulation of heavy metals in a long-term poultry waste amended soil. **Soil Science**, v. 165, p. 260–268, 2000.

HAO, X.-Z.; ZHOU, D.-M.; CHEN, H.-M.; DONG, Y.-H. Leaching of copper and zinc in a garden soil receiving poultry and livestock manures from intensive farming. **Pedosphere**, v. 18, p. 69–76, 2008.

HEIDMANN, I.; CHRISTL, I.; KRETZSCHMAR, R. Sorption of Cu and Pb to kaolinite-fulvic acid colloids: Assessment of sorbent interactions. **Geochimica et Cosmochimica Acta**, v. 69, p. 1675–1686, 2005.

HESTERBERG, D. Biogeochemical cycles and processes leading to changes in mobility of chemicals in soils. **Agriculture, Ecosystems & Environment**, v. 67, n. 2-3, p. 121-133, 1998.

HILLEL, D. **Introduction to Environmental Soil Physics**. 1st ed. Academic Press, 2003.

HLAVAY, J.; PROHASKA, T.; WEISZ, M.; WENZEL, W.W.; STINGEDER, G.J. Determination of trace elements bound to soils and sediment fractions. IUPAC Technical Report. **Pure and Applied Chemistry**, v. 76, p. 415-442, 2004.

HSEU, Z.-Y. Extractability and bioavailability of zinc over time in three tropical soils incubated with biosolids. **Chemosphere**, v. 63, n. 5, p. 762–771, 2006.

HSU, J.-H.; LO, S.-L. Effect of composting on characterization and leaching of copper, manganese, and zinc from swine manure. **Environmental Pollution**, v. 114, p. 119–127, 2001.

HUGEN, C.; MIQUELLUTI, D. J.; CAMPOS, M. L; ALMEIDA, J. A.; FERREIRA, E. R. N. C.; POZZAN, M. Teores de Cu e Zn em perfis de solos de diferentes litologias em Santa Catarina. **Revista Brasileira de Engenharia Agrícola e Ambiental**, n. 49, p. 622–628, 2013.

ISAURE, M. P.; MANCEAU, A.; GEOFFROY, N.; LABOUDIGUE, A.; TAMURA N.; MARCUS, M. A. Zinc mobility and speciation in soil covered by contaminated dredged sediment using micrometer-scale and bulk-averaging X-ray fluorescence, absorption and diffraction techniques. **Geochimica et Cosmochimica Acta**, v. 69, n. 5, p. 1173–1198, 2005.

JACOBSON, A. R.; DOUSSET, S.; ANDREUX F.; BAVEYE P. C. Electron microprobe and synchrotron X-ray fluorescence mapping of the heterogeneous distribution of copper in high-copper vineyard soils. **Environmental Science & Technology**, v. 41, p. 6343–6349, 2007.

JACQUAT, O.; VOEGELIN, A.; KRETZSCHMAR, R. Local coordination of Zn in hydroxy-interlayered minerals and implications for Zn retention in soils. **Geochimica et Cosmochimica Acta** v. 73, n. 2, 348–363, 2009a.

JACQUAT, O.; VOEGELIN, A.; KRETZSCHMAR, R. Soil properties controlling Zn speciation and fractionation in contaminated soils. **Geochimica et Cosmochimica Acta**, v. 73, n. 18, p. 5256–5272, 2009b.

JACQUAT, O.; VOEGELIN, A.; VILLARD, A.; MARCUS, M. A.; KRETZSCHMAR, R. Formation of Zn-rich phyllosilicates, Zn-layered double hydroxide and hydrozincite in contaminated calcareous soils. **Geochimica et Cosmochimica Acta**, v. 72, p. 5034–5057, 2008.

JONDREVILLE, C.; REVY, P.; DOURMAD, J. Dietary means to better control the environmental impact of copper and zinc by pigs from weaning to slaughter. **Livestock Production Science**, v. 84, n. 2, p. 147–156, 2003.

JONES, D. L.; PRABOWO, A. M.; KOCHIAN, L. V. Kinetics of malate transport and decomposition in acid soils and isolated bacterial populations: The effect of microorganisms on root exudation of malate under Al stress. **Plant and Soil**, v. 182, p. 239-247, 1996.

JUILLOT, F.; MORIN, G.; ILDEFONSE, P.; TRAINOR, T. P.; BENEDETTI, M.; GALOISY, L.; CALAS, G.; BROWN, G. E. Occurrence of Zn/Al hydrotalcite in smelter-impacted soils from northern France: evidence from EXAFS spectroscopy and chemical extractions. **American Mineralogist**, v. 88, p. 509–526, 2003.

KABALA, C.; SINGH, R.R. Fractionation and mobility of copper, lead, and zinc in soil profiles in the vicinity of a copper smelter. **Journal of Environmental Quality**, v. 30, p. 485–492, 2001.

KARATHANASIS, A. D.; JOHNSON, D. M.; MATOCHA, C. J. Biosolid colloid-mediated transport of copper, zinc, and lead in waste-amended soils. **Journal of Environmental Quality**, v. 34, p. 1153–1164, 2005.

KRAUSS, M.; WILCKE, W. Persistent organic pollutants in soil density fractions: distribution and sorption strength. **Chemosphere**, v. 59, n. 10, p. 1507–1515, 2005.

KIRPICHTCHIKOVA, T. A.; MANCEAU, A.; SPADINI, L.; PANFILI, F.; MARCUS, M. A; JACQUET, T. Speciation and solubility of heavy metals in contaminated soil using X-ray microfluorescence, EXAFS spectroscopy, chemical extraction, and thermodynamic modeling. **Geochimica et Cosmochimica Acta**, v. 70, p. 2163–2190, 2006.

L'HERROUX, L.; LE ROUX, S.; APPRIOU, P.; MARTINEZ, J. Behaviour of metals following intensive pig slurry applications to a natural field treatment process in Brittany (France). **Environmental Pollution**, v. 97, n. 1, p. 119–130, 1997.

LA FORCE, M. J.; FENDORF S. Solid-phase iron characterization during common selective sequential extractions. **Soil Science Society of America Journal**, v. 64, p. 1608–1615, 2000.

LEBEDEV, A. **Database: publications on x-ray absorption spectroscopy**. Available at <http://scon155.phys.msu.su/~papers/>. Accessed: 14/09/2015.

LEE, Y. J.; ELZINGA, E.; REEDER, R. J. Cu(II) adsorption a the calcite- water interface in the presence of natural organic matter: kinetic studies and molecular-scale characterizations. **Geochimica et Cosmochimica Acta**, v. 69, p. 49–61, 2005.

LEGROS, S.; DOELSCH, E.; MASION, A.; ROSE, J.; BORSCHNECK, D.; PROUX, O.; HAZEMANN, J-L.; SAINT-MACARY, H.; BOTTERO, J-Y. Combining size fractionation, scanning electron microscopy, and X-ray absorption spectroscopy to probe zinc speciation in pig slurry. **Journal of Environmental Quality**, v. 39, n. 2, p. 531–540, 2010a.

LEGROS, S.; CHAURAND, P.; ROSE, J.; MASION, A.; BRIOIS, V.; FERRASSE, J-H.; MACARY, H. S.; BOTTERO, J-Y.; DOELSCH, E. Investigation of copper speciation in pig slurry by a multitechnique approach. **Environmental Science & Technology**, v. 44, n. 18, p. 6926–6932, 2010b.

LEGROS, S.; DOELSCH, E.; FEDER, F. MOUSSARD, G.; SANSOULET, J.; GAUDET, J. P.; RIGAUD, S.; BASILE DOELSCH, I.; MACARY, H. S.; BOTTERO, J. Y. Fate and behaviour of Cu and Zn from pig slurry spreading in a tropical water–soil–plant system. **Agriculture, Ecosystems & Environment**, v. 164, p. 70-79, 2013.

LIBARDI, P.L. **Dinâmica da água no solo**. São Paulo: EDUSP, 335p., 2005.

LIPOTH, S. L.; SCHOENAU, J. J. Copper, zinc, and cadmium accumulation in two prairie soils and crops as influenced by repeated applications of manure. **Journal of Plant Nutrition and Soil Science**, v. 170, n. 3, p. 378–386, 2007.

LIU, S. H.; WANG, H. P. In situ studies of copper-humic substances in a contaminated soil during electrokinetic remediation. **Journal of Environmental Quality**, v. 33, p. 1280–1287, 2004.

MALLMAN, F. J. K. **Modelagem da transferência de cobre e zinco em solos contaminados por dejeto líquido de suínos**. 104 p. Ph.D. thesis (Doutorado em Ciência do Solo), Universidade Federal de Santa Maria, 2013.

MALLMANN, F. J. K.; SANTOS, D. R. D.; CERETTA, C. A.; CELLA, C.; ŠIMŮNEK, J.; VAN OORT, F. Modeling field-scale vertical movement of zinc and copper in a pig slurry-amended soil in Brazil. **Journal of Hazardous Materials**, v. 243, p. 223–231, 2012.

MANCEAU, A. ; LANSON, B. ; SCHLEGEL, M.L. ; HARGE, J.C.; MUSSO, M.; EYBERT-BERARD, L.; HAZEMANN, J.L.; CHATEIGNER, D.; LAMBLE, G.M. Quantitative Zn speciation in smelter-contaminated soils by EXAFS spectroscopy. **American Journal of Science**, v. 300, p. 289–343, 2000.

MANCEAU, A.; MARCUS, M. A.; TAMURA, N.; PROUX, O.; GEOFFROY, N.; LANSON, B. Natural speciation of Zn at the micrometer scale in a clayey soil using X-ray fluorescence, absorption and diffraction. **Geochimica et Cosmochimica Acta**, v. 68, p. 2467–2483, 2004.

MANCEAU, A.; MATYNIA, A. The nature of Cu bonding to natural organic matter. **Geochimica et Cosmochimica Acta**, v. 74, n. 9, p. 2556–2580, 2010.

MANCEAU, A.; TAMURA, N.; CELESTRE, R. S.; MACDOWELL, A. A.; GEOFFROY, N.; SPOSITO, G.; PADMORE, H. A. Molecular-scale speciation of Zn and Ni in soil ferromanganese nodules from loess soils of the Mississippi basin. **Environmental Science & Technology**, v. 37, p. 75–80, 2003.

MANCEAU, A.; TOMMASEO, C.; RIHS, S.; GEOFFROY, N.; CHATEIGNER, D.; SCHLEGEL, M.; TISSERAND, D.; MARCUS, M. A.; TAMURA, N.; CHEN, Z.-S. Natural speciation of Mn, Ni, and Zn at the micrometer scale in a clayey paddy soil using X-ray fluorescence, absorption, and diffraction. **Geochimica et Cosmochimica Acta**, v. 69, n. 16, p. 4007–4034, 2005.

MANCEAU, A.; MARCUS, M. A.; TAMURA N. Quantitative speciation of heavy metals in soils and sediments by synchrotron X-ray techniques. In: **Applications of Synchrotron Radiation in Low-temperature Geochemistry and Environmental Science**, v. 49. Washington, DC: Mineralogical Society of America, 2002.

MARTINEZ, C. E.; MOTTO, H. L. Solubility of lead, zinc and copper added to mineral soils. **Environmental Pollution**, v. 107, p. 153–158, 2000.

MCBRIDE, M. B. **Environmental Chemistry of Soils**. New York: Oxford University Press, 405 p., 1994.

MCBRIDE, M. B. Toxic metals in sewage sludge-amended soils: has promotion of beneficial use discounted the risks? **Advances in Environmental Research**, v. 8, n. 1, p. 5–19, 2003.

MILLER, J. O.; KARATHANASIS, A. D.; MATOCHA, C. J. in situ generated colloid transport of Cu and Zn in reclaimed mine soil profiles associated with biosolids application. **Applied and Environmental Soil Science**, v. 2011, 9 p., 2011.

MORTON, J. D.; SEMRAU, J. D.; HAYES, K. F. An X-ray absorption spectroscopy study of the structure and reversibility of copper adsorbed on montmorillonite clay. **Geochimica et Cosmochimica Acta**, v. 65, p. 2709–2722, 2001.

MORTVEDT, J. J. Heavy metal contaminants in inorganic and organic fertilizers. **Fertilizer Research**, v. 43, p. 55-61, 1996.

NACHTEGAAL, M.; MARCUS, M. A.; SONKE, J. E.; VANGRONSVELD, J.; LIVI, K. J. T.; VAN DER LELIE, D.; SPARKS D. L. Effects of in situ remediation on the speciation and bioavailability of zinc in a smelter contaminated soil. **Geochimica et Cosmochimica Acta**, v. 69, p. 4649–4664, 2005.

NASCIMENTO, C. W. A.; FONTES, R. L. F.; NEVES, J. C. L.; MELÍCIO, A. C. D. F. Fracionamento, dessorção e extração química de Zinco em Latossolos. **Revista Brasileira de Ciência do Solo**, v. 26, n. 1, p. 599-606, 2002.

NEWVILLE. M. Fundamentals of XAFS. **Reviews in Mineralogy and Geochemistry**, v. 78, p. 33-74, 2004.

NOVAK, J. M.; WATTS, D. W.; STONE, K. C. Copper and zinc accumulation, profile distribution, and crop removal in coastal plain soils receiving long−term, intensive applications of swine manure. **American Society of Agricultural Engineers**, v. 47, n. 5, p. 1513–1522, 2004.

ORIHARA, K.; KAMIYAMA, K.; FUJIWARA, S. Characteristics of heavy metal content in animal manure compost. **Japanese Society of Soil Science and Plant Nutrition**, v. 73, p. 403−409, 2002.

PANDOLFO, C.; BRAGA, H. J.; SILVA JÚNIOR, V. P. **Atlas climatológico digital do Estado de Santa Catarina**. Florianópolis: Epagri, 2002.

PANFILI, F.; MANCEAU, A.; SARRET, G.; SPADINI, L.; KIRPICHTCHIKOVA, T.; BERT, V.; LABOUDIGUE, A.; MARCUS, M. A.; AHAMDACH, N.; LIBERT, M. F. The effect of phytostabilization on Zn speciation in a dredged contaminated sediment using scanning electron microscopy, X-ray fluorescence, EXAFS spectroscopy, and principal components analysis. **Geochimica et Cosmochimica Acta**, v. 69, n. 9, p. 2265-2284, 2005.

PELOZATO, M. **Valores de referência de cádmio, cobre, manganês e zinco para solos de Santa Catarina**. 70 p. M.Sc. thesis (Mestrado em Ciência do Solo), Universidade Estadual de Santa Catarina, 2008.

PEU, P.; BIRGAND, F.; MARTINEZ, J. Long term fate of slurry derived nitrogen in soil: A case study with a macro-lysimeter experiment having received high loads of pig slurry (Solepur). **Bioresource Technology**, v. 98, p. 3228–3234, 2007.

PINTO, M. A. B.; FABBRIS, C.; BASSO, C. J.; SANTI, A. L.; GIROTTO, E. Aplicação de dejeto líquido de suínos e manejo do solo na sucessão aveia/milho. **Agricultural Research in the Tropics**, v. 44, n. 2, p. 205-212, 2014.

PLEKHANOVA, I. O. Effect of wetting conditions on the fractional composition of heavy metal compounds in agrosoddy-podzolic soils contaminated with sewage sludge. **Eurasian Soil Science**, v. 45, n. 7, p. 657-664, 2012.

POULSEN, H. D. Zinc and copper as feed additives, growth factors or unwanted environmental factors. **Journal of Animal and Feed Sciences**, v. 7, p. 135-142, 1998.

QIAO, X. L.; LUO, Y. M.; CHRSTIE, P.; WONG, M. H. Chemical speciation and extractability of Zn, Cu and Cd in two contrasting biosolids-amended clay soil. **Chemosphere**, v. 50, p. 823-829, 2003.

RAO, C. R. M.; SAHUQUILLO, A.; Sanchez, J. F. L. A review of the different methods applied in environmental geochemistry for single and sequential extraction of trace elements in soils and related materials. **Water, Air & Soil Pollution**, v. 189, p. 291–333, 2008.

RATUZNY, T.; GONG, Z.; WILKE, B.-M. Total concentrations and speciation of heavy metals in soils of the Shenyang Zhangshi Irrigation Area, China. **Environmental Monitoring and Assessment**, v. 156, p. 171–180, 2009.

RAVEL, B.; NEWVILLE,M. Athena, Artemis, Hephaestus: data analysis for X-ray absorption spectroscopy using IFEFFIT. **Journal of Synchrotron Radiation**, v. 12, p. 537–541, 2005.

REEDER, R. J.; SCHOONEN, M. A. A.; LANZIROTTI, A. Metal speciation and its role in bioaccessibility and bioavailability. **Reviews in Mineralogy and Geochemistry**, v. 64, p. 59–113, 2006.

REINERT, D. J.; REICHERT, J. M. **Propriedades físicas do solo**. Santa Maria, 2006.

RIEUWERTS J. S.; ASHNORE, M. R.; FARAGO, M. E.; THORNTON, I. The influence of soil characteristics on the extractability of Cd, Pb and Zn in upland and moorland soils. **Science of the Total Environment**, v. 366, p. 64–875, 2006.

ROBERTS, D. R.; SCHEINOST, A C.; SPARKS, D. L. Zinc speciation in a smelter-contaminated soil profile using bulk and microspectroscopic techniques. **Environmental Science & Technology**, v. 36, n. 8, p. 1742–1750, 2002.

SAMPAIO, A. O. Afinal, queremos ou não viabilizar o uso agrícola do lodo produzido em estações de esgoto sanitário? Uma avaliação crítica da Resolução CONAMA 375. **Revista DAE**, n. 193, 2013.

SANCHEZ, E. **Propriedades físicas do solo e produtividade de soja em sucessão a plantas de cobertura de inverno**, Unicentro-PR, 2012.

SARRET, G.; BALESDENT, J.; BOUZIRI, L.; GARNIER, J. M.; MARCUS, M. A.; GEOFFROY, N.; PANFILI, F; MANCEAU, A. Zn speciation in the organic horizon of a contaminated soil by micro-X-ray fluorescence, micro- and powder-EXAFS spectroscopy, and isotopic dilution. **Environmental Science & Technology**, v. 38, p. 2792–2801, 2004.

SARRET, G.; SCHROEDER, W. H.; MARCUS, M. A.; GEOFFROY, N.; MANCEAU, A. Localization and speciation of Zn in mycorrihizd roots by μSXRF and μEXAFS.. **Journal de Physique IV France**, v. 107, p.1193-1196, 2003.

SARRET, G.; SAUMITOU-LAPRADE, P.; BERT, V.; PROUX, O.; HAZEMANN, J. L.; TRAVERSE, A.; MARCUS, M. A.; MANCEAU A. Forms of zinc accumulated in the hyperaccumulator *Arabidopsis halleri*. **Plant Physiology**, v. 130, p. 1815–1826, 2002.

SASKATCHEWAN-CANADÁ. **Nutrient Values of Manure.** Saskatchewan Agriculture and Food. 4p., 2013.

SBSC – SOCIEDADE BRASILEIRA DE CIÊNCIA DO SOLO. Comissão de Química e Fertilidade do Solo. **Manual de adubação e de calagem para os Estados do Rio Grande do Sul e de Santa Catarina**. 10. ed., Porto Alegre, 2004. 400 p.

SCHEINOST, A. C.; KRETZSCHMAR, R.; PFISTER, S.; ROBERTS, D. R. Combining selective sequential extractions, X-ray absorption spectroscopy, and principal component analysis for quantitative zinc speciation in soil. **Environmental Science & technology**, v. 36, n. 23, p. 5021-5028, 2002.

SCHLEGEL, M. L.; MANCEAU, A. Zn incorporation in hydroxy-Al- and Keggin Al-13-intercalated montmorillonite: a powder and polarized EXAFS study. **Environmental Science & Technology**, v. 41, p. 1942–1948, 2007.

SELIM, H. M.; AMACHER, M. C. **Reactivity and Transport of Heavy Metals in Soils**. 1 Ed. Boca Raton: CRC Press, 1996, 224p.

SEMA/IAP – SECRETARIA DE ESTADO DO MEIO AMBIENTE E RECURSOS HÍDRICOS. INSTITUTO AMBIENTAL DO PARANÁ. Instrução Técnica CEP/DTA N. 001/2002**: Dispõe sobre a utilização agrícola de lodo de estação de tratamento de esgoto sanitário.** 2002.

SHUMAN, L.M. Effect of liming on the distribution of manganese, copper, iron, and zinc among soil fractions. **Soil Science Society of America Journal**, v. 50, p. 1236–1240, 1986.

SILVEIRA, M. L.; ALLEONI, L. R. F.; O'CONNOR, G. A.; CHANG, A. C. Heavy metal sequential extraction methods – A modification for tropical soils. **Chemosphere**, v. 64, p. 1929–1938, 2006.

SIMS, J. L.; PATRICK JR.; W. H., The distribution of micronutrients cations in soil under conditions of varying redox potential and pH. **Soil Science Society of America Journal**, v. 42, p. 259–262, 1978.

SMITH, D. R.; MOORE JR., P. A.; MAXWELL, C. V.; HAGGARD, B. E.; DANIEL, T. C. Reducing phosphorus runoff from swine manure with dietary phytase and aluminum Chloride. **Journal of Environmental Quality**, v. 33, p. 1048–1054, 2004.

STRAWN, D. G.; PALMER, N. P.; FURNARE, L.; GOODELL, C.; AMONETTE, J.; KUKKADAPU, R. Mechanisms of copper sorption on smectites. **Clays and Clay Minerals**, v. 52, p. 321–333, 2004.

STRAWN, D. G. & BAKER, L. L. Speciation of Cu in a contaminated agricultural soil measured by XAFS, μ-XAFS, and μ-XRF. **Environmental Science & Technology**, v. 42, p. 37–42, 2008.

SCHUWIRTH, N.; VOEGELIN, A.; KRETZSCHMAR, R.; HOFMANN, T. Vertical distribution and speciation of trace metals in weathering flotation residues of a zinc/lead sulfide mine. **Journal of Environmental Quality**, v. 36, p. 61–69, 2007.

TAVARES, C. J. Produção e caracterização de revestimentos nanoestruturados em multicamadas de TiAlN/Mo. Ph.D. thesis (Doutoramento em Ciências, área de especialização em Física). Universidade do Minho. Braga, 2002. 198p.

TEDESCO, M. J.; GIANELLO, C.; BISSANI, C. A.; BOHNEN, H.; VOLKWEISS, S. J. **Análise de solo, plantas e outros materiais**. 2nd ed. Porto Alegre: Departamento de Solos/UFRGS, 174p., 1995.

TEO, B.K., **EXAFS: Basic Principles and Data Analysis**. Berlin: Springer-Verlag, 1986.

TESSIER, A.; CAMPBELL, P. G. C.; BISSON, M. Sequential extraction procedure for the speciation of particulate trace metals. **Analytical Chemistry**, v. 51, n. 7, p. 844-851, 1979.

TOWE, K.M.; BRADLEY, W.F. Mineralogical constitution of colloidal "hydrous ferric oxides". **Journal of Colloid and Interface Science**, v. 24, p. 384-392, 1967.

URE, A. M.; QUEVAUVILLER, PH.; MUNTAU, H.; GRIEPINK, B. Speciation of heavy metals in solids and sediments. An account of the improvement and harmonization of extraction techniques undertaken under the auspices of the BCR of the Commission of the European Communities. **International Journal Environmental Analytical Chemistry**, v. 51, p. 135- 151, 1993.

URE, A.M.; DAVIDSON, C.M. **Chemical speciation in the environment**. 2nd ed. Oxford: Blackwell Science, 452p., 2002.

USDA – UNITED STATES DEPARTMENT OF AGRICULTURE. **Soil survey staff, keys to soil taxonomy**. 9th ed. Washington: Natural Resources Conservation Service, USDA, 2003.

USDA – UNITED STATES DEPARTMENT OF AGRICULTURE. **Soil texture calculator**, 2013. Available at: <http://soils.usda.gov/technical/aids/investigations/texture/>. Accessed 2013, May 2nd.

USEPA - UNITED STATES ENVIRONMENTAL PROTECTION AGENCY**. Hazardous Waste Land Treatment. Response SW-874.** Office of Solid Waste and Emergency, Washington, 1983.

USEPA – UNITED STATES ENVIRONMENTAL PROTECTION AGENCY. Method 3051A: Microwave assisted acid digestion of sediments, sludges, soils, and oils, In: **Sw-846 test methods for evaluation solid waste: physical/chemical methods**. Washington, 2007.

USEPA - UNITED STATES ENVIRONMENTAL PROTECTION AGENCY. Standards for the use and disposal of sewage sludge. In: **40 CFR – Part 503**. Federal Region, Washington, v. 58, p. 9387-9415, 1993.

USEPA - UNITED STATES ENVIRONMENTAL PROTECTION AGENCY. Understanding Variation in Partition Coefficient, Kd, Values – Volume I: The Kd Model, Methods of Measurements and Application of Chemical Reaction Codes**.** In: **EPA/402-R-99-004A**. Office of Air and Radiation, Washington. 212p. 1999.

USEPA – UNITED STATES ENVIRONMENTAL PROTECTION AGENCY. **Terminology Services: Terms & Acronyms**. 2016. Available at: <https://iaspub.epa.gov/sor_internet/registry/termreg/searchandretrieve/termsandacronyms/search.do>. Accessed 2016, April 8th.

USEPA - UNITED STATES ENVIRONMENTAL PROTECTION AGENCY. **ISIS - Integrated Risk Information System.** 2015. Available at: <http://www.epa.gov/iris>. Accessed 2015, December 30th.

USPCE – UNITED STATES PORK CENTER OF EXCELLENCE. **Quick facts: the pork industry at a glance**. 2009. Available at: < http://www.porkgateway.org/FileLibrary/PIGLibrary/References/NPB%20Quick%20%20Facts%20book.pdf>. Accessed 2015, June 19th.

VAZ, A. J.; LIMA, I. V. D. Imunotoxicologia dos Metais. In: F. A. de Azevedo; A. A. da M. Chasin (Eds.); **Metais - Gerenciamento da Toxicidade**. 1st ed. São Paulo: Atheneu, p. 399-414, 2003.

VEIGA, M.; PANDOLFO, C. M.; JUNIOR, A .A .B.; SPAGNOLLO, E. Chemical attributes of a Hapludox soil after nine years of pig slurry application. **Pesquisa Agropecuária Brasileira**, v. 47, p. 1766-1773, 2012.

VLAIC, G.; OLIVI, L. EXAFS Spectroscopy: a Brief Introduction. **Croatica Chemica Acta**, v. 77, n. 3, p. 427–433, 2004.

VOEGELIN, A.; PFISTER, S.; SCHEINOST, A.C.; MARCUS, M.A.; KRETZSCHMAR, R. Changes in zinc speciation in field soil after contamination with zinc oxide. **Environmental Science & Technology**, v. 39, p. 6616–6623, 2005.

VOEGELIN, A.; JACQUAT, O.; PFISTER, S.; BARMETTLER, K.; SCHEINOST, A. C.; KRETZSCHMAR, R. Time-dependent changes of zinc speciation in four soils contaminated with zincite or sphalerite. **Environmental Science & Technology**, v. 45, p. 255–261, 2011.

WAGAI, R.; KAJIURA, M.; ASANO, M.; HIRADATE, S. Nature of soil organo-mineral assemblage examined by sequential density fractionation with and without sonication: Is allophanic soil different? **Geoderma**, v. 241-242, p. 295–305, 2015.

WAYCHUNAS, G. A.; FULLER, C. C.; DAVIS, J. A. Surface complexation and precipitate geometry for aqueous Zn(II) sorption on ferrihydrite: I. X-ray absorption extended fine structure spectroscopy analysis. **Geochimica et Cosmochimica Acta**, v. 66, p. 1119-1137, 2002.

WILCKE, W.; GUSCHKER, C.; KOBŽA, J.; ZECH, W. Heavy metal concentrations, partitioning, and storage in Slovak forest and arable soils along a deposition gradient. **Journal of Plant Nutrition and Soil Science**, v. 162, p. 223–229, 1999.

XIANG, H. F.; TANG, H. A.; YING, Q. H. Transformation and distribution of forms of zinc in acid, neutral and calcareous soils of China. **Geoderma**, v. 66, p. 121–135, 1995.

XUE, H.; NHAT, P. H.; GÄCHTER, R.; HOODA, P. S. The transport of Cu and Zn from agricultural soils to surface water in a small catchment. **Advances in Environmental Research**, v. 8, p. 69–76, 2003.

YIN, Y.; IMPELLITTERI, C. A.; YOU, S.−J; ALLEN H. E. The importance of organic matter distribution and extract soil: solution ratio on the desorption of heavy metals from soils. **Science of the Total Environment**, v. 287, p. 107−119, 2002.

ZHENG, C.; BENNETT, G. D. **Applied contaminant transport modeling**. 2nd ed. New York: John Wiley & Sons, 656 p., 2002.

ZIMMERMAN, A. J.; WEINDORF, D. C. Heavy metal and trace metal analysis in soil by sequential extraction: a review of procedures. **International Journal of Analytical Chemistry**, v. 2010, p. 1–7, 2010.

ZHOU, W.; HESTERBERG, D.; HANSEN, P. D. H.; HUTCHISON, K. J.; SAYERS, D. E. Stability of copper sulfide in a contaminated soil. **Journal of Synchrotron Radiation**, v. 6, p. 630–632, 1999.

ZOU, X.; YUAN, T.; ZHU, Y.; ZHANG, X.; FENG, S.; SHEN, Z.; WANG, W. Heterogeneous distribution of copper in different grain size and density fractions of contaminated surface sediment from Nansi Lake (China). **Environmental Geology**, v. 51, n. 5, p. 813–820, 2006.

ZUBLENA, J. P.; BARKER, J. C.; PARKER, J. W.; STANISLAW, C. M. Swine Manure as a Fertilizer Source. **Soil Facts**. North Carolina Cooperative Extension Service College of Agricultural & Life Sciences. North Carolina State University. 6p. 2004.

APPENDICES

Supporting Information SI-1.

Cu fractions and SUMF concentrations (mean ± SD) within the soil layers of the CT, PS50, PS100 and PS200 plots.

Soil layer	Plot	F1*	F2	F3	F4	F5	F6	SUMF
(cm)		(mg kg^{-1})						
0—5	CT	0.23 ± 0.04	1.48 ± 0.15	19.39 ± 2.25	7.62 ± 1.77	8.27 ± 0.72	88.29 ± 3.61	125.28 ± 6.52
	PS50	0.48 ± 0.02	3.90 ± 0.51	37.73 ± 5.82	9.42 ± 2.16	10.23 ± 0.52	88.93 ± 5.06	150.69 ± 3.15
	PS100	0.75 ± 0.07	6.37 ± 1.62	39.59 ± 4.61	9.80 ± 1.28	10.29 ± 0.94	87.90 ± 4.96	154.70 ± 9.88
	PS200	1.03 ± 0.22	10.23 ± 1.03	55.53 ± 8.14	12.89 ± 0.84	11.73 ± 0.21	88.81 ± 1.63	180.22 ± 9.49
5—10	CT	0.15 ± 0.04	1.61 ± 0.15	21.18 ± 1.55	6.45 ± 0.53	8.10 ± 0.57	90.05 ± 4.60	127.54 ± 5.55
	PS50	0.28 ± 0.05	3.16 ± 0.74	31.30 ± 3.24	7.20 ± 1.17	8.69 ± 0.61	87.01 ± 2.81	137.65 ± 5.15
	PS100	0.39 ± 0.04	4.24 ± 0.57	30.16 ± 1.68	7.10 ± 1.78	8.55 ± 0.66	87.50 ± 3.58	137.94 ± 6.66
	PS200	0.61 ± 0.20	6.68 ± 1.22	38.81 ± 6.93	7.60 ± 0.55	8.85 ± 0.91	86.79 ± 5.93	149.34 ± 14.13
10—15	CT	0.08 ± 0.02	1.74 ± 0.02	20.10 ± 0.98	6.69 ± 1.29	7.62 ± 0.20	92.54 ± 1.24	128.76 ± 1.45
	PS50	0.15 ± 0.01	2.06 ± 0.31	25.33 ± 3.38	5.92 ± 0.72	7.72 ± 0.28	93.49 ± 4.30	134.68 ± 2.48
	PS100	0.25 ± 0.03	2.62 ± 0.46	24.69 ± 3.49	5.57 ± 0.51	7.40 ± 0.27	93.47 ± 6.92	134.01 ± 5.57
	PS200	0.31 ± 0.08	3.82 ± 0.58	28.80 ± 2.20	5.79 ± 0.16	7.52 ± 0.37	93.03 ± 2.18	139.28 ± 2.51
15—20	CT	0.07 ± 0.01	1.85 ± 0.12	20.59 ± 0.82	6.95 ± 1.39	7.45 ± 0.58	88.91 ± 0.80	125.81 ± 2.29
	PS50	0.12 ± 0.01	1.80 ± 0.21	24.84 ± 4.37	5.52 ± 0.52	7.70 ± 0.24	88.83 ± 4.60	128.81 ± 0.93
	PS100	0.15 ± 0.01	2.14 ± 0.15	22.43 ± 2.29	4.88 ± 0.23	7.13 ± 0.19	90.37 ± 7.48	127.10 ± 5.44
	PS200	0.22 ± 0.06	2.70 ± 0.40	25.45 ± 2.07	4.77 ± 0.21	7.46 ± 0.16	86.50 ± 4.19	127.10 ± 5.26
20—25	CT	0.10 ± 0.01	1.87 ± 0.11	20.26 ± 0.69	7.34 ± 1.20	7.51 ± 0.48	90.77 ± 2.04	127.86 ± 2.35
	PS50	0.10 ± 0.02	1.73 ± 0.28	25.98 ± 2.95	5.73 ± 1.20	7.51 ± 0.04	81.48 ± 2.10	122.54 ± 3.79
	PS100	0.13 ± 0.02	2.03 ± 0.12	24.39 ± 1.34	4.67 ± 0.61	6.86 ± 0.23	83.20 ± 3.61	121.27 ± 4.07
	PS200	0.18 ± 0.05	2.34 ± 0.39	25.79 ± 1.02	4.54 ± 0.03	7.06 ± 0.25	82.30 ± 1.13	122.21 ± 1.60
25—30	CT	0.10 ± 0.03	1.97 ± 0.12	21.64 ± 0.61	6.66 ± 1.78	7.43 ± 0.24	87.79 ± 0.39	125.59 ± 1.61
	PS50	0.12 ± 0.02	1.73 ± 0.26	26.20 ± 2.50	5.49 ± 1.27	7.37 ± 0.60	90.50 ± 3.21	131.41 ± 2.16
	PS100	0.14 ± 0.02	2.08 ± 0.36	24.85 ± 1.13	4.42 ± 0.40	7.07 ± 0.30	90.37 ± 3.38	128.93 ± 4.75
	PS200	0.18 ± 0.04	2.29 ± 0.42	25.54 ± 0.58	4.27 ± 0.30	6.20 ± 1.44	86.97 ± 2.26	125.45 ± 3.48

* F1 = exchangeable; F2 = adsorbed; F3 = organic matter; F4 = amorphous oxyhydroxides; F5 = crystalline oxides; F6 = residual; SUMF = sum of fractions.

Supporting Information SI-2.

Zn fractions and SUMF concentrations (mean ± SD) within the soil layers of the CT, PS50, PS100 and PS200 plots.

Soil layer	Plot	F1*	F2	F3	F4	F5	F6	SUMF
(cm)		(mg kg^{-1})						
0—5	CT	0.15 ± 0.03	1.34 ± 0.29	9.08 ± 1.14	2.91 ± 1.41	9.71 ± 0.07	77.21 ± 3.54	100.40 ± 5.32
	PS50	3.13 ± 1.77	13.32 ± 4.65	25.91 ± 5.72	8.18 ± 2.58	15.13 ± 2.90	82.17 ± 2.79	147.83 ± 14.98
	PS100	6.71 ± 2.95	24.27 ± 6.28	29.47 ± 4.78	9.18 ± 1.12	15.37 ± 0.30	78.32 ± 0.24	163.31 ± 14.63
	PS200	11.65 ± 4.76	31.88 ± 2.86	35.69 ± 3.34	11.41 ± 1.13	15.71 ± 0.27	81.79 ± 0.80	188.13 ± 8.83
5—10	CT	0.10 ± 0.04	0.50 ± 0.16	8.02 ± 1.04	1.26 ± 0.40	9.99 ± 1.11	76.70 ± 7.92	96.56 ± 8.37
	PS50	1.51 ± 0.61	3.93 ± 1.47	16.27 ± 1.89	3.50 ± 0.64	11.26 ± 0.46	77.79 ± 4.65	114.26 ± 7.54
	PS100	2.67 ± 1.44	6.91 ± 1.75	17.19 ± 2.28	4.54 ± 1.13	12.41 ± 1.08	72.88 ± 5.29	116.60 ± 11.68
	PS200	5.26 ± 1.30	11.06 ± 1.61	21.28 ± 2.38	5.15 ± 0.68	13.02 ± 1.09	77.83 ± 5.59	133.60 ± 9.31
10—15	CT	0.08 ± 0.08	0.49 ± 0.35	7.01 ± 0.43	1.13 ± 0.55	9.83 ± 1.03	80.49 ± 4.09	99.03 ± 4.55
	PS50	0.43 ± 0.27	0.79 ± 0.69	10.87 ± 0.68	1.70 ± 0.48	9.30 ± 0.47	83.16 ± 1.57	106.25 ± 2.13
	PS100	0.76 ± 0.71	2.07 ± 0.96	12.52 ± 2.50	2.36 ± 0.64	11.09 ± 0.81	79.24 ± 10.49	108.04 ± 12.79
	PS200	1.75 ± 0.84	4.24 ± 0.22	14.95 ± 0.72	3.03 ± 0.32	10.50 ± 0.90	83.22 ± 2.91	117.70 ± 3.82
15—20	CT	0.14 ± 0.05	0.29 ± 0.12	7.37 ± 0.38	0.96 ± 0.43	8.66 ± 0.40	75.21 ± 4.29	92.62 ± 5.06
	PS50	0.26 ± 0.20	0.20 ± 0.26	10.54 ± 1.45	1.11 ± 0.35	9.60 ± 0.35	80.86 ± 4.12	102.57 ± 4.39
	PS100	0.37 ± 0.23	0.83 ± 0.25	10.28 ± 1.79	1.45 ± 0.05	10.27 ± 0.87	73.26 ± 6.95	96.45 ± 6.50
	PS200	0.61 ± 0.40	1.75 ± 0.44	11.70 ± 1.13	1.58 ± 0.17	9.82 ± 0.95	74.75 ± 7.22	100.21 ± 9.19
20—25	CT	0.18 ± 0.11	0.34 ± 0.29	6.83 ± 0.65	1.07 ± 0.38	8.45 ± 0.59	81.20 ± 4.61	98.07 ± 5.05
	PS50	0.14 ± 0.12	0.05 ± 0.32	10.25 ± 1.21	0.83 ± 0.38	8.02 ± 0.90	76.63 ± 7.76	95.92 ± 8.83
	PS100	0.22 ± 0.14	0.32 ± 0.02	11.55 ± 0.81	1.39 ± 0.41	9.17 ± 0.28	70.83 ± 8.27	93.47 ± 9.13
	PS200	0.29 ± 0.18	0.89 ± 0.22	11.60 ± 0.35	1.17 ± 0.13	9.55 ± 1.14	72.88 ± 2.33	96.38 ± 3.74
25—30	CT	0.09 ± 0.08	0.17 ± 0.23	7.45 ± 0.66	0.67 ± 0.14	8.31 ± 0.43	80.19 ± 9.57	96.87 ± 9.49
	PS50	0.07 ± 0.06	0.00 ± 0.06	10.21 ± 2.29	0.90 ± 0.35	8.99 ± 0.46	83.22 ± 1.10	103.38 ± 0.58
	PS100	0.14 ± 0.07	0.17 ± 0.21	11.37 ± 0.58	0.90 ± 0.21	10.41 ± 1.42	81.10 ± 2.44	104.09 ± 2.57
	PS200	0.17 ± 0.10	0.56 ± 0.09	11.21 ± 0.26	0.86 ± 0.10	8.90 ± 1.53	79.17 ± 3.00	100.87 ± 4.87

* F1 = exchangeable; F2 = adsorbed; F3 = organic matter; F4 = amorphous oxyhydroxides; F5 = crystalline oxides; F6 = residual; SUMF = sum of fractions.

Supporting Information SI-3.

X-ray diffractograms of kaolinite and purified montmorillonite clays used in Cu sorption experiments.

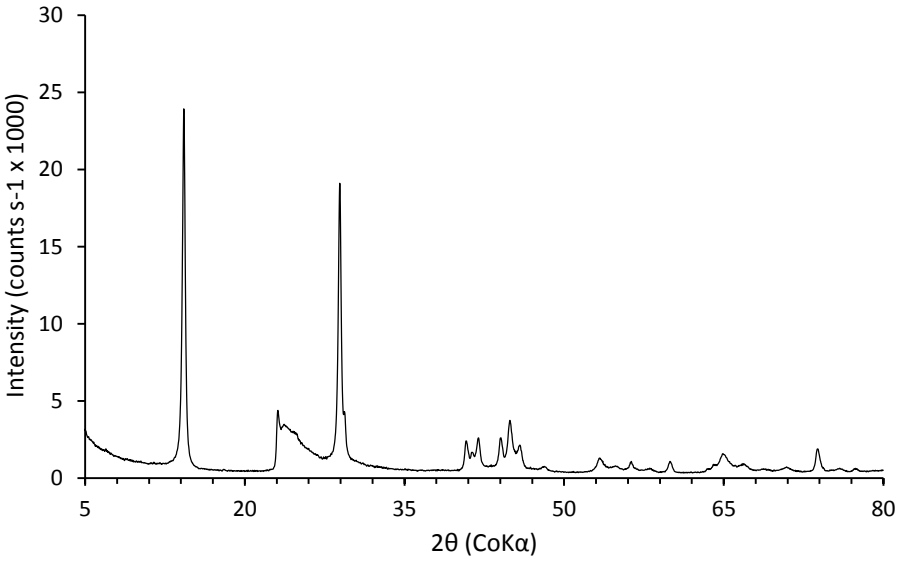

Figure SI-3a – X-ray diffraction patterns of kaolinite.

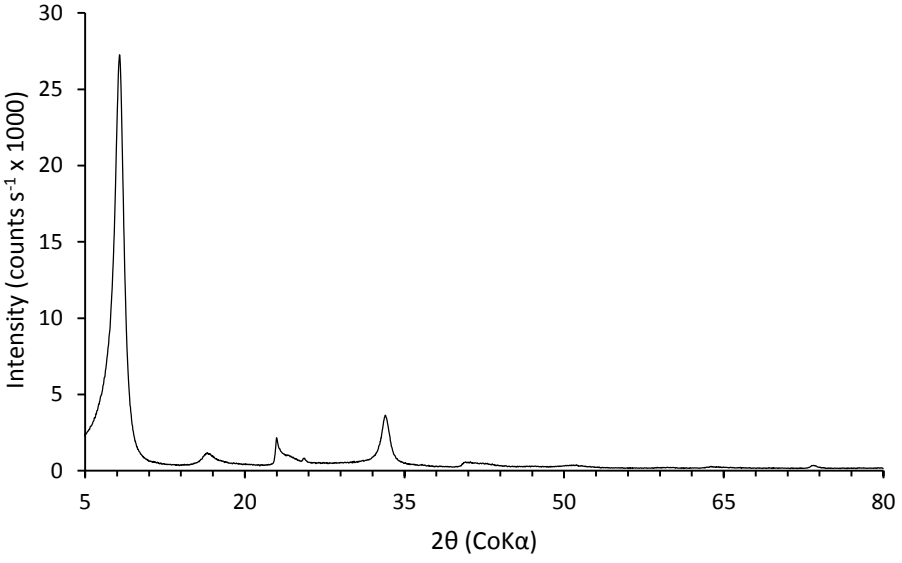

Figure SI-3b – X-ray diffraction patterns of purified montmorillonite.

Supporting Information SI-4.

Cu uptake as a function of time in kaolinite and montmorillonite clays

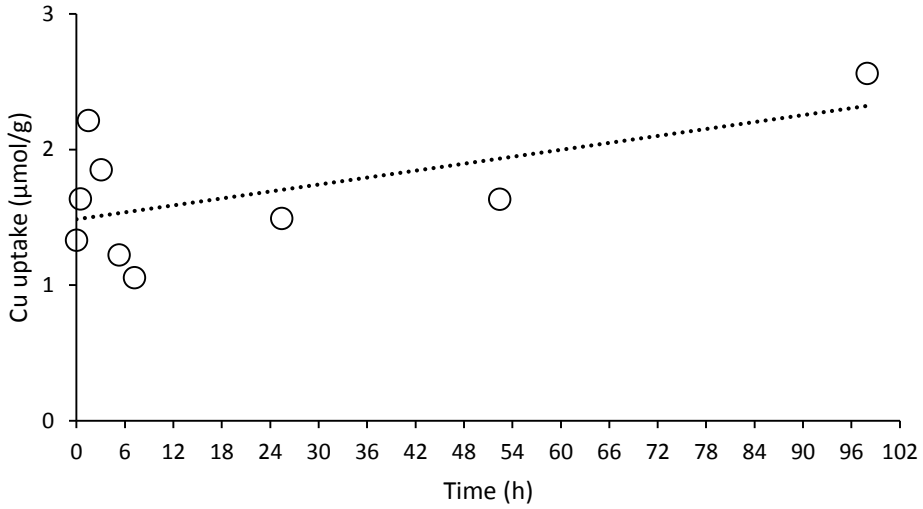

Figure SI-4a – Cu uptake as function of time in 2 g l^{-1} kaolinite (pH = 5.7, [Cu] total = 33 µM).

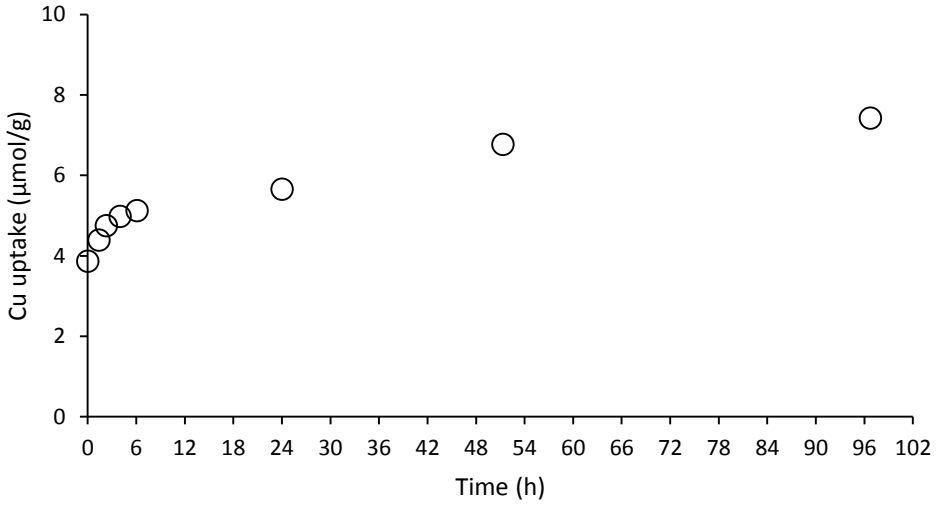

Figure SI-4b – Cu uptake as function of time in 2 g l^{-1} montmorillonite (pH = 5.7, [Cu] total = 33 µM).

Supporting Information SI-5.

Cu uptake by kaolinite and montmorillonite clays for different initial Cu concentrations (pH = 5.7, clay = 2 g l^{-1}, reaction time = 4h).

	Kaolinite			Montmorillonite			
	Cu-kaol 33[(1)]	Cu-kaol 100	Cu-kaol 300	Cu-Mont 13[(1)]	Cu-Mont 33	Cu-Mont 100	Cu-Mont 300
[Cu] initial (µM)[(2)]	32.6	97.0	282.6	13.1	32.8	97.3	283.4
Cu uptake (µmol g^{-1})	3.3	6.3	20.2	3.8	6.0	9.3	27.6
Cu uptake (mg kg^{-1})	208.6	400.6	1283.1	244.5	380.5	589.4	1755.8

(1) 13, 33, 100 and 300: target Cu initial concentration in the reaction solution, in µM.
(2) Cu initial concentration corrected for the volume of base added to raise the pH.